# LATE-GLACIAL ALPINE GLACIER ADVANCE AND EARLY HOLOCENE TEPHRAS, NORTHERN BRITISH COLUMBIA

by

Thomas Ryan Lakeman
B.Sc., University of Alberta, 2004

THESIS SUBMITTED IN PARTIAL FULFILLMENT OF THE REQUIREMENTS FOR THE DEGREE OF

MASTER OF SCIENCE

In the
Department
of
Earth Sciences


SIMON FRASER UNIVERSITY
Fall 2006

# APPROVAL

**Name:** **Thomas Lakeman**

**Degree:** **Master of Science**

**Title of Thesis:** **Late-Glacial Alpine Glacier advance and early Holocene Tephras, Northern British Columbia**

**Examining Committee:**

**Chair:** **Dr. Derek Thorkelson**
Professor, Department of Earth Sciences

---

**Dr. John Clague**
Senior Supervisor
Professor, Department of Earth Sciences

---

**Dr. Brent Ward**
Supervisor
Associate Professor, Department of Earth Sciences

---

**Dr. Brian Menounos**
Supervisor
University of British Columbia

---

**Dr. Peter Bobrowsky**
External Examiner
Geological Survey of Canada

**Date Defended/Approved:** November 10, 2006

# ABSTRACT

Two related studies in northern British Columbia are presented. The first documents moraines in Finlay River area that record an advance of alpine glaciers. A minimum age of 9230 radiocarbon yr BP and the relation of moraines to ice-stagnation deposits suggest the advance is Younger Dryas in age. The advance demonstrates Younger Dryas glacier expansion differs in magnitude in western Canada, suggesting a complex glacier response to late-glacial climate change.

The second study describes four early Holocene tephras. Two phonolitic tephras, older than 9180 radiocarbon yr BP, were found in sediments from Finlay River and Dease Lake areas. Their source may be a large volcano in northwest British Columbia. Two other tephras were recovered from Bob Quinn Lake. A lower basaltic tephra was produced by an eruption near Iskut River 8400 radiocarbon yr ago. The upper phonolitic tephra is 6000-7000 radiocarbon yr old.

**Keywords:** Cordilleran Ice Sheet, Younger Dryas, British Columbia, tephras, northern Cordilleran volcanic province.

# ACKNOWLEDGEMENTS

This project was supported by NSERC grants to John Clague and Brian Menounos, and student grants from the Geological Society of America and the Northern Scientific Training Program. I am grateful to John Clague and Brian Menounos for the opportunity to work in northern British Columbia and for their encouragement, support, and mentorship over the past two years. Valuable comments from Brent Ward regarding fieldwork, research articles, and aerial photographs are gratefully acknowledged. Gerald Osborn (University of Calgary) provided samples for microprobe analysis, helpful discussions, and financial support for fieldwork in the Dease Lake area. Duane Froese and Britta Jensen provided laboratory assistance at the University of Alberta and advice on interpreting microprobe data. Ian Spooner (Acadia University) and David Mazzucchi (University of Victoria) provided samples for microprobe analysis. I thank Ben Edwards (Dickinson College) for discussions of Quaternary volcanism in northern British Columbia, Yukon, and Alaska. Rolf Mathewes (Simon Fraser University) provided access to his laboratory.

Denny Capps (Simon Fraser University) assisted in the field. Melanie Grubb assisted with splitting, logging, and sampling cores in the sedimentological laboratory at the University of Northern British Columbia and provided information on late-glacial moraines in the southern Coast Mountains. Kim Menounos and Milo are gratefully acknowledged for hospitable accommodation and exceptional meals during my endless visits to the University of Northern British Columbia. Simon and Darrel provided safe floatplane and helicopter transport, respectively, in the field.

I thank Janice Brahney, Denny Capps, Jesse Dykstra, Michelle Hansen, Greg Hartman, Marit Heideman, Joe Koch, Robin McKillop, John Orwin, Jon Reidel, Dan Shugar, and Kenna Wilkie for their friendship and humour over the past two years. I am very grateful to my family for their continuing support and encouragement. Finally, I would like to thank Chantel Nixon for her love and advice; she continues to amaze and inspire.

# TABLE OF CONTENTS

# LIST OF FIGURES

# LIST OF TABLES

# CHAPTER 1:

## Introduction

Knowledge of Quaternary paleoenvironments provides a framework for testing relations between various components of the Earth system, including the atmosphere, oceans, glaciers, ecosystems, and sedimentary environments. Quaternary paleoenvironmental research in British Columbia has focused mainly on physical environments and ecosystems of the Late Wisconsinan (25,000-10,000 years ago) and the Holocene (10,000 years ago-present). Researchers have used a variety of methods, including geomorphology, stratigraphy, radiocarbon dating, tephrochronology, paleolimnology, microfossil and macrofossil analyses, computer modeling, and geochemical analyses of ice core records to determine former climates, atmospheric and oceanic circulation patterns, sea levels, and ecosystems, among others. Much of the body of paleoenvironmental research in British Columbia has been in the southern third of the province. In contrast northern British Columbia has received little attention. In this thesis, I present and discuss the results of two paleoenvironmental studies in northern British Columbia.

Chapter 2 presents evidence for a late-glacial advance of alpine glaciers in the Finlay River area of northern British Columbia. The advance built large, well preserved, lateral and terminal moraines at the mouths of many high-elevation tributary valleys in the watershed. Deglacial landforms and sediments, which constrain the style, pattern and timing of contemporaneous ice sheet retreat, are mapped and described in detail. Terrestrial plant matter in sediment cores recovered from lakes dammed by late-glacial moraines provides minimum limiting ages for construction of the moraines and for

regional deglaciation. The style of deglaciation in the study area is described and compared to that in other areas of British Columbia. The magnitude and scale of the late-glacial advance are discussed in the context of other advances of the same or similar age in western North America.

Chapter 3 describes and interprets four, previously unrecognized tephras found in lake sediment cores from northern British Columbia. The grain size, colour, thickness, glass shard morphology, phenocryst mineralogy, major element composition, distribution, and age of the tephras are described, and their possible sources are discussed. The tephras, which are early Holocene in age, are phonolitic to basaltic in composition, and are products of eruptions in the northern Cordilleran volcanic province.

Chapter 4 consists of general conclusions from the two studies and suggestions for future work in the region. The final part of the thesis includes four appendices: A – a map of all glacial landforms and deposits in the study area; B – a description of the method used to reconstruct past glacier equilibrium line altitudes and the results of the analysis; C – a summary of all lake core data; and D – a summary of tephra and rock microprobe data.

## CHAPTER 2:

# Late-glacial advance of alpine glaciers in the Finlay River area: Implications for ice sheet retreat and the nature of late-glacial climate change in northern British Columbia


### Abstract

Large, sharp-crested lateral and terminal moraines record a significant late Pleistocene advance of alpine glaciers in the Finlay River area of northern British Columbia. The moraines are regional in extent and character, and appear to record climatic deterioration near the end of the last glaciation. Lateral moraines are bulky and up to 120 m high. Terminal moraines are up to 9 km beyond Little Ice Age deposits and terminate between 1100 and 1200 m above sea level. Several lateral moraines are crosscut by lateral meltwater channels, which record downwasting of trunk valley ice of the northern Cordilleran Ice Sheet. Other lateral moraines merge with ice-stagnation deposits in trunk valleys. These relationships confirm the interaction of advancing alpine glaciers with the regionally decaying Cordilleran Ice Sheet and verify a late-glacial age for the moraines (i.e. younger than 15,000 $^{14}$C yrs BP). Sediment cores were collected from eight lakes dammed by the late-glacial moraines. Two phonolitic tephras occur in basal sediments of several lakes, demonstrating that the moraines are the same age. Radiocarbon dating of plant macrofossils from sediment cores provides a minimum limiting age of 9230 ± 50 $^{14}$C yr BP for abandonment of the moraines. The moraines record a regional alpine glacial advance, here named the Finlay advance, which is probably correlative with the Younger Dryas chronozone (11,000-10,000 $^{14}$C yr BP). The Finlay advance correlates with other advances in western Canada dated to the

Younger Dryas. Moraines of similar size and regional extent have not been identified elsewhere in the Canadian Cordillera. The different response of alpine glaciers in western Canada to Younger Dryas cooling indicates differing rates and magnitudes of late-glacial climate change, different styles of deglaciation, different temperature and precipitation gradients, and variable effects of remnant ice masses on local atmospheric circulation.

**Introduction**

Little is known about the decay of the northern half of the Cordilleran Ice Sheet, which covered an area of nearly 500,000 $km^2$ in northern British Columbia and southern Yukon Territory (Clague, 1989; Jackson et al., 1991; Ryder and Maynard, 1991; Bobrowsky and Rutter, 1992; Clague and James, 2002). The northern part of the ice sheet probably began to decay about 16,000-15,000 $^{14}C$ yr BP, when glaciers with source areas in the northern Coast Mountains retreated from the Queen Charlotte Islands (Blaise et al., 1990). By 13,000 $^{14}C$ yr BP, the ice sheet had retreated from Hecate Strait and its outlet glaciers terminated along the mainland coast and in fiords (Clague, 1985; Barrie and Conway, 1999). Similarly, glaciers in southeast Alaska had retreated from the continental shelf by 13,500 $^{14}C$ yr BP (Mann and Hamilton, 1995). The eastern margin of the ice sheet had withdrawn from the northern Rocky Mountains by 13,500-12,500 $^{14}C$ yr BP, although alpine glaciers persisted in the northern Rocky Mountains after the ice sheet decayed (Bednarski, 1999, 2000, 2001). Deglaciation was probably complete in northern British Columbia before 9500 $^{14}C$ yr BP (Clague, 1981). Other than the broad constraints on deglaciation provided above, the timing and pattern of ice sheet decay are unknown in

northern British Columbia. Importantly, nothing is known about the effects of late-glacial climatic oscillations, such as the Younger Dryas (11,000-10,000 $^{14}$C yrs BP; Alley, 2000), on remnants of the Cordilleran Ice Sheet in British Columbia.

The Younger Dryas, which began 11,000 $^{14}$C yrs ago and lasted about 1300 calendar years, was a severe cold period at the end of the last glaciation (Alley, 2000). Abundant evidence suggests widespread Northern Hemisphere, and possibly global, cooling of the atmosphere and oceans during the Younger Dryas (Mayewski et al., 1993; Peteet, 1995; Mikolajewicz et al., 1997; Steig et al., 1998), with the greatest temperature depressions in the North Atlantic region (Alley, 2000). The cause of Younger Dryas cooling continues to be a matter of debate (Broecker, 2003, 2006), but the favoured hypothesis involves disruption of North Atlantic Deep Water formation by a large influx of meltwater from North America, with attendant reduction in the poleward flux of ocean heat (Broecker et al., 1989; Lehman and Keigwin, 1992; Bjorck et al., 1996; Fanning and Weaver, 1997; Clark et al., 2001, 2002; Teller et al., 2002, 2005; Broecker, 2003, 2006; Tarasov and Peltier, 2005, 2006; Meissner and Clark, 2006; Peltier et al., 2006). Meltwater discharges from the Baltic Ice Lake and the Barents Sea Ice Sheet have also been suggested as a possible triggering mechanism (Bjork et al., 1996).

A change in ocean circulation and cooling of climate in the northeast Pacific Ocean coincident with the Younger Dryas have been documented in north-coastal British Columbia and adjacent Alaska (Engstrom et al., 1990; Mathewes, 1993; Mathewes et al., 1993; Peteet and Mann, 1994; Hu et al., 1995, 2002; Patterson et al., 1995; Hansen and Engstrom, 1996; Hendy et al., 2002; Hetherington and Reid, 2003; Lacourse, 2005). Glacier advances of Younger Dryas age have been identified in the central and southern

Coast Mountains of British Columbia (Clague, 1985; Friele and Clague, 2002a), the southern Canadian and northern American Rocky Mountains (Reasoner et al., 1994; Osborn and Gerloff, 1997), the northern Cascade Range of Washington (Kovanen and Easterbrook, 2001; Riedel et al., 2003), and southwestern Alaska (Briner et al., 2002).

The Younger Dryas, however, was not the only cold interval during the late-glacial period. Advances several hundred years to more than 1000 years earlier than the Younger Dryas have been identified in southwest British Columbia (Armstrong, 1981; Saunders et al., 1987; Clague et al., 1997; Friele and Clague, 2002b) and in the southern Canadian and northern American Rocky Mountains (Osborn and Gerloff, 1997). Their regional climatic significance, however, remains unknown.

The Finlay River area of north-central British Columbia (Fig. 2.1) contains large, sharp-crested lateral and terminal moraines that record a resurgence of alpine glaciers during final decay of the Cordilleran Ice Sheet. The moraines are regional in extent, appear to be of equivalent age, and record significant climatic deterioration during late-glacial time (i.e. younger than 15,000 $^{14}$C yr BP; Clague, 1981). This paper documents and discusses these moraines and related deglacial sediments and landforms. The objectives are to: 1) describe the late-glacial moraines, 2) infer the pattern of deglaciation in the area, 3) present information on the age of the advance that constructed the moraines, 4) discuss the paleoclimatic significance of the moraines, and 5) compare the inferred late-glacial climate of the Finlay River area to that of other areas in the Canadian Cordillera where late-glacial moraines have been identified. The paper considers the relation of late-glacial alpine glacier resurgence in northern British Columbia and late-glacial advances elsewhere in the Canadian Cordillera.

**Study area**

The Finlay River watershed is located in north-central British Columbia, in the rain shadow of the northern Coast Mountains (Fig. 2.1). The study area comprises approximately 3200 $km^2$ of mountainous terrain straddling the northern Omineca and southern Cassiar mountains (Fig. 2.2). The Continental Divide runs through the centre of the study area, separating Pacific from Arctic drainages. Finlay River flows north and then east into the northern Rocky Mountain Trench, which borders the study area to the east. Chukachida River drains the western part of the study area and flows into Stikine River on Spatsizi Plateau west of the map area.

Climate in the study area is continental, with mean annual temperatures ranging from 0° C to –2° C and average annual precipitation ranging from 400 to 500 mm (Environment Canada, 2002). Most moisture is derived from the Pacific Ocean approximately 600 km to the west. White and black spruce (*Picea glauca, Picea mariana*), subalpine fir (*Picea engelmannii*), lodgepole pine (*Pinus contorta*), and aspen (*Populus tremuloides*) dominate vegetation at low elevations in the study area (Meidinger and Pojar, 1991).

The highest peaks exceed 2500 m above sea level (asl), and local relief is up to 1400 m. Small cirque glaciers are restricted to sites above 1800 m asl on the flanks of a few of the highest peaks (Fig. 2.2). The study area was extensively glaciated during the Pleistocene. Cirques, broad U-shaped valleys, and arêtes formed during repeated, lengthy periods of alpine glaciation. The Cordilleran Ice Sheet also covered the area

repeatedly during the Pleistocene, but probably for much shorter intervals than alpine glaciers.

**Methods**

Glacial landforms and deposits were mapped on Province of British Columbia aerial photographs flown in 1986 and 1999. The photographs have nominal scales of 1:60,000 and 1:35,000, respectively. Mapped features were entered into a GIS, and checked during an aircraft-supported field survey in 2005 (Appendix A). Identification of large moraine complexes; meltwater channels; ice-contact deltas, fans, and a landslide; eskers; and glaciolacustrine sediments enabled a detailed reconstruction of latest Pleistocene glacier activity and the regional pattern of deglaciation. Equilibrium line altitudes of former glaciers were estimated to determine their paleoclimatic significance using the accumulation area ratio (AAR) method (Porter, 1975; Appendix B).

Sediment cores were collected from eight lakes impounded by late-glacial moraines to constrain the time of deglaciation. The cores were collected from lake ice in January 2005 and from the floats of a De Havilland DHC-2 Beaver in July 2005, using a percussion coring system (Reasoner, 1993). The cores were transported to the University of Northern British Columbia, where they were split, logged, photographed, analyzed for bulk physical properties (grain size, magnetic susceptibility, and organic content), and sampled for terrestrial macrofossils and tephras. Terrestrial macrofossils extracted from the cores were radiocarbon dated at IsoTrace Laboratory (University of Toronto) and Beta Analytic Inc. by accelerator mass spectrometry. Two tephras were found in most cores. The major element compositions of glass shards, which were isolated from the

tephras using a heavy liquid separation procedure, were determined using the electron microprobe at the Department of Geology and Geophysics, University of Calgary (Chapter 3). The radiocarbon ages and tephras provide constraints on the absolute age of the late-glacial moraines and the time of deglaciation in the study area.

**Early deglaciation in the Finlay River area**

During the Fraser Glaciation, the northern half of the Cordilleran Ice Sheet was fed from accumulation centres located over the northern Coast, the Skeena, and the northernmost Cassiar mountains (Fig. 2.3; Mathews 1980; Ryder and Maynard, 1991; Stumpf et al., 2000; McCuaig and Roberts, 2002). Radial flow from the northern Skeena Mountains directed ice north into the Cassiar Mountains and Liard Plateau, east into the northern Rocky Mountains and foothills, and south into the Omineca Mountains and Nechako Plateau (Mathews, 1980; Ryder and Maynard, 1991; Bobrowsky and Rutter, 1992; Bednarski, 1999, 2000, 2001; Stumpf et al., 2000; McCuaig and Roberts, 2002). The Skeena Mountains also fed glaciers flowing west along major valleys through the northern Coast Mountains (Ryder and Maynard, 1991). Smaller ice divides over the northern Coast Mountains and northernmost Cassiar Mountains directed ice westward onto the continental shelf and north into the Yukon, respectively (Ryder and Maynard, 1991).

The Finlay River area was covered by ice flowing from the northern Skeena Mountains (Fig. 2.3; Mathews, 1980; Ryder and Maynard, 1991). Ice flow through the study area at the last glacial maximum may have been relatively unobstructed by topography. This condition, however, was probably short-lived, and for much of the

Fraser Glaciation, mountain ranges and valleys in the study area controlled the pattern of ice flow. Numerous meltwater channels traversing alpine ridges and valley sides record drawdown of the ice sheet during initial deglaciation. At this time, glaciers continued to flow north and east from the northern Skeena Mountains along major valleys through the study area.

## Late-glacial moraines

*Description*

Large, regionally extensive lateral and terminal moraines provide evidence for an advance of alpine glaciers in the Finlay River area during late-glacial time (Fig. 2.4). The moraines are bulky, sharp-crested, up to 120 m high (Figs. 2.5 and 2.6), and extend up to 9 km beyond Little Ice Age terminal moraines (Fig. 2.7), which, in contrast, are much smaller (Fig. 2.8). Most of the late-glacial terminal moraines terminate between 1100 and 1200 m asl. Two or three nested moraines are present in most areas, indicating multiple episodes of moraine construction. The moraines are distributed uniformly throughout the study area (Fig. 2.4). Morphologically similar moraines occur north and west of the study area in the Cassiar Mountains, but were not investigated in this study.

Lateral moraines are common in valleys below high cirques (Fig. 2.4). Associated terminal moraines are broad, undulating to flat surfaces (Fig. 2.8). More commonly, however, terminal moraines are weakly developed or absent altogether (Fig. 2.5). Some terminal moraines may have been eroded as deglaciation progressed, but this explanation cannot explain their widespread absence in the study area, especially given the presence of nearby, well preserved lateral moraines. Lateral moraines with no

associated terminal moraine commonly merge with ice-stagnation deposits, such as ice-contact alluvial fans, kames, eskers, and kettles that cover trunk valley floors (Fig. 2.9). Some lateral moraines curve at the mouths of tributary valleys, suggesting that tributary and trunk glaciers coalesced (Fig. 2.9). Lateral meltwater channels, formed during downwasting and retreat of trunk glaciers, crosscut many of the lateral moraines (Fig. 2.5).

*Relative age*

Based on the distribution of meltwater channels, I infer that a labyrinth of active (i.e. non-stagnant), but decaying glaciers in trunk valleys in the study area formed the digitate margin of the retreating northern Cordilleran Ice Sheet when the tributary valley moraines were being constructed (Fig. 2.10). Trunk glaciers in the Finlay, Toodoggone, and Chukachida River valleys were sourced in the Skeena Mountains. The large trunk glacier in the Chukachida River valley diverged into several smaller trunk glaciers situated in the Geese Creek, Cushing Creek, and intervening valleys (Fig. 2.10). Abandoned fragments of Cordilleran ice occupied many north-south trending valleys in the study area, such as Belle, Midas, Mulvaney, Junkers, and Jack Lee Creek valleys (Fig. 2.10). Crosscutting lateral meltwater channels (Fig. 2.5) and the spatial association of the moraines with sediments deposited during final wastage of the Cordilleran Ice Sheet (Fig. 2.9) demonstrate that the moraines were built during final deglaciation of northern British Columbia and are thus late Pleistocene in age.

*Late-glacial advance*

There are few exposures in tributary valleys that contain lateral and end moraines, and no stratigraphic evidence was found to unequivocally demonstrate that alpine

glaciers advanced during late-glacial time. However, some alpine glaciers clearly constructed moraines in areas that had previously been deglaciated (Fig. 2.8), which is strong evidence for an advance of alpine glaciers during or after retreat of the ice sheet. Elsewhere, alpine glaciers constructed lateral moraines abutting active but decaying ice in trunk valleys (Figs. 2.5 and 2.9). The moraines record a discrete advance and not a stillstand during separation of tributary alpine glaciers from trunk glaciers, because the size and character of the moraines can only be explained by abundant remobilization of late-glacial sediments (e.g. the Red Barrel moraines; Fig. 2.8). Equilibrium line altitudes calculated for alpine glaciers that did not coalesce with remnant Cordilleran ice in trunk valleys, at the time of moraine construction, suggest that snowline was 1650-1750 m asl compared to approximately 1900-1950 m asl during the Little Ice Age (Appendix B). No stratigraphic or geomorphic evidence was found for a late-glacial resurgence or thickening of remnant tongues of the northern Cordilleran Ice Sheet in trunk valleys.

**Deglaciation following the late-glacial advance**

*Deglacial landforms and sediments*

Trunk glaciers in the Toodoggone and Finlay River valleys were up to 200-300 m thick and thinned eastward and northward, respectively, at the time of the late-glacial advance. Ice thicknesses were estimated from the elevations of lateral meltwater channels crosscutting late-glacial moraines and from the elevations of terminal moraines that were constructed against trunk ice by resurgent tributary glaciers. Hummocky terrain and large meltwater channels in the Finlay River valley adjacent to the Rocky Mountain Trench and large kettles and eskers farther up-valley record final wastage of

the Finlay trunk glacier following the late-glacial advance. The terminus of the Finlay trunk glacier was likely a narrow lobe of thin stagnant ice that reached into the northern Rocky Mountain Trench at the time of the late-glacial advance (Fig. 2.10). Two tributary glaciers deposited kame terraces against the decaying trunk glacier in the Finlay River valley (Fig. 2.9). These kame terraces suggest that the Finlay trunk glacier was 60-80 m thick at the time the tributary glaciers abandoned their moraines. Following the advance, large eskers and numerous kettles formed in the Finlay and Toodoggone River valleys. In addition, abundant subglacial meltwater channels were cut into the valley sides along Toodoggone River.

Elevations of lateral meltwater channels crosscutting moraines show that the trunk glacier in Geese Creek valley was up to 200 m thick at the time of the late-glacial advance. Resurgent alpine glaciers constructed lateral moraines, but terminal moraines are absent and were probably not built because active ice occupied the adjacent trunk valley (Fig. 2.5). The Geese Creek trunk glacier thinned to the east where it overtopped a low pass and terminated against resurgent alpine glaciers in the northwest tributary of Thudaka Creek (Fig. 2.5). Shortly after the advance, several eskers and ice-contact alluvial fans were deposited in Geese Creek valley below lateral moraines lying in adjacent cirques and tributary valleys (Fig. 2.5).

The trunk glacier in Cushing Creek valley was up to 200 m thick at the time of the late-glacial advance. It thinned eastward and terminated near Thudaka Creek (Fig. 2.10). As the trunk glacier retreated, a large rock avalanche fell from the north flank of Mount Cushing onto the glacier terminus (Fig. 2.11). The glacier diverted the blocky debris downvalley, preventing it from being deposited where trunk ice remained. Exotic,

rounded, granite cobbles and boulders are present in the rock avalanche debris and were deposited by the trunk glacier where it abutted the rock avalanche (Fig. 2.11). Farther west in the valley, numerous eskers were deposited during final wastage of the trunk glacier.

Advancing alpine glaciers constructed moraines against abandoned fragments of the Cordilleran Ice Sheet in many north-trending valleys in the study area, including Belle, Midas, Mulvaney, Junkers, and Jack Lee Creek valleys (Fig. 2.10). Lateral meltwater channels crosscutting the late-glacial moraines indicate that trunk glaciers in these valleys were up to 250 m thick during the late-glacial advance. Late-glacial terminal moraines built by alpine glaciers are well preserved on trunk valley floors. Lateral and subglacial meltwater channels abut several ice-contact deltas that prograded into lakes dammed by abandoned Cordilleran ice in north-trending valleys and by trunk glaciers in the Toodoggone and Chukachida River valleys. Meltwater from retreating alpine glaciers and stagnating Cordilleran ice deposited large ice-contact alluvial fans in the Chukachida River valley (Fig. 2.12).

Alpine glaciers occupied most of Thudaka Creek valley and its tributaries during the late-glacial advance (Fig. 2.10). A large lobe of the Cordilleran Ice Sheet did, however, cover a section of Thudaka Creek valley north of Red Barrel Lake where three tributary valleys converge (Fig. 2.8). The western margin of the Cordilleran lobe coalesced with an eastward-flowing Cordilleran trunk glacier in an adjacent valley at the time of the late-glacial advance (Fig. 2.10). Kame terraces and meltwater channels mark the eastern limit of the Cordilleran lobe, and demonstrate that it terminated just up-valley of the moraine that impounds Red Barrel Lake (Fig. 2.8). The Red Barrel moraines have

no crosscutting features recording interaction between the alpine glacier and the adjacent Cordilleran lobe. During final deglaciation, the Cordilleran lobe impounded a small glacial lake in the westernmost tributary of Thudaka Creek (Fig. 2.8). It also may have temporarily dammed two other tributaries, but meltwater probably flowed freely under or around the thin glacier terminus during most of the late-glacial advance (Fig. 2.8). Following the advance, alpine glaciers abandoned their moraines and the Cordilleran lobe stagnated.

*Pattern and style of ice retreat*

Landforms and sediments in the study area suggest that the northern Cordilleran Ice Sheet thinned early during deglaciation but retained an active network of trunk glaciers at its periphery prior to the late-glacial advance (Fig. 2.10). However, some trunk valleys in the study area, such as lower Thudaka Creek valley, had become ice-free prior to the advance (Fig. 2.8). The thickness and geometry of glaciers in trunk valleys at the time of the late-glacial advance can be reconstructed from abundant, well preserved, lateral meltwater channels that crosscut many late-glacial moraines (e.g. Geese Creek valley; Fig. 2.5). The lateral meltwater channels indicate that trunk glaciers thinned and retreated rapidly following the late-glacial advance. Eskers and deeply incised, subglacial meltwater channels in many of the major valleys record stagnation and final wastage of trunk glaciers. Alpine glaciers abandoned their moraines and retreated back into cirques following the advance. Some alpine glaciers constructed small moraines during retreat, but recessional moraines are uncommon.

**Age of the moraines**

Two black phonolitic tephras occur near the contact between inorganic and overlying organic-rich sediments in sediment cores collected from Katharine, Red Barrel, and Cushing lakes (Fig. 2.13). Red Barrel and Cushing lakes are impounded behind late-glacial terminal and lateral moraines, respectively (Figs. 2.6 and 2.8), whereas Katharine Lake lies on the distal side of a late-glacial terminal moraine (Fig. 2.4). The tephras comprise fine sand to silt-sized mineral grains and glass shards. They are coarser than the bounding sediments and lie within 2-4 cm of one another in the cores (Fig. 2.13). A radiocarbon age of 8960 ± 80 $^{14}$C yr BP was obtained on a piece of wood 2 cm above the upper tephra in a core from Red Barrel Lake (Fig. 2.13; Table 2.1). Unidentified plant material 1 cm above the upper tephra in Cushing Lake returned an age of 9180 ± 80 $^{14}$C yr BP (Fig. 2.13; Table 2.1).

A sediment core from Deep Lake contains one phonolitic tephra near its base. This lake is located in a cirque that supported the glacier that constructed the terminal moraine impounding Red Barrel Lake (Fig. 2.8). A core from Black Lake, which is dammed by a late-glacial alluvial fan, also contains a single basal phonolitic tephra. The occurrence of phonolitic tephras in basal sediments from five lakes in the study area indicates that deglaciation was complete by no later than 9180 ± 80 $^{14}$C yr BP. This age is also a minimum for construction and abandonment of the late-glacial moraines.

Another minimum date for deglaciation is a radiocarbon age of 9230 ± 50 $^{14}$C yr BP, obtained from basal sediments in a core from Sandwich Lake (Fig. 2.13; Table 2.1). Sandwich Lake lies within a lateral meltwater channel at the same elevation as adjacent

meltwater channels that crosscut late-glacial lateral moraines. The radiocarbon age is thus a minimum limiting age for abandonment of the moraines.

Data from the Rocky Mountains to the east provide a maximum age constraint on the late-glacial advance in the Finlay River watershed. Bednarski (1999, 2000, 2001) obtained three surface exposure cosmogenic ages on striated rock surfaces high in the northern Rocky Mountains. He concluded from the three ages that the northern Cordilleran Ice Sheet withdrew from the northern Rocky Mountains before 14,000-13,000 cal yr BP, which corresponds to approximately 13,500-12,500 $^{14}$C yr BP. Ice cover in the Finlay River area at that time must have been greater than during the late-glacial advance, because the exposure ages were obtained on high ridges that had been covered by ice flowing east from the Skeena ice divide 200-300 km to the west and 150 km west of the Finlay River area (Fig. 2.3; Mathews, 1980; Ryder and Maynard, 1991). Thus, the Finlay advance happened after the Cordilleran Ice Sheet withdrew from the northern Rocky Mountains, sometime after 13,000 $^{14}$C yrs BP.

## Discussion

### *Pattern and style of deglaciation*

The Finlay advance occurred when valley glaciers were present at intermediate and high elevations in the northern Omineca and southern Cassiar mountains. At the same time, remnant tongues of decaying Cordilleran ice flowing from the northern Skeena Mountains occupied many trunk valleys in the study area (Fig. 2.10). The advance occurred at a time of deglaciation that Fulton (1967, 1991) termed the *transitional upland phase*, when downwasting of the ice sheet uncovered upland areas,

but regional ice flow continued in valleys. In the Finlay River area, drawdown rapidly transformed the ice sheet into a labyrinth of rapidly ablating valley glaciers. Under this scenario, the regional equilibrium line was sufficiently low that alpine glaciers could persist at intermediate to high elevations. These alpine glaciers later advanced and constructed large moraines when equilibrium line fell to 1650-1750 m asl. It is possible that alpine glaciers completely disappeared prior to the late-glacial advance, but this scenario seems unlikely given the size of the moraines and the glaciers that constructed them. Following the advance, a large and rapid rise in equilibrium line forced alpine glaciers to retreat and trunk glaciers to stagnate as the latter became detached from their source areas in the northern Skeena Mountains. By approximately 9500 $^{14}$C yrs BP, glaciers in northern British Columbia were likely no more extensive than today (Clague, 1981).

The pattern of deglaciation in the Finlay River area, excluding final stagnation of trunk glaciers, appears to differ from that documented in southern British Columbia by Fulton (1967, 1991). Fulton concluded that upland areas in southern British Columbia appeared through the ice sheet first due to downwasting and complex frontal retreat. Cirques at intermediate and, locally, high elevations on the southern Interior Plateau were deglaciated during late-glacial time. In contrast, ice persisted in high mountain valleys in the northern Skeena, Omineca, and Cassiar mountains while the ice sheet downwasted. The alpine physiography of the study area and its proximity to major ice accumulation areas in the northern Skeena Mountains are probably the reasons alpine glaciers persisted at intermediate to high elevations during late-glacial time. Temperature and precipitation regimes favourable for glacier growth or persistence during rapid latest Pleistocene

climatic amelioration may also partly account for widespread persistence of alpine glaciers in northern British Columbia.

*Finlay advance*

The size and regional extent of the Finlay moraines imply that regional climatic deterioration was important in triggering the late-glacial advance in the study area. Apart from Crowfoot moraines in the Canadian Rocky Mountains (Reasoner et al., 1994), no other large concentration of late-glacial moraines has been identified in the Canadian Cordillera.

A drop in equilibrium line altitude in the Finlay River area to 1650-1750 m asl allowed alpine glaciers to advance and construct lateral and terminal moraines in high tributary valleys and in areas where trunk glaciers were stagnant or absent (Figs. 2.8 and 2.9). Trunk glaciers did not subsequently override and remove late-glacial moraines because the trunk glaciers were lower than both the equilibrium line altitude and the adjacent moraines. The complex geometry of the trunk glacier network and the distance of these glaciers from major source areas in the northern Skeena Mountains likely attenuated the effects of positive mass balance that would have otherwise led to their thickening and advance. Ice in the northern Skeena Mountains may have thinned so much earlier during deglaciation that accumulation centres were unable to nourish their distal, complex, valley glacier network when alpine glaciers advanced in the Finlay River area.

The large size of the lateral moraines requires explanation, given that the length of time available for their construction is no more than 1000 years, assuming, as seems likely, that the Finlay advance occurred during the Younger Dryas chronozone, 11,000-

10,000 $^{14}$C yr BP. The size of the lateral moraines is perhaps a result of the large amount of sediment available to the glaciers at the time of the advance. As mentioned above, alpine glaciers at intermediate and high elevations survived initial downwasting and retreat of the Cordilleran Ice Sheet with attendant transport and deposition of large amounts of supraglacial and subglacial debris. In particular, rockfall and landslides from freshly deglaciated cirque headwalls probably contributed large amounts of debris, which was transported down-glacier and deposited in the moraines.

*Correlative landforms and deposits*

Younger Dryas glacier advances have been identified at many sites in western North America, including the central and southern Coast Mountains of British Columbia (Clague, 1985; Friele and Clague, 2002a, 2002b), the southern Canadian Rocky Mountains (Reasoner et al., 1994), southwestern Alaska (Briner et al., 2002), the northern Cascade Range (Kovanen and Easterbrook, 2001; Riedel et al., 2003), and other areas in the western United States (Gosse et al., 1995; Menounos and Reasoner, 1997; Owen et al., 2003; Licciardi et al., 2004). Friele and Clague (2002a, 2002b) documented a Younger Dryas advance of the glacier that occupied the Squamish River valley in the southern Coast Mountains, 50 km north of Vancouver, British Columbia. Some valley glaciers on the west side of the Coast Mountains reached fiord heads at this time (Clague, 1985; Friele and Clague, 2002a). East of the crest of the southernmost Coast Mountains, glaciers were restricted to cirques and high valleys with accumulation areas above about 2000 m asl (Souch, 1989; Friele and Clague, 2002a). Clague (1985) reported a Younger Dryas advance of a tidewater glacier in the central Coast Mountains near Terrace, British Columbia, however, its climatic significance is uncertain. Crowfoot moraines record

small Younger Dryas glacier advances in the Canadian Rocky Mountains (Reasoner et al., 1994). They commonly lie immediately outside Little Ice Age moraines or have been incorporated into them, thus Crowfoot glaciers were comparable in extent to those of the Little Ice Age (Reasoner et al., 1994; Osborn and Gerloff, 1997; Osborn et al., 2001). The small size of Crowfoot glaciers suggests that they had decayed significantly from their maximum Late Wisconsinan limits and, in some cases, may have formed in cirques that had been completely deglaciated prior to the onset of the Younger Dryas (Reasoner et al., 1994; Osborn and Gerloff, 1997; Osborn et al., 2001). Briner et al. (2002) suggested that the late-glacial Mount Waskey advance in the Ahklun Mountains of southwestern Alaska might be Younger Dryas in age, based on cosmogenic surface exposure ages of boulders on moraines. During this advance, resurgent valley glaciers constructed large terminal and lateral moraines several kilometres downvalley of modern glacier termini. The Mount Waskey moraines are about 80 km inside the maximum limit of Late Wisconsinan glaciation in the region, indicating that the advance occurred after substantial deglaciation during late-glacial time.

Late-glacial advances prior to the Younger Dryas have been documented at several localities in the Canadian Cordillera. Clague et al. (1997) presented evidence for two late-glacial advances of a lobe of the Cordilleran Ice Sheet in southwest British Columbia, both of which occurred before the onset of the Younger Dryas. Saunders et al. (1987) reported contemporaneous advances in the Chilliwack River valley, southwest British Columbia. A correlative advance or stillstand of the trunk glacier in Squamish River valley is marked by an end moraine at Porteau Cove, 15 km south of Squamish (Friele and Clague, 2002b).

Other undated late-glacial moraines and deposits have been documented elsewhere in the North American Cordillera. Some moraines in the Canadian and American Rocky Mountains pre-date the Crowfoot advance and record local stillstands or advances during the late-glacial interval (Reasoner et al., 1994; Osborn and Gerloff, 1997). Undated moraines have been reported from at least four sites in northern British Columbia: the Tuya-Teslin area (Watson and Mathews, 1944), Level Mountain (Hamilton, 1981), the Atlin area (Tallman, 1975), and the Omineca Mountains (Roots, 1954). Late-glacial advances and stillstands of the northern Cordilleran Ice Sheet have been reported from several valleys of southern Yukon Territory (Hughes, 1990; Jackson et al., 1991; Bond, 2004; Kennedy and Bond, 2004; Bond and Kennedy, 2005).

Late-glacial moraines in the Cassiar Mountains near Dease Lake are similar in size and character to the Finlay moraines (T. Lakeman, unpublished data). Many of the valley glaciers that constructed the moraines coalesced with trunk glaciers that were part of the northern Cordilleran Ice Sheet. Sediment cores recovered from lakes inside the moraines in the Dease Lake area contain the same phonolitic tephras as lake cores from the Finlay River area (Chapter 3). The presence of the same tephras in the two areas some 250 km apart suggests that the moraine complexes are correlative and are the product of the same late-glacial climate event.

*Late-glacial climate of northern British Columbia*

Paleoecological data from north-coastal British Columbia record regional climate change during deglaciation. The most pronounced and consistent change in the records is the Younger Dryas climate deterioration (Engstrom et al., 1990; Mathewes, 1993; Mathewes et al., 1993; Hetherington and Reid, 2003; Lacourse, 2005). Mathewes (1993)

and Mathewes et al. (1993) documented a late-glacial shift from closed forest to open, herb-rich parkland at two sites near Cape Ball, Graham Island; the parkland persisted from about 10,700 to 10,000 $^{14}$C yr BP. Lacourse (2005) presented similar evidence for Younger Dryas climatic cooling from northern Vancouver Island. Mathewes et al. (1993) showed that waters on the central British Columbia continental shelf were cooler from 11,100 to 10,200 $^{14}$C yr BP than either earlier or later, based on abundances of the cold-water benthic foraminifera, *Cassidulina reniforme*, in several marine sediment cores. Similarly, Hecate Strait was cooler from 10,900 to 10,300 $^{14}$C yr BP than at times immediately earlier or later, based on the absence of most bivalves, except species tolerant of low sea surface temperatures (Hetherington and Reid, 2003). Engstrom et al. (1990) reported that pine parkland on Pleasant Island, southeastern Alaska, was replaced by shrub- and herb-dominated tundra about 10,800 $^{14}$C yr BP; tundra persisted in the area to about 9800 $^{14}$C yr BP.

These studies document a return to cool and wet conditions in northern British Columbia and southeast Alaska during the Younger Dryas. The records show no evidence of a comparable late-glacial climate oscillation either before or after the Younger Dryas. Thus, the Younger Dryas was likely the most significant event of its kind in northern British Columbia during the late glacial period.

*Regional synthesis*

Consideration of available paleoecological data from northern British Columbia and southeast Alaska indicates that the Finlay moraines record a regional advance of alpine glaciers during the Younger Dryas chronozone. Differences in the magnitude of

the advances in the Finlay River area and elsewhere in the Canadian Cordillera point to variable responses of glaciers to climate change during terminal Pleistocene deglaciation.

The Finlay moraines indicate that the timing and pattern of ice sheet retreat were important in determining glacier extents at the onset of late-glacial climate deterioration. Different styles and rates of deglaciation were probably primary mechanisms causing varied glacier responses to late-glacial climate change. Generally larger advances in coastal and northern alpine areas near former accumulation centres or ice divides where extensive ice persisted early during deglaciation (e.g. the Squamish and Finlay advances) support this assertion. Near-complete deglaciation of the southern Canadian Rocky Mountains by Younger Dryas time and perhaps relatively less precipitation may explain the comparatively smaller Crowfoot advances. Different temperature and precipitation gradients and the variable effects of remnant, large ice masses on local atmospheric circulation may have also contributed to the complexity in glacier fluctuations during deglaciation in western North America.

**Conclusions**

Glaciers flowing from the northern Skeena Mountains covered the Finlay River area of northern British Columbia at the climax of the Fraser Glaciation. Large alpine glaciers persisted at intermediate and high elevations early during deglaciation as the Cordilleran Ice Sheet decayed by downwasting and frontal retreat.

Large terminal and lateral moraines were constructed in tributary valleys in the Finlay River area during a regional late-glacial advance of alpine glaciers following early deglaciation. The advance occurred when regional equilibrium line altitudes fell to 1650-

1750 m asl and it coincided with final decay of a network of remnant, thin tongues of the northern Cordilleran Ice Sheet in trunk valleys. Trunk glaciers were below both resurgent alpine glaciers and the lowered regional equilibrium line altitude that allowed alpine glaciers to advance. The late-glacial moraines are well preserved and clearly record interaction between alpine glaciers and decaying trunk glaciers. The large size of the moraines is probably due the abundance of sediment available for transport during deglaciation.

Two phonolitic tephras slightly older than 9180 ± 80 $^{14}$C yr BP occur in the study area and closely delimit the time of abandonment of the late-glacial moraines. A radiocarbon age of 9230 ± 50 $^{14}$C yr BP from a meltwater channel cut during retreat of trunk glaciers from the area confirms a late-glacial age for the moraines. The advance likely occurred after the Cordilleran Ice Sheet had withdrawn from the northern Rocky Mountains ca. 13,000 $^{14}$C yr BP.

The widespread distribution of the Finlay moraines points to regional climatic deterioration as a likely trigger for the late-glacial advance of alpine glaciers. Paleoecological records from northern British Columbia indicate that the most severe cold interval during late-glacial time coincided with the Younger Dryas chronozone. Therefore, it is likely that the late-glacial moraines in the Finlay River area record a regional advance of alpine glaciers during that time.

Younger Dryas and older glacier advances in the southern Coast Mountains of British Columbia, the southern Canadian Rocky Mountains, southwestern Alaska, the northern Cascade Range, and other areas in the western United States differ in size, suggesting variable glacier responses to late-glacial climate change. The different

responses probably reflect different styles of deglaciation, different temperature and precipitation gradients, differing rates and magnitudes of late-glacial climate change, and variable effects of remnant ice masses on local atmospheric circulation. The stochastic nature of rapid changes in the atmosphere and oceans at the end of the last glaciation probably accounts for the sporadic occurrence and variable scale of Younger Dryas glacier advances in western North America.

Table 2.1. Radiocarbon ages from the Finlay River area.

| Location (latitude, longitude) | $^{14}$C age[1] (years BP) | Calibrated age range[2] (years BP) | Laboratory number[3] | Dated material | Depth in core (cm) |
|---|---|---|---|---|---|
| Red Barrel Lake (57°40.623′ N, 126°44.029′ W) | 3930 ± 80 | 4100-4580 | TO-12469 | Conifer needle | 60.5 |
| | 3920 ± 60 | 4160-4520 | TO-12470 | Twig | 82.5 |
| | 5240 ± 70 | 5890-6210 | TO-12471 | Spruce terminal bud | 98.5 |
| | 7250 ± 70 | 7950-8190 | TO-12472 | Twig | 115.0 |
| | 8270 ± 90 | 9030-9460 | TO-12473 | Conifer needle | 121.5 |
| | 8960 ± 80 | 9780-10,250 | TO-12474 | Wood | 139.5 |
| Cushing Lake (57°35.607′ N, 126°54.450′ W) | 9180 ± 80 | 10,220-10,560 | TO-12475 | Terrestrial plant matter | 77.5 |
| Bronlund Lake (57°25.463′ N, 126°35.460′ W) | 8270 ± 50 | 9090-9430 | Beta-202608 | Conifer needles | 89.5 |
| Sandwich Lake (57°01.565′ N, 126°29.747′ W) | 9230 ± 50 | 10,250-10,550 | Beta-202609 | Wood | 93.5 |

[1] Laboratory-reported errors are 1-sigma.
[2] Calibrated ages determined using the program OxCal v4.0 Beta, which uses the IntCal04 calibration curve (Reimer et al., 2004). The range represents the 95% confidence interval (± 2 sigma).
[3] Beta - Beta Analytic Inc.; TO - IsoTrace Laboratory (University of Toronto).

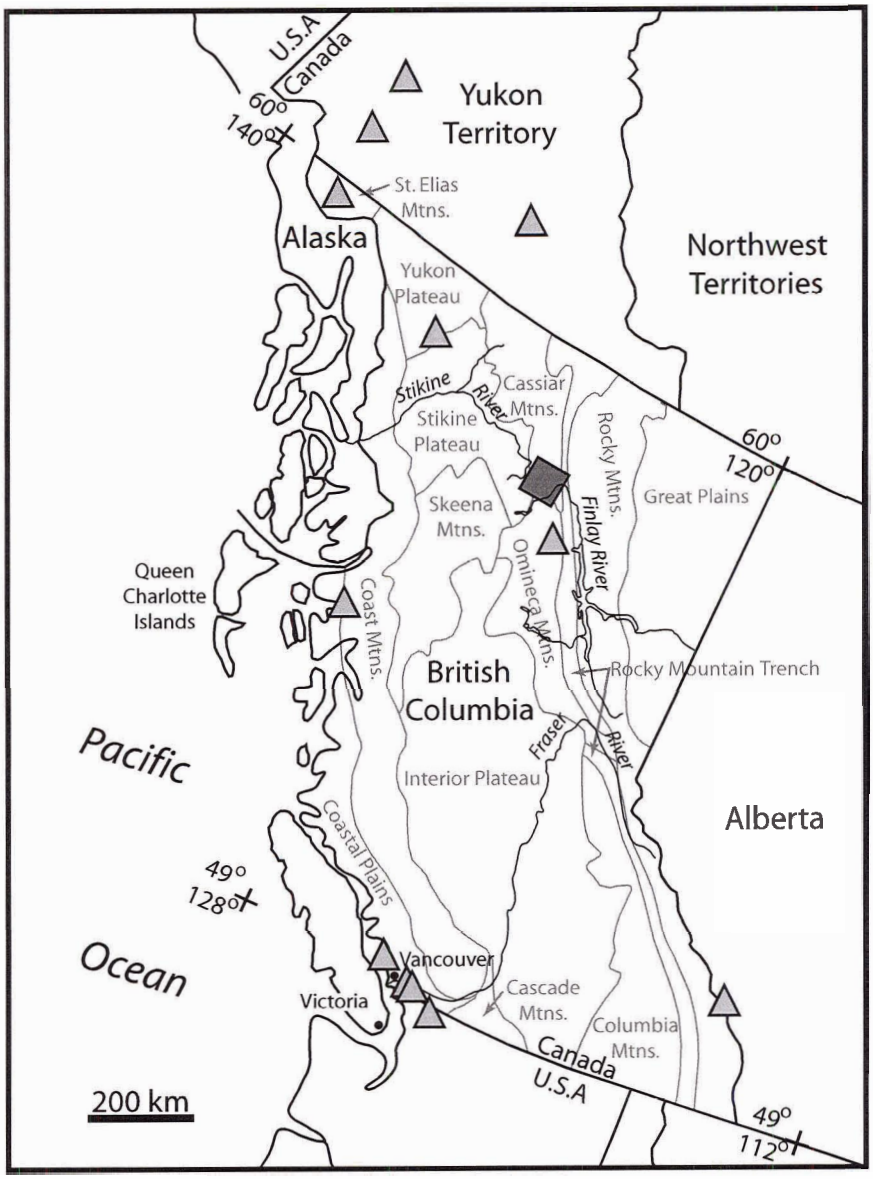


Figure 2.1. British Columbia showing its major physiographic regions (based on Mathews, 1986). Grey box indicates study area. Triangles mark sites where late-glacial glacier advances have been identified.

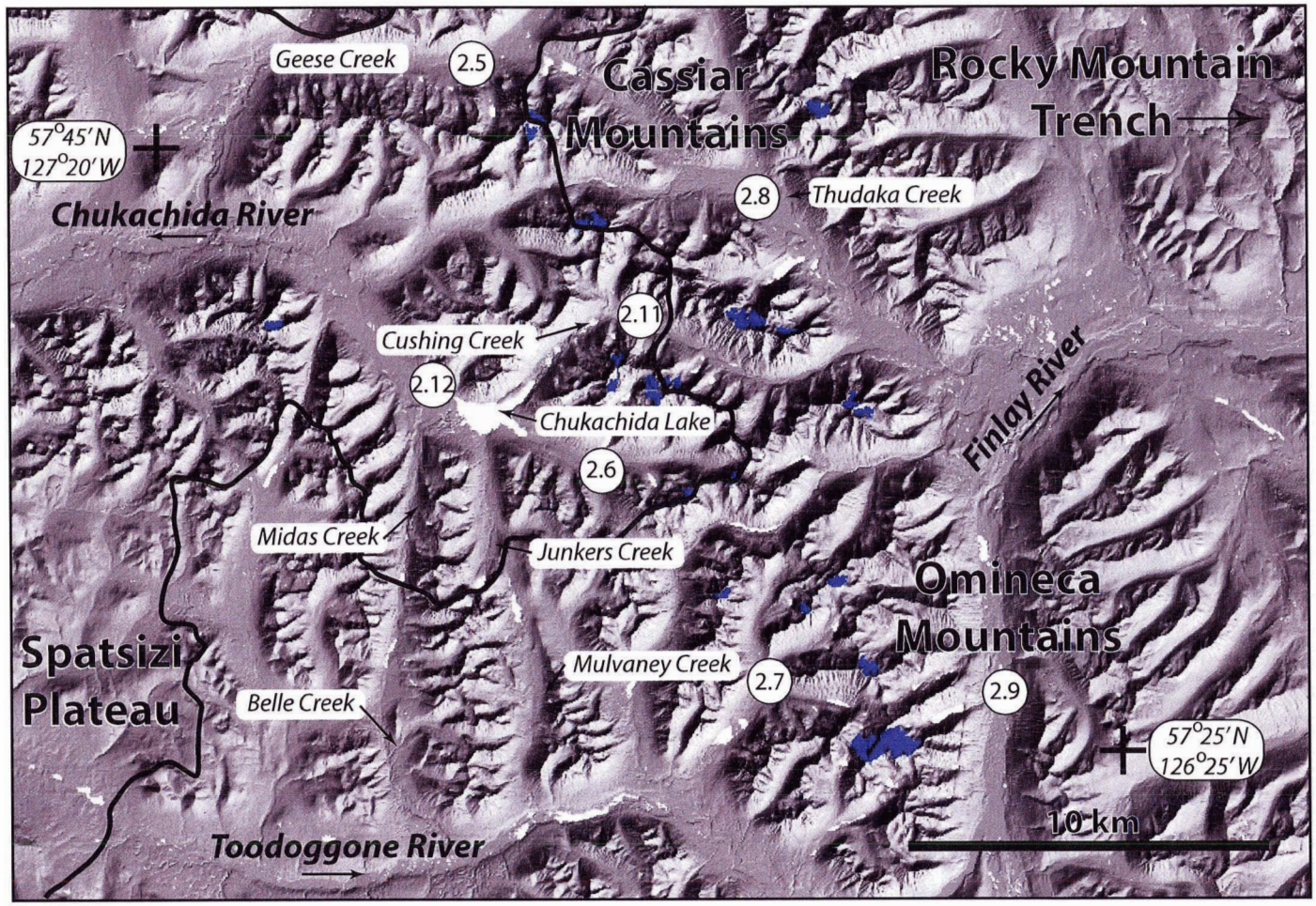


Figure 2.2. Hillshaded digital elevation model of the study area. Numbers indicate figure locations. Bold line delineates watershed divide between Pacific and Arctic drainages. Present-day glaciers are shown in blue. Hillshade map was produced with permission using digital elevation data from the Province of British Columbia, Base Mapping and Geomatic Services Branch.

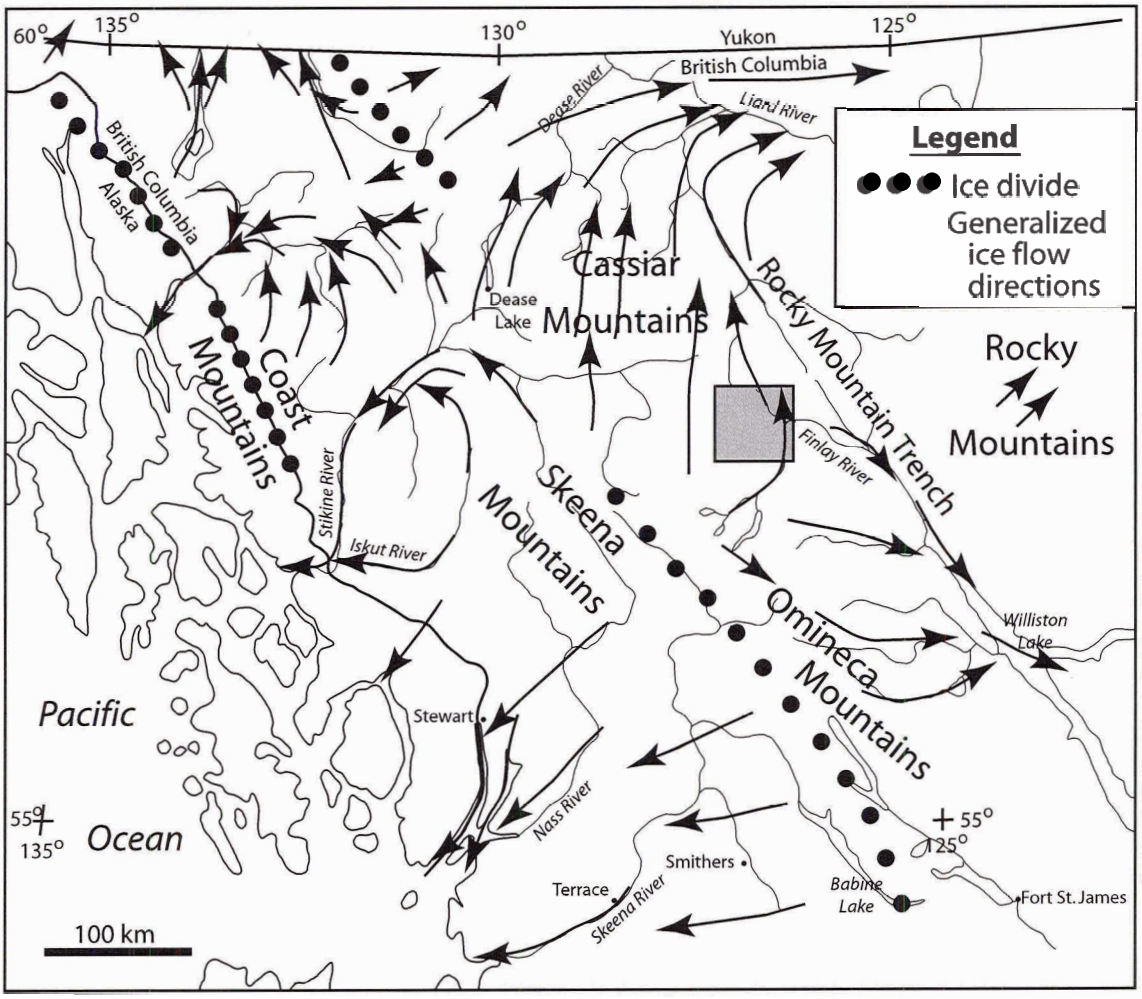


Figure 2.3. Generalized ice flow directions in northern British Columbia at the maximum of the Fraser Glaciation. Grey box indicates study area. Modified with permission from Ryder and Maynard (1991), with data from Bednarski (1999), Stumpf et al. (2000), and McCuaig and Roberts (2002).

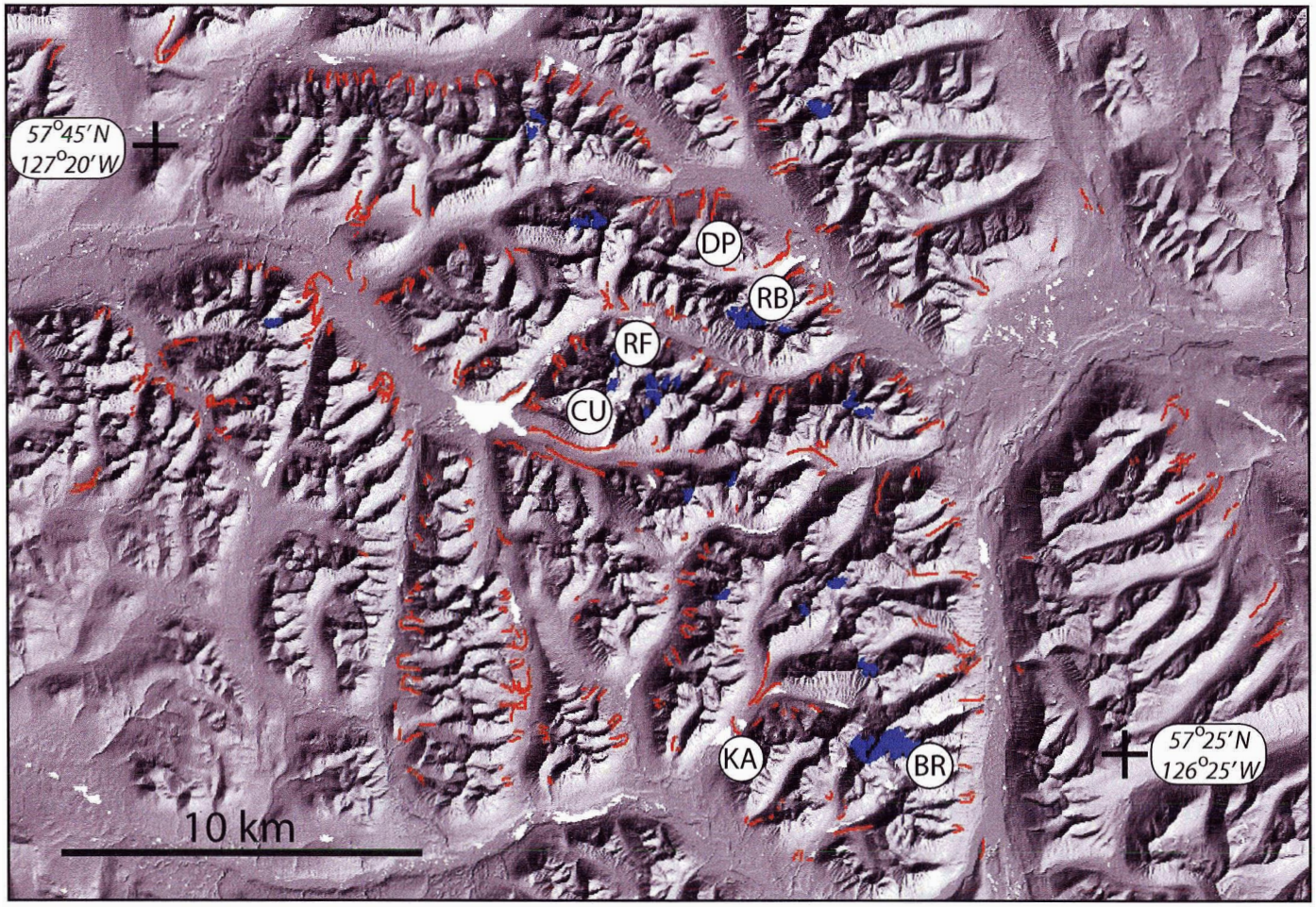


Figure 2.4. Distribution of late-glacial moraines (orange) in the study area and location of cored lakes: Deep Lake (DP), Red Barrel Lake (RB), Rock Fall Lake (RF), Cushing Lake (CU), Katharine Lake (KA), and Bronlund Lake (BR). Present-day glaciers are shown in blue. Hillshade map was produced with permission using digital elevation data from the Province of British Columbia, Base Mapping and Geomatic Services Branch.

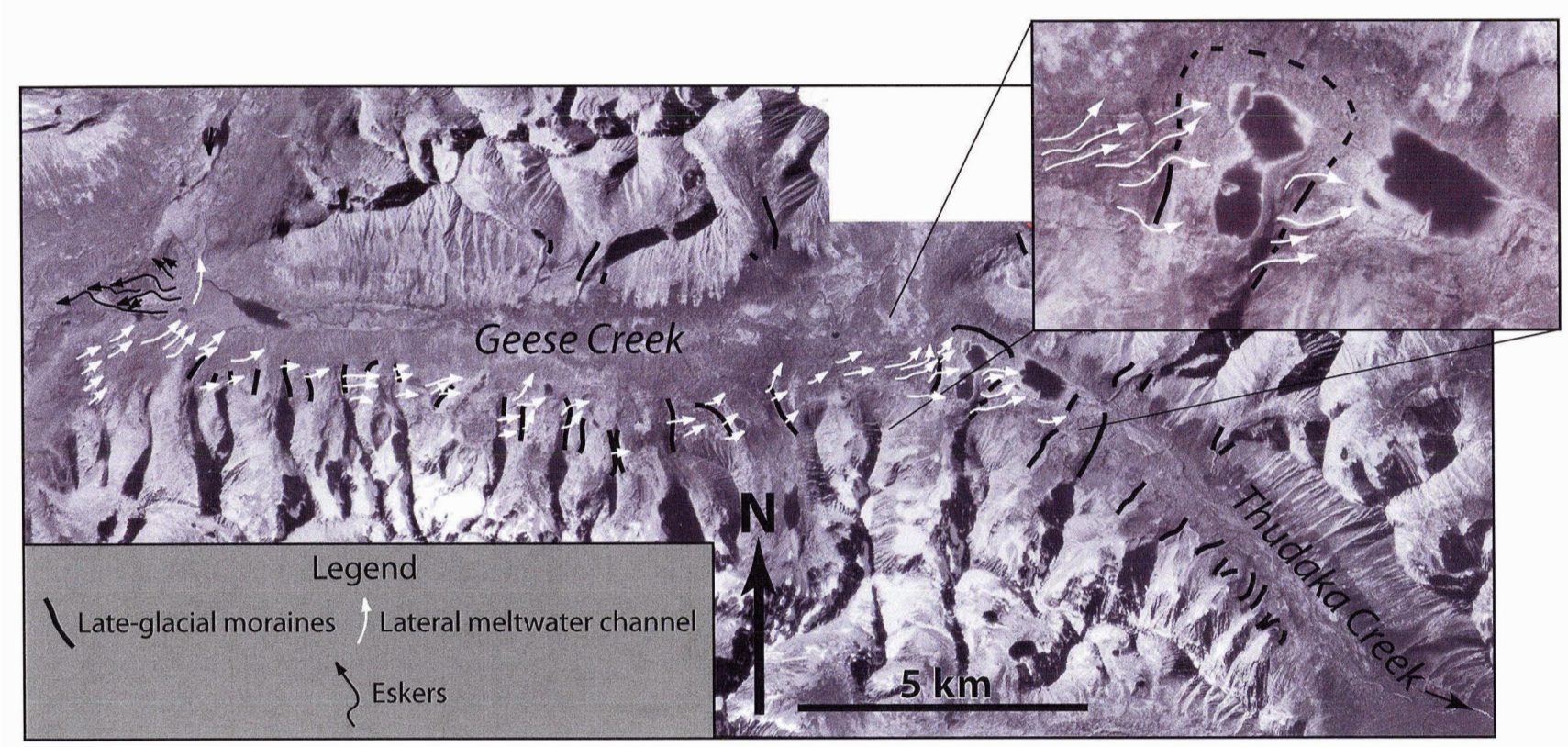


Figure 2.5. Aerial photograph mosaic of late-glacial landforms in Geese Creek valley. Ice-marginal meltwater channels demarcate the margin of a trunk glacier. The channels crosscut lateral moraines constructed by resurgent alpine glaciers. Inset shows the approximate terminus of the trunk glacier in Geese Creek valley when it was in contact with resurgent alpine glaciers; note deep lateral meltwater channels cut into lateral moraines. Aerial photographs 15BC86082-002, 003, and 004; reproduced with permission of British Columbia Ministry of Agriculture and Lands, Base Mapping and Geomatic Services Branch.

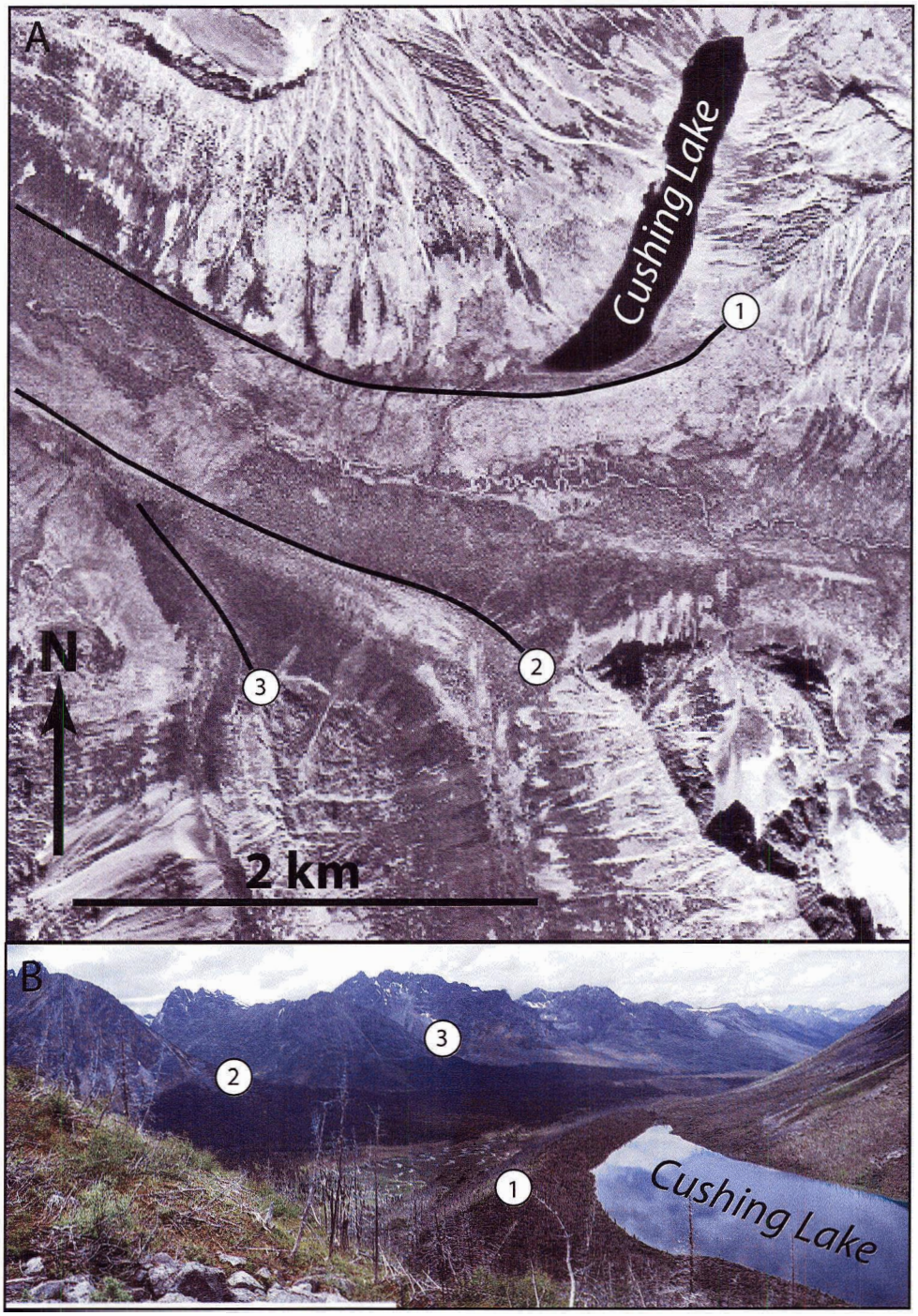


Figure 2.6. A) Aerial photograph of Cushing Lake, which is dammed by a late-glacial lateral moraine, labeled 1. B) Photograph of late-glacial lateral and medial moraines looking west downvalley towards Chukachida Lake (Fig. 2.2). Moraines 2 and 3 are labeled on both photgraphs. Aerial photgraph 15BCB99017-131; reproduced with permission of British Columbia Ministry of Agriculture and Lands, Base Mapping and Geomatic Services Branch.

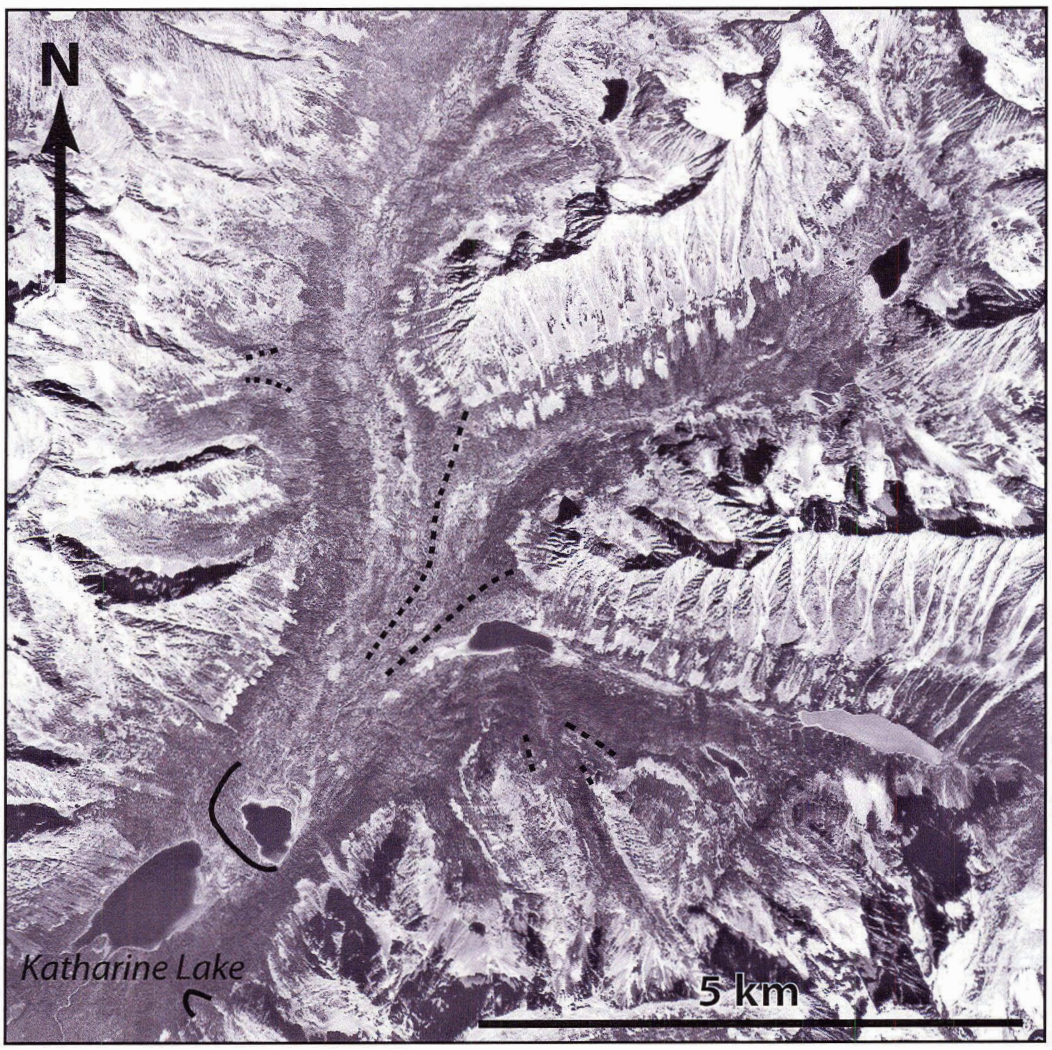


Figure 2.7. Aerial photograph of Katharine Lake, which lies on the distal side of a late-glacial terminal moraine (solid black line) 9 km downvalley from the source cirque. Several recessional lateral and medial moraines are marked by dashed black lines. Aerial photograph 15BCB99016-134; reproduced with permission of British Columbia Ministry of Agriculture and Lands, Base Mapping and Geomatic Services Branch.

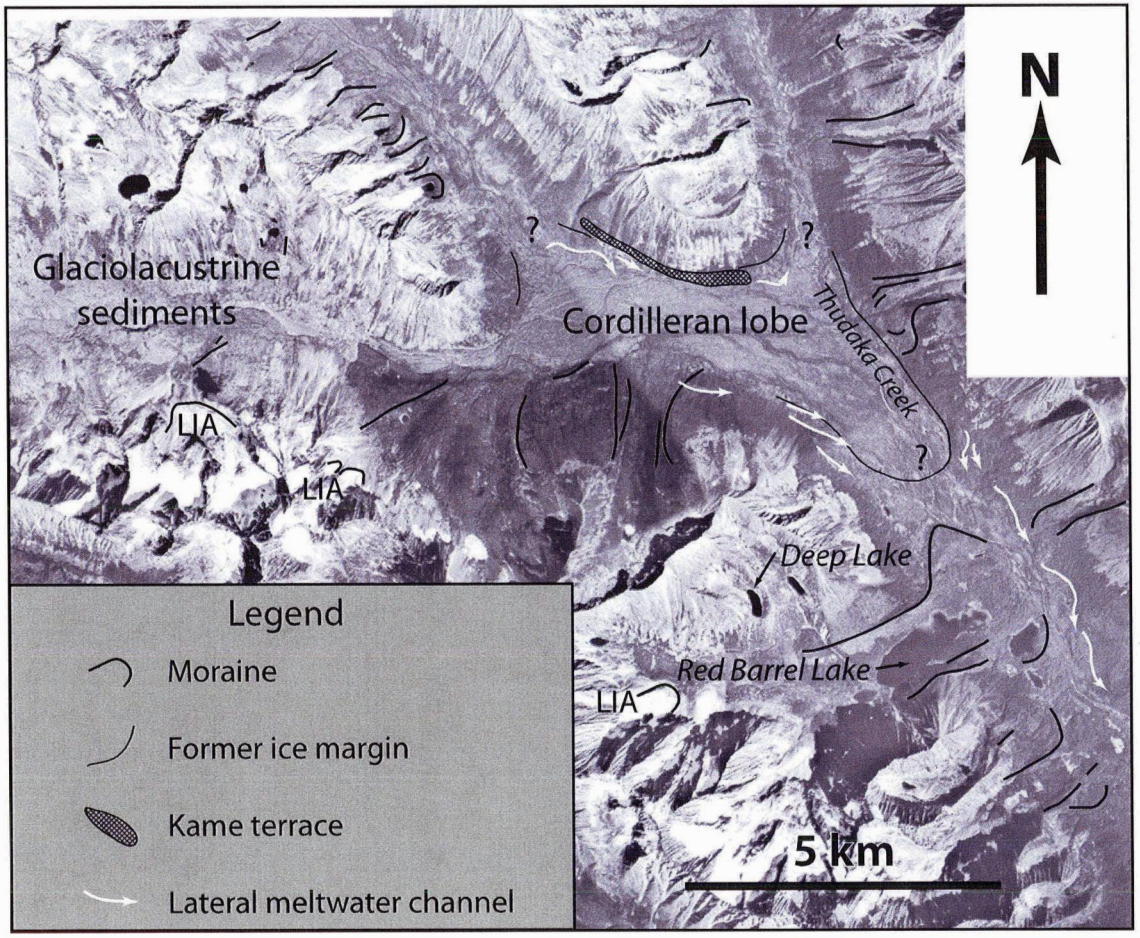


Figure 2.8. Aerial photograph mosaic of late-glacial landforms in Thudaka Creek valley. LIA - Little Ice Age moraine. Aerial photographs 15BCB99018-097, 164, 165, 166, and 167; reproduced with permission of British Columbia Ministry of Agriculture and Lands, Base Mapping and Geomatic Services Branch.

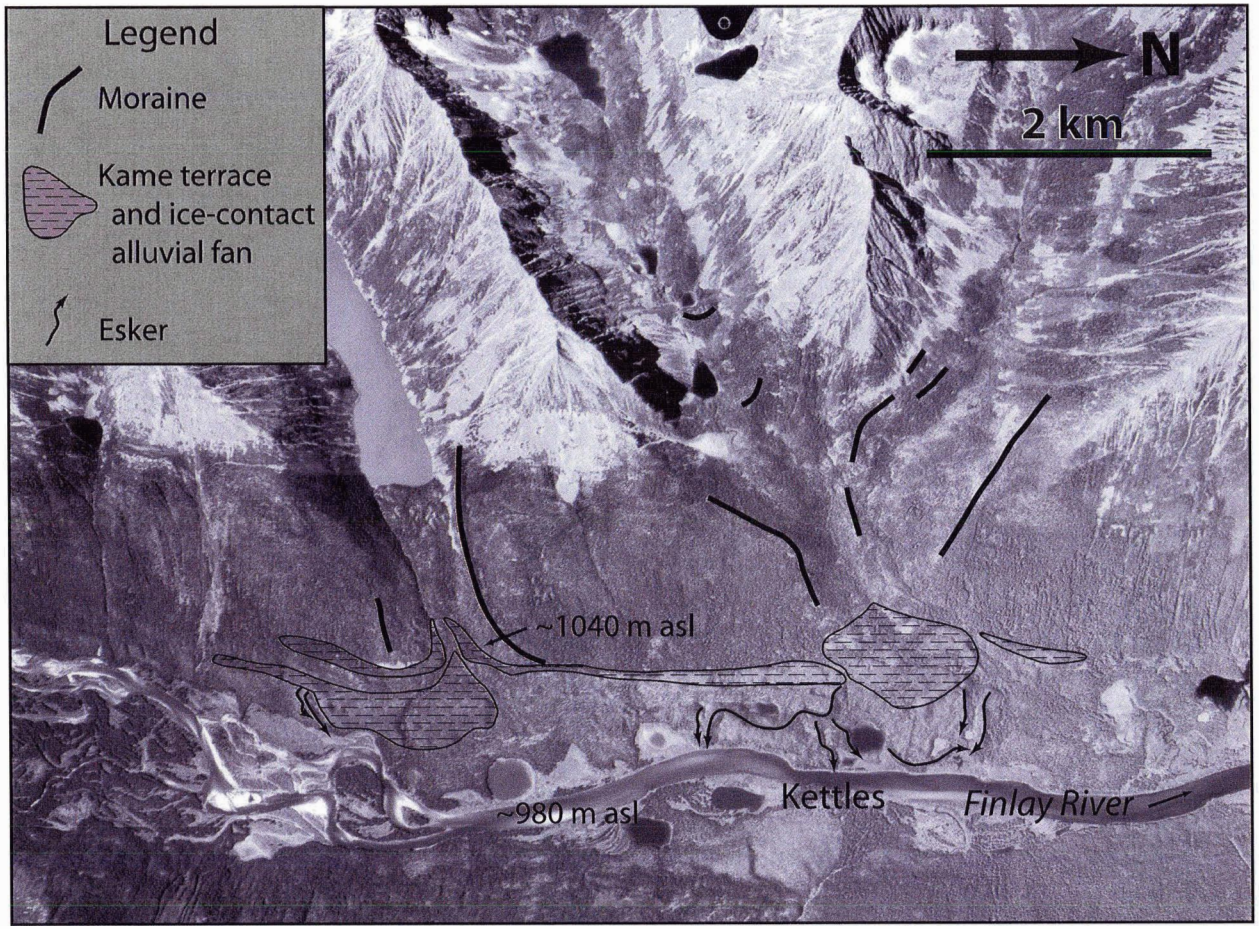


Figure 2.9. Aerial photograph of late-glacial landforms in Finlay River valley and its tributaries. When alpine glaciers abandoned their lateral moraines, they built kame terraces and ice-contact alluvial fans against trunk ice in the Finlay River valley. Aerial photograph 15BCB99016-137; reproduced with permission of British Columbia Ministry of Agriculture and Lands, Base Mapping and Geomatic Services Branch.

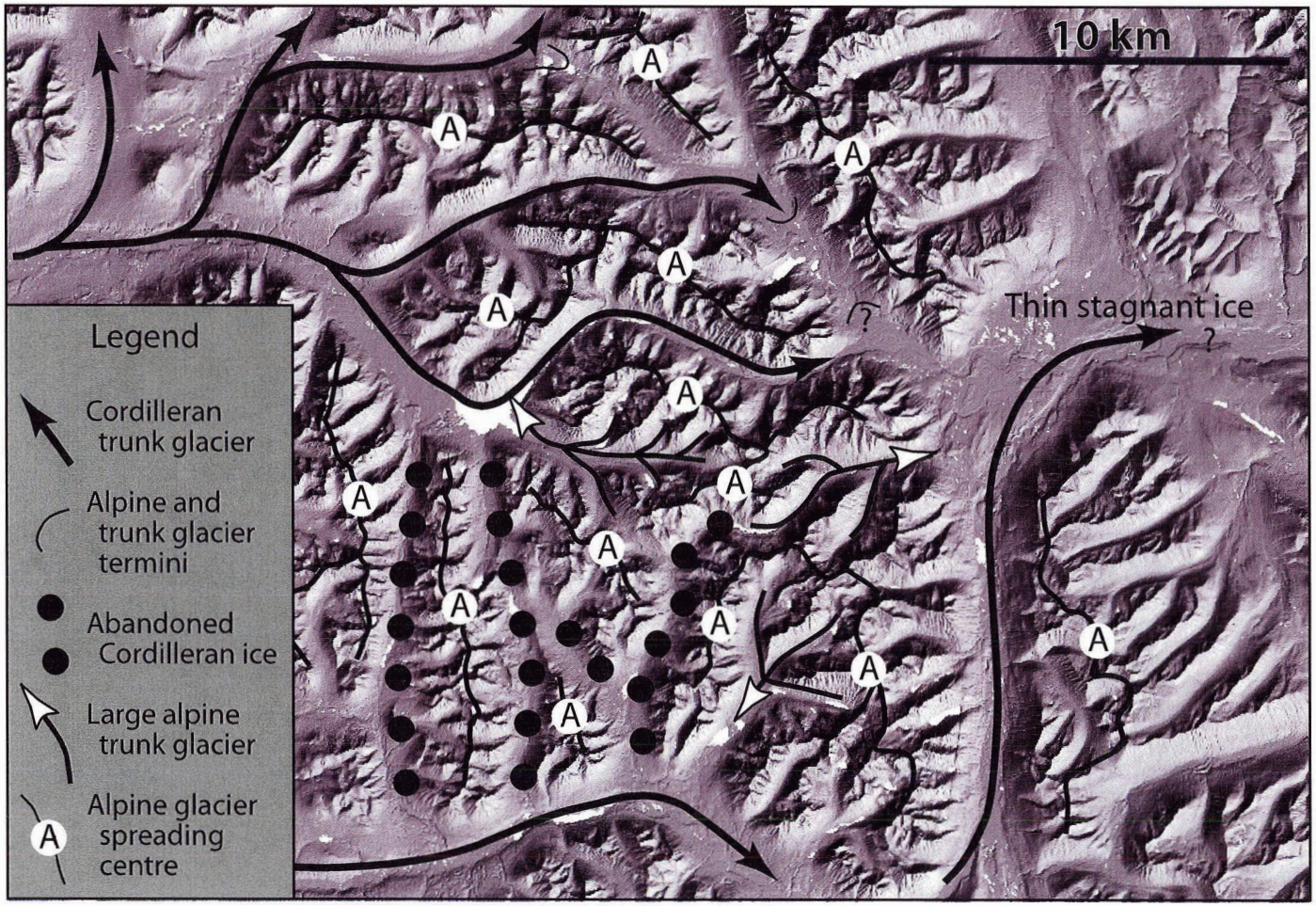


Figure 2.10. Hillshaded digital elevation model of the study area showing the pattern of ice flow during the late-glacial advance. Hillshade map was produced with permission using digital elevation data from the Province of British Columbia, Base Mapping and Geomatic Services Branch.

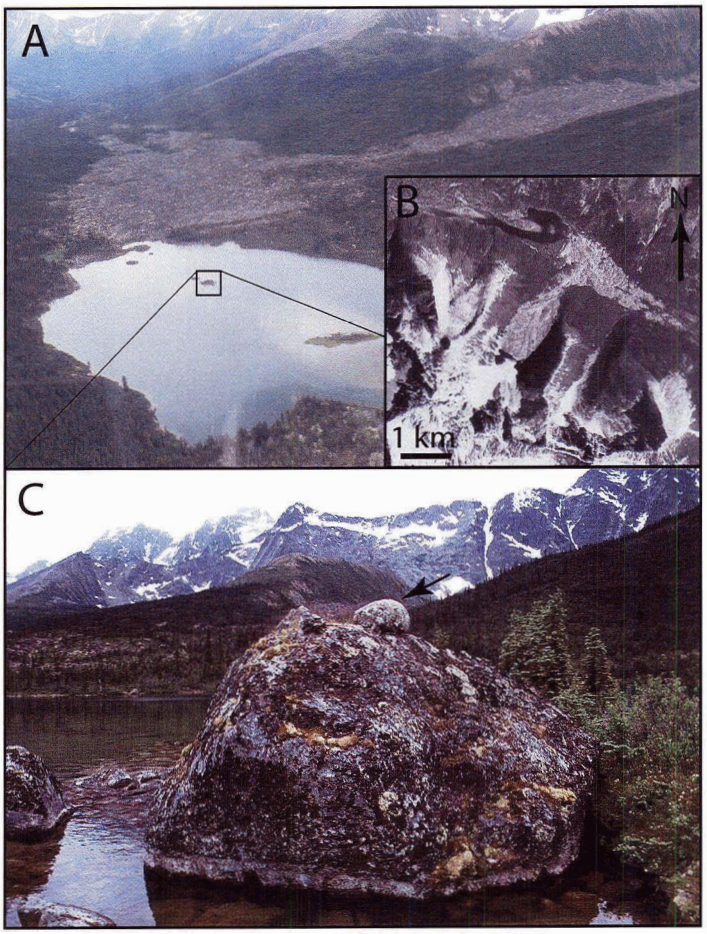


Figure 2.11. A) Rock avalanche debris damming Rock Fall Lake. Box indicates location of C. B) Aerial photograph of rock avalanche debris. C) Exotic, rounded granite boulder (arrowed) sitting on top of rock avalanche debris that was redeposited by the trunk glacier in Cushing Creek valley. Aerial photograph 15BCB99018-046; reproduced with permission of British Columbia Ministry of Agriculture and Lands, Base Mapping and Geomatic Services Branch.

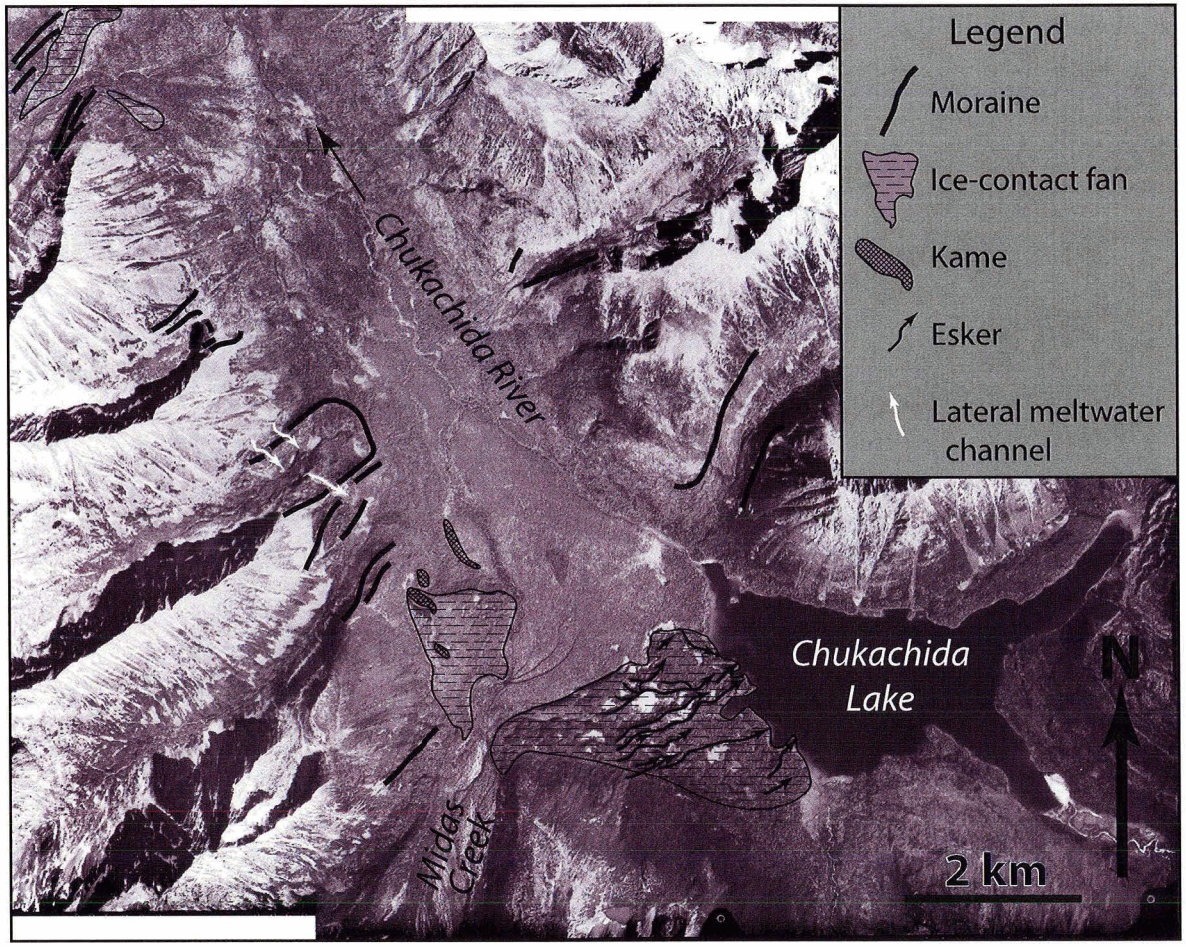


Figure 2.12. Aerial photograph mosaic of late-glacial landforms in Chukachida River valley showing a large ice-contact fan deposited by meltwater derived from stagnating ice and ice-dammed lakes in Midas Creek valley. Eskers, kettles, and kames are preserved on the fan surface. Aerial photographs 15BCB99018-50 and 51; reproduced with permission of British Columbia Ministry of Agriculture and Lands, Base Mapping and Geomatic Services Branch.

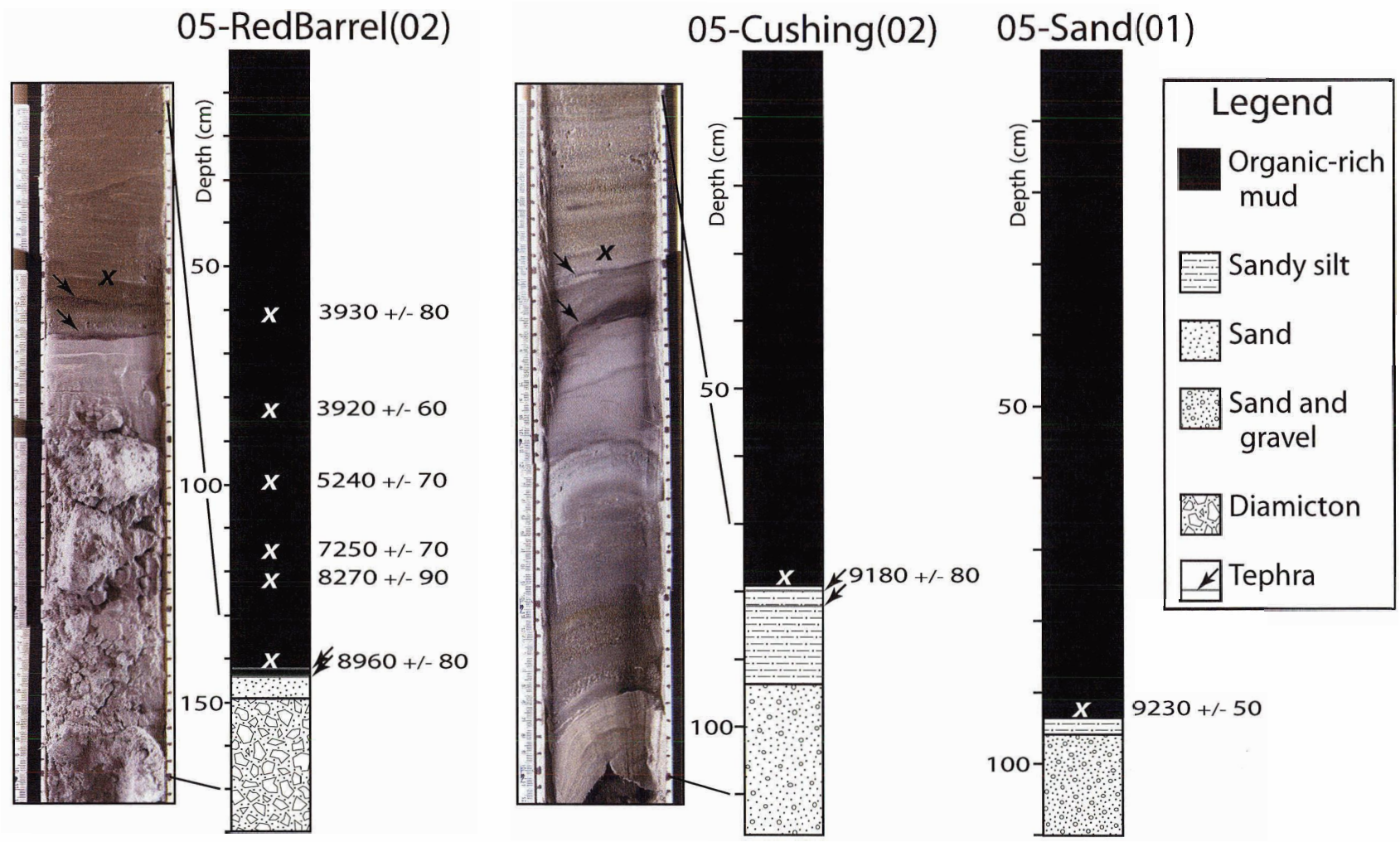


Figure 2.13. Stratigraphic logs and radiocarbon ages from Red Barrel, Cushing, and Sandwich lakes. Tephras are thin black laminae delineated by arrows in the core photos. White and black X's are locations of radiocarbon ages.

# CHAPTER 3:

## Early Holocene tephras in northwest British Columbia


### Abstract

Four, previously undocumented tephras have been found in sediment cores recovered from alpine and sub-alpine lakes up to 250 km apart in northwest British Columbia. Two black phonolitic tephras, each 5-10 mm thick occur within 2-4 cm of one another in basal sediments from seven lakes in the Finlay River and Dease Lake areas. They are slightly older than 9180 ± 80 $^{14}$C yr BP (10,220-10,560 cal yr BP) and likely originate from two closely spaced eruptions of one or two large volcanoes in the northern Cordilleran volcanic province. The Finlay tephras occur at the transition between deglacial sediments and organic-rich postglacial mud in the lake cores, and thus closely delimit the termination of the Fraser Glaciation in northern British Columbia. Sediments in Bob Quinn Lake, which lies on the eastern edge of the northern Coast Mountains, contain two additional black tephras that differ in age and composition from the Finlay tephras. The lower Bob Quinn tephra is 3-4 mm thick, basaltic in composition, and is derived from an eruption in the Iskut River volcanic field about 8400 $^{14}$C yr ago (9400 cal yr BP). The upper Bob Quinn tephra is 12 mm thick, phonolitic in composition, and probably 6000-7000 $^{14}$C yr old. The four tephras are valuable chronostratigraphic markers for future paleoenvironmental studies in northern British Columbia.


### Introduction

The northern Cordilleran volcanic province consists of over 100 late Cenozoic volcanic centres in northwest British Columbia, Yukon, and Alaska (Fig. 3.1; Edwards

and Russell, 1999, 2000). The dominant volcanic rocks are alkali olivine basalt and hawaiite, but highly alkaline rocks such as nephelinite, basanite, peralkaline phonolite, trachyte, and comendite are locally common (Edwards and Russell, 2000). Volcanic centres range from small cinder cones to large shield volcanoes and have a broad range of eruptive styles. Cinder cones consisting of basalt and hawaiite are most abundant (Edwards and Russell, 2000). Large volcanic complexes, including Hoodoo Mountain, Mount Edziza, Level Mountain, and Heart Peaks, are shield and composite volcanoes with numerous cinder cones (Fig. 3.1). They are, by far, the largest volcanoes in the northern Cordilleran volcanic province and show the greatest range in petrology (Edwards and Russell, 2000).

Several postglacial (i.e. younger than 10,000 yr BP) lava flows have been identified and mapped in northwest British Columbia (Read et al., 1989; Souther, 1992; Villeneuve et al., 1998; Edwards et al., 1999, 2000, 2002; Russell and Hauksdóttir, 2000). Distal tephras related to this volcanic activity have not been reported, even though some of the Holocene eruptions were large and thick tephra deposits have been found near several volcanoes and cinder cones (Read et al., 1989; Souther, 1992; Villeneuve et al., 1998; Edwards et al., 1999, 2000, 2002; Russell and Hauksdóttir, 2000).

Four, previously undocumented, early Holocene tephras are reported in this paper. They occur in sediment cores from lakes up to 250 km apart in northwest British Columbia (Figs. 3.1 and 3.2). Two phonolitic tephras are present in lake sediments in the Finlay River and Dease Lake areas (Fig. 3.3). Sediment cores recovered from Bob Quinn Lake contain two additional tephras that are basaltic and phonolitic in composition (Fig. 3.3). The objectives of this paper are to: 1) describe the geomorphic and stratigraphic

setting of the tephras, 2) document their distribution, 3) characterize the morphology and major element composition of their glass shards, and 4) discuss their importance for future paleoenvironmental studies in the region.

**Methods**

Eighteen sediment cores were collected from twelve lakes in three areas of northwest British Columbia using a percussion coring system (Reasoner, 1993). Sediment cores were recovered from lake ice in January 2005 and February 2006, and from the floats of a De Havilland DHC-2 Beaver in July 2005. Red Barrel, Cushing, Katharine, Deep, Black, Bronlund, Rock Fall, and Sandwich lakes were cored in the Finlay River area; of these, Red Barrel, Cushing, Katharine, Deep, and Black lakes contain tephras (Fig. 3.2). Little Glacier, Hungry, and Sister lakes were cored in the Dease Lake area; tephra was found in sediments from Little Glacier and Hungry lakes (Fig. 3.2). Bob Quinn Lake, at the eastern edge of the northern Coast Mountains, was also cored; it too contains tephras (Fig. 3.2). All lake names, except Bob Quinn Lake, are informal. Sediment cores were transported to the University of Northern British Columbia in Prince George where they were split, logged, photographed, and analyzed for bulk physical properties (organic matter, magnetic susceptibility, and grain size). Lithologic and magnetic susceptibility logs for selected cores are presented in this chapter, whereas lithologic, magnetic susceptibility, and percent organic matter logs for all the cores taken in this study are presented individually in Appendix C. Samples of terrestrial plant macrofossils and tephras were extracted from the cores. Plant macrofossils were washed in distilled water, air-dried, and stored in glass vials.

Radiocarbon ages were determined by accelerator mass spectrometry at IsoTrace Laboratory (University of Toronto) and Beta Analytic Inc.

Glass shards were separated from tephras using a heavy liquid separation procedure at the Department of Earth and Atmospheric Sciences, University of Alberta. The mineralogy of glass shard phenocrysts was determined by thin section analysis. The shards, together with shards from previously identified Holocene scoria and tephra deposits on Mount Edziza were analyzed using a JEOL JXA-8200 electron microprobe in the Department of Geology and Geophysics, University of Calgary to determine their major element compositions. Analyses were performed with the microprobe operating at 15 keV accelerating voltage, a 10μm beam diameter, and a 10 ηA beam current. A reference sample of Old Crow tephra (UT1434, University of Toronto) was analyzed repeatedly to track changes in the analytical accuracy of the microprobe. Data were corrected and normalized to 100% on a water free basis and are shown in Tables 3.1 and 3.2. Uncorrected values from individual glass shard analyses are presented in Appendix D.

**Geomorphic and stratigraphic setting**

Sediment cores from the Finlay River and Dease Lake areas were collected from lakes dammed by moraines built during a late-glacial advance of alpine glaciers in northwest British Columbia (Chapter 2). Two tephras were found in most of the cores near the contact between older inorganic silt, sand, and gravel, and younger organic-rich mud (Fig. 3.3). This facies boundary records the transition from deglacial sedimentation to organic-rich postglacial sedimentation, and marks the termination of the late-glacial

advance (Chapter 2) and the Fraser Glaciation in northern British Columbia. The tephras are black, range in thickness from less than 5 mm to 10 mm, and occur within 2-4 cm of one another in the cores (Fig. 3.4a). The two tephras from the Finlay River and Dease Lake areas are equivalent and are referred to hereafter as the Finlay tephras.

Bob Quinn Lake cores contain two tephras that are different from the Finlay tephras (Fig. 3.3). The lower Bob Quinn tephra is 3-4 mm thick and lies about 5 cm above a contact between organic-rich mud and underlying inorganic silt (Fig. 3.5a). A second tephra, 12 mm thick, lies 40 cm above the lower tephra, within organic-rich mud (Fig. 3.5a).

**Composition and age**

The two Finlay tephras have fine sand and coarse silt textures. Glass shards in the two tephras are similar in morphology. They are dominantly blocky in shape and have spherical vesicles; needle-shaped shards with lineated, lensoid vesicles are also present but are less common (Fig. 3.4b). Phenocrysts in glass shards of both tephras are dominantly plagioclase with subordinate orthopyroxene. Both tephras are phonolitic to trachytic in composition and rich in FeO (Figs. 3.6 and 3.7; Table 3.1). The two tephras have nearly identical major element composition, indicating that they are likely derived from the same source.

Terrestrial plant macrofossils directly overlying the upper Finlay tephra yielded ages of 8960 ± 80 $^{14}$C yr BP (9780 -10,250 cal yr BP) and 9180 ± 80 $^{14}$C yr BP (10,220-10,560 cal yr BP) (Fig. 3.3; Table 3.3). The two tephras are thus early Holocene in age, deposited immediately after deglaciation (Clague, 1981).

The lower Bob Quinn tephra has a medium-coarse sand texture. Glass shards are blocky and needle-shaped, up to 5 mm in length, and contain plagioclase, clinopyroxene, and minor orthopyroxene phenocrysts (Fig. 3.5b). Most of the blocky shards contain spherical vesicles, whereas the needle-shaped shards have lineated, lensoid vesicles (Fig. 3.5b). The lower tephra is trachybasaltic in composition with 11-12 wt. % FeO (Figs. 3.6 and 3.8; Table 3.1).

The upper Bob Quinn tephra has a silty fine sand texture. Glass shards have spherical vesicles and are dominantly blocky in shape (Fig. 3.5b). Phenocrysts in glass shards are dominantly plagioclase; pyroxene and potassium feldspar crystals are also present, although rare. The tephra is phonolitic in composition, like the Finlay tephras (Fig. 3.6). However, it has about 2% less $SiO_2$, 1.5% more $Al_2O_3$, and more $TiO_2$, CaO, and MgO than the Finlay tephras (Fig. 3.7; Table 3.1).

Terrestrial plant macrofossils directly above and below the lower Bob Quinn tephra yielded ages of 8450 ± 50 $^{14}$C yr BP (9320-9540 cal yr BP) and 8370 ± 40 $^{14}$C yr BP (9270-9500 cal yr BP), respectively (Fig. 3.3; Table 3.3). The calibrated age ranges overlap and indicate that the tephra was deposited about 8400 $^{14}$C yr ago (9400 cal yr BP). The upper Bob Quinn tephra has not been directly dated, but its stratigraphic position suggests an age of 6000-7000 $^{14}$C yr BP (Fig. 3.3).

**Sources of tephras**

Based on their distributions, thicknesses, and compositions, the tephras likely were erupted from one or more volcanic centres in the northern Cordilleran volcanic province (Figs. 3.1 and 3.2). Highly alkaline rocks with compositions similar to the

phonolitic tephras documented in this study are characteristic of the northern Cordilleran volcanic province (Fig. 3.6; Edwards and Russell, 1999, 2000). Tephras derived from volcanoes in the Wrangell volcanic belt and Aleutian Arc, for example Dawson tephra (Westgate et al., 2000) and White River tephra (Lerbekmo and Campbell, 1969; Lerbekmo et al., 1975; Clague et al., 1995), are dominantly rhyolitic, indicating that those regions are unlikely source areas for the tephras in northern British Columbia (Preece et al., 1992, 1999; Richter et al., 1995; Mangan et al., 2003). Late Pleistocene tephras from Mount Edgecumbe, southeastern Alaska (Fig. 3.1), range in composition from basaltic to rhyolitic, and all but one are local in extent (Heusser, 1960; McKenzie, 1970; Yehle, 1974; Riehle et al., 1992). The only Edgecumbe tephra of regional extent is dacitic in composition and approximately 11,300 $^{14}$C yr old (Riehle et al., 1992; Begét and Motyka, 1998), older than the tephras of this study. Nevertheless, possible, unidentified volcanic centres in southeast Alaska and northwest British Columbia that are presently below sea level or covered by glaciers cannot be ruled out as possible sources for the Finlay and Bob Quinn tephras.

*Finlay tephras*

The two Finlay tephras are distributed across northwest British Columbia and possibly extend into the northern Rocky Mountains. Based on their distribution, thickness, and major element composition, the likely source is one of the large shield or composite volcanoes in northwest British Columbia, specifically Hoodoo Mountain, Mount Edziza, Level Mountain, or Heart Peaks (Figs. 3.1 and 3.2). Some cinder cones in the northern Cordilleran volcanic province erupted following deglaciation during the late

Pleistocene or early Holocene, but they are too small to account for the thickness and distribution of the Finlay tephras.

The major element compositions of the Finlay tephras are most similar to those of whole-rock samples from Hoodoo Mountain (Figs. 3.6 and 3.7; Tables 3.1 and 3.4), a large composite volcano with a long history of phonolitic and trachytic eruptive activity dating from 85,000 to 9000 yr BP (Edwards, 1997; Edwards et al., 2002). Two phonolitic lava flows on the south flank of Hoodoo Mountain are estimated to be postglacial in age, based on $^{40}Ar/^{39}Ar$ dates of 10,000-9,000 yr BP (Villeneuve et al., 1998; Edwards et al., 1999; 2002) and observations that the flows have not been glaciated (Edwards et al., 2002). The average whole-rock chemistry of the two postglacial phonolitic flows is similar to the glass composition of the Finlay tephras (Figs. 3.6 and 3.7; Tables 3.1 and 3.4). No pyroclastic deposits or tephras are known to be associated with the eruptions that produced these lava flows (Edwards et al., 2002). The core from Bob Quinn Lake, which is only 60 km northeast of Hoodoo Mountain and lies along the trajectory that any ash plume would take moving from that volcano to the Finlay River and Dease Lake areas (Figs. 3.1 and 3.2), does not contain the Finlay tephras. The base of that core, however, is about 1000 years younger than the Finlay tephras. The compositional data indicate that Hoodoo Mountain is the most likely source for the Finlay tephras, but other possible sources must be considered.

Mount Edziza is another large volcanic complex in the northern Cordilleran volcanic province and a possible source of the Finlay tephras. It is a broad plateau consisting of multiple, large, ice-covered composite cones and numerous small cinder cones (Figs. 3.1 and 3.2; Souther, 1992). The volcanic complex has a diverse suite of

rocks ranging from basaltic to peralkaline felsic in composition (Souther, 1992). These rocks are generally less alkaline than the Finlay tephras, although some are similar composition (Figs. 3.6 and 3.7; Tables 3.1 and 3.2). Comenditic trachyte pumice of the Sheep Track Member of the Big Raven Formation is postglacial in age and covers an area of about 40 $km^2$ on the west flank of Mount Edziza (Souther, 1992). The pumice is white, markedly richer in $SiO_2$, and poorer in FeO than the Finlay tephras (Fig. 3.7). Older formations of possible late Pleistocene to early Holocene age are dominantly basaltic and limited in extent (Souther, 1992). However, their absolute ages and chemical compositions are poorly known, therefore Mount Edziza cannot be ruled out as a possible source for the Finlay tephras.

Level Mountain and Heart Peaks are large volcanic complexes similar in size and chemistry to Mount Edziza and Hoodoo Mountain (Figs. 3.1 and 3.2; Casey, 1980; Hamilton, 1981, 1991; Souther and Yorath, 1991; Edwards and Russell, 2000). They have received little scientific study, and it is not known whether Holocene deposits are present and, if they are, whether they are extensive. Consequently, further field and laboratory investigations are required to assess whether the Finlay tephras originated from Level Mountain or Heart Peaks.

*Bob Quinn tephras*

The age and composition of the lower Bob Quinn tephra strongly suggest that it is derived from the Iskut River volcanic field. This volcanic field consists of eight volcanic centres situated between Iskut and Unuk rivers, approximately 40 km southwest of Bob Quinn Lake (Figs. 3.1 and 3.2). The presence of large, needle-shaped glass shards in the tephra indicates that Bob Quinn Lake is near the source of the eruption. Volcanism in the

Iskut River volcanic field ranges in age from approximately 70,000 to 150 yr BP (Russell and Hauksdóttir, 2000). Read et al. (1989) demonstrated that two basalt flows temporarily dammed Iskut River during the early Holocene. The flows originate from the Iskut River volcanic centre, about 4 km east-southeast of Iskut Canyon (Fig. 3.2; Read et al., 1989; Russell and Hauksdottir 2000). Read et al. (1989) reported ages of 8730 ± 600 $^{14}$C yr BP from charcoal underlying one of the basalt flows and 8780 ± 150 $^{14}$C yr BP from plant material bounding basaltic tephra that mantles nearby slopes (Table 3.3). The major element composition of whole-rock samples collected from the Iskut River volcanic field is similar to that of the lower Bob Quinn tephra (Figs. 3.6 and 3.8; Tables 3.1 and 3.4).

The upper Bob Quinn tephra is similar in composition to the Finlay tephras and to whole-rock samples from Hoodoo Mountain and Mount Edziza (Figs. 3.6 and 3.7; Tables 3.1, 3.2, and 3.4). Its composition is closest to that of the two postglacial phonolitic lava flows on Hoodoo Mountain, but the ages of the flows must be better constrained to confirm the tentative correlation made here.

The areal distributions of the upper and lower Bob Quinn tephras are poorly constrained. The lower Bob Quinn tephra probably extends along Iskut River, south of Mount Edziza, based on its affinity to the Iskut River volcanic field. However, it may not be present much farther east in northern British Columbia because of its coarse grain size and limited thickness. The upper Bob Quinn tephra may extend farther east than the lower tephra based on its grain size and thickness.

**Conclusions**

Four, previously unrecognized tephras are reported from northern British Columbia. Their distribution and major element composition indicate sources at one or more volcanic centres in the northern Cordilleran volcanic province. Two phonolitic tephras in the Finlay River and Dease Lake areas are products of two closely spaced eruptions shortly before 9180 ± 80 $^{14}$C yr BP (10,220-10,560 cal yr BP). The Finlay tephras are regional in extent and occur at the transition from deglacial sedimentation to deposition of organic-rich Holocene mud. They closely delimit the time of terminal Pleistocene deglaciation in northern British Columbia and the termination of a regional, late-glacial glacier advance. Cores from Bob Quinn Lake also contain two tephras, but they are different in age and composition from the Finlay tephras. A lower basaltic tephra at Bob Quinn Lake is 8400 $^{14}$C yr old (9400 cal yr old) and is likely derived from the Iskut River volcanic centre, which is one of eight volcanoes forming the Iskut River volcanic field. The upper phonolitic tephra at Bob Quinn Lake is 6000-7000 $^{14}$C yr old; its source is unknown.

The Finlay and Bob Quinn tephras are valuable chronostratigraphic markers for future paleoenvironmental studies in northern British Columbia.

Table 3.1. Average major element composition of glass shards from the Finlay and Bob Quinn tephras.

| | Lower Finlay tephra | | | | | | Upper Finlay tephra | | | | | | Upper Finlay tephra (?) | | | |
|---|---|---|---|---|---|---|---|---|---|---|---|---|---|---|---|---|
| | UA1144* | | UA1165 | | UA1168 | | UA1143* | | UA1164 | | UA1169 | | UA1166 | | UA1167 | |
| $SiO_2$ | 61.84 | (3.09) | 60.66 | (0.26) | 60.90 | (0.96) | 62.57 | (1.13) | 60.46 | (0.31) | 60.39 | (0.48) | 60.45 | (0.37) | 60.52 | (0.38) |
| $TiO_2$ | 0.67 | (0.41) | 0.20 | (0.02) | 0.29 | (0.14) | 0.24 | (0.03) | 0.20 | (0.02) | 0.22 | (0.03) | 0.20 | (0.03) | 0.21 | (0.02) |
| $Al_2O_3$ | 18.87 | (0.62) | 16.52 | (0.17) | 16.95 | (0.92) | 17.00 | (0.31) | 16.60 | (0.20) | 16.48 | (0.28) | 16.50 | (0.16) | 16.56 | (0.17) |
| FeO(t) | 5.09 | (2.36) | 7.83 | (0.17) | 6.95 | (1.46) | 8.17 | (0.21) | 7.92 | (0.25) | 8.07 | (0.35) | 7.89 | (0.26) | 8.03 | (0.28) |
| MnO | 0.14 | (0.05) | 0.20 | (0.02) | 0.18 | (0.06) | 0.23 | (0.03) | 0.21 | (0.02) | 0.22 | (0.02) | 0.22 | (0.03) | 0.21 | (0.03) |
| CaO | 2.48 | (1.21) | 1.17 | (0.03) | 1.36 | (0.42) | 1.24 | (0.08) | 1.15 | (0.06) | 1.17 | (0.06) | 1.17 | (0.03) | 1.12 | (0.13) |
| MgO | 0.64 | (0.57) | 0.01 | (0.01) | 0.15 | (0.19) | 0.01 | (0.01) | 0.01 | (0.01) | 0.01 | (0.01) | 0.01 | (0.01) | 0.01 | (0.01) |
| $Na_2O$ | 5.67 | (2.19) | 8.57 | (0.23) | 8.01 | (0.77) | 6.06 | (1.55) | 8.56 | (0.37) | 8.54 | (0.21) | 8.74 | (0.27) | 8.52 | (0.51) |
| $K_2O$ | 4.58 | (0.86) | 4.83 | (0.10) | 5.21 | (0.49) | 4.47 | (0.08) | 4.88 | (0.08) | 4.91 | (0.07) | 4.82 | (0.13) | 4.81 | (0.07) |
| $H_2O$(d) | 1.20 | (1.28) | 0.56 | (0.74) | 0.48 | (0.67) | 1.46 | (1.20) | 1.55 | (0.55) | 0.00 | (0.69) | 0.24 | (0.65) | 0.11 | (1.01) |
| n | 14 | | 18 | | 17 | | 18 | | 20 | | 20 | | 19 | | 20 | |

| | Lower Bob Quinn tephra | | Upper Bob Quinn tephra | |
|---|---|---|---|---|
| | UA1163 | | UA1162 | |
| $SiO_2$ | 47.45 | (0.28) | 58.48 | (1.43) |
| $TiO_2$ | 2.34 | (0.12) | 0.92 | (0.30) |
| $Al_2O_3$ | 16.93 | (0.27) | 18.12 | (0.29) |
| FeO(t) | 11.76 | (0.23) | 6.22 | (0.78) |
| MnO | 0.18 | (0.03) | 0.14 | (0.02) |
| CaO | 9.05 | (0.18) | 2.68 | (0.73) |
| MgO | 6.12 | (0.20) | 0.77 | (0.27) |
| $Na_2O$ | 5.20 | (0.12) | 7.79 | (1.08) |
| $K_2O$ | 0.97 | (0.06) | 4.88 | (0.51) |
| $H_2O$(d) | 0.98 | (0.51) | 0.85 | (1.00) |
| n | 24 | | 25 | |

Notes:

All analyses normalized to 100% on a water-free basis. UA1162 - laboratory number (University of Alberta); standard deviation in parentheses; n - number of analyses; FeO(t) - total iron oxide as FeO; $H_2O$(d) - water by difference.

*Samples UA1143 and UA1144 were run prior to recalibration of the microprobe and are therefore not comparable to the other analyses.

Table 3.2. Average major element composition of Holocene scoria and pumice from Mount Edziza.

| | Sheep Track Member | | | | Holocene Cinder Cones | | | | | |
|---|---|---|---|---|---|---|---|---|---|---|
| | Sheep Track Pumice | | | | Sheep Track Pumice (?) | | Williams Cone | | Englacial cinders | | Cinders on tundra | |
| | UA1155 | | UA1156 | | UA1157 | | UA1149 | | UA1150 | | UA1153 | |
| $SiO_2$ | 62.84 | (0.28) | 63.01 | (0.19) | 62.52 | (0.33) | 51.41 | (0.24) | 49.81 | (1.01) | 51.08 | (0.32) |
| $TiO_2$ | 0.21 | (0.03) | 0.22 | (0.03) | 0.21 | (0.02) | 2.48 | (0.11) | 2.79 | (0.07) | 2.67 | (0.07) |
| $Al_2O_3$ | 18.13 | (0.10) | 18.20 | (0.12) | 17.99 | (0.13) | 15.85 | (0.13) | 15.32 | (0.16) | 15.81 | (0.18) |
| FeO(t) | 4.67 | (0.06) | 4.53 | (0.11) | 4.68 | (0.09) | 11.24 | (0.18) | 12.41 | (0.29) | 11.51 | (0.20) |
| MnO | 0.14 | (0.03) | 0.13 | (0.02) | 0.13 | (0.02) | 0.19 | (0.02) | 0.18 | (0.03) | 0.19 | (0.02) |
| CaO | 0.99 | (0.05) | 0.97 | (0.04) | 0.98 | (0.03) | 7.11 | (0.15) | 7.93 | (0.81) | 7.18 | (0.14) |
| MgO | 0.11 | (0.01) | 0.11 | (0.03) | 0.11 | (0.02) | 3.21 | (0.12) | 3.73 | (0.60) | 3.27 | (0.10) |
| Na O | 7.69 | (0.29) | 7.49 | (0.16) | 8.00 | (0.24) | 5.98 | (0.30) | 5.77 | (0.29) | 5.90 | (0.23) |
| $K_2O$ | 5.22 | (0.14) | 5.34 | (0.13) | 5.38 | (0.16) | 2.53 | (0.13) | 2.06 | (0.41) | 2.39 | (0.08) |
| $H_2O$(d) | -0.71 | (0.75) | 1.52 | (0.39) | -0.70 | (0.48) | 0.53 | (0.36) | 0.44 | (0.61) | 0.32 | (0.78) |
| n | 18 | | 18 | | 15 | | 17 | | 20 | | 20 | |

Notes:
All analyses normalized to 100% on a water-free basis. UA1150 - laboratory number (University of Alberta); standard deviation in parentheses; n - number of analyses; FeO(t) - total iron oxide as FeO; $H_2O$(d) - water by difference.

Table 3.3. Radiocarbon ages from the Finlay River, Dease Lake, and Iskut River areas.

| Location (latitude, longitude) | $^{14}$C age[1] (years BP) | Calibrated age range[2] (years BP) | Laboratory number[3] | Dated material | Depth in core (cm) | Reference |
|---|---|---|---|---|---|---|
| Red Barrel Lake (57°40.623'N, 126°44.029'W) | 3930 ± 80 | 4100-4580 | TO-12469 | Conifer needle | 60.5 | this study |
| | 3920 ± 60 | 4160-4520 | TO-12470 | Twig | 82.5 | this study |
| | 5240 ± 70 | 5890-6210 | TO-12471 | Spruce terminal bud | 98.5 | this study |
| | 7250 ± 70 | 7950-8190 | TO-12472 | Twig | 115.0 | this study |
| | 8270 ± 90 | 9030-9460 | TO-12473 | Conifer needle | 121.5 | this study |
| | 8960 ± 80 | 9780-10,250 | TO-12474 | Wood | 139.5 | this study |
| Cushing Lake (57°35.607'N, 126°54.450'W) | 9180 ± 80 | 10,220-10,560 | TO-12475 | Terrestrial plant matter | 77.5 | this study |
| Bob Quinn Lake (56°58.573'N, 130°15.623'W) | 8450 ± 50 | 9320-9540 | Beta-216498 | Wood | 206.5 | this study |
| | 8370 ± 50 | 9270-9500 | Beta-216499 | Terrestrial plant matter | 207.5 | this study |
| Iskut River (56°41.448'N, 130°36.748'W) | 8730 ± 600 | 8390-11,630 | ? | Charcoal | - | Read et al. (1989) |
| | 8750 ± 150 | 9540-10,200 | SFU-??? | ? | - | |

[1] Laboratory-reported errors are 1-sigma.
[2] Calibrated ages determined using the program OxCal v4.0 Beta, which uses the IntCal04 calibration curve (Reimer et al., 2004). The range represents the 95% confidence interval (± 2 sigma).
[3] Beta - Beta Analytic Inc.; SFU - Simon Fraser University; TO - IsoTrace Laboratory (University of Toronto).

Table 3.4. Average whole-rock major element compositions of postglacial phonolitic flows at Hoodoo Mountain and Holocene basalt flows from several volcanic centres in the Iskut River volcanic field.

| | Hoodoo Mountain | | Iskut River volcanic centres | | | | | | | | | | | | | |
|---|---|---|---|---|---|---|---|---|---|---|---|---|---|---|---|---|
| | | | Iskut River | | Tom MacKay Ck. | | Snippaker Ck. | | Cone Glacier | | Cinder Mountain | | King Ck. | | Second Canyon | | Lava Fork | |
| $SiO_2$ | 60.12 | n/a | 48.53 | (0.55) | 48.08 | n/a | 48.36 | (0.43) | 48.24 | (0.69) | 49.63 | (1.08) | 49.44 | n/a | 46.10 | n/a | 46.57 | (0.12) |
| $TiO_2$ | 0.29 | n/a | 2.30 | (0.07) | 2.30 | n/a | 2.30 | (0.03) | 2.37 | (0.17) | 2.41 | (0.41) | 2.24 | n/a | 2.57 | n/a | 2.83 | (0.03) |
| $Al_2O_3$ | 16.81 | n/a | 16.61 | (0.30) | 15.57 | n/a | 16.65 | (0.35) | 16.47 | (0.41) | 16.11 | (0.03) | 16.58 | n/a | 14.90 | n/a | 16.95 | (0.03) |
| $Fe_2O_3$ | 4.59 | n/a | 2.97 | (0.68) | 3.26 | n/a | 3.32 | (1.35) | 4.48 | (1.77) | 3.95 | (0.81) | 2.77 | n/a | 4.30 | n/a | 3.53 | (1.01) |
| FeO | 3.26 | n/a | 8.76 | (0.62) | 8.51 | n/a | 8.53 | (1.06) | 7.65 | (1.45) | 9.25 | (0.78) | 8.52 | n/a | 8.29 | n/a | 9.19 | (0.94) |
| MnO | 0.19 | n/a | 0.18 | (0.01) | 0.18 | n/a | 0.18 | (0.00) | 0.19 | (0.01) | 0.25 | (0.02) | 0.18 | n/a | 0.18 | n/a | 0.18 | (0.00) |
| CaO | 1.68 | n/a | 9.07 | (0.19) | 10.03 | n/a | 9.37 | (0.15) | 9.18 | (0.35) | 6.67 | (0.82) | 8.58 | n/a | 10.25 | n/a | 8.90 | (0.05) |
| MgO | 0.21 | n/a | 6.48 | (0.36) | 7.83 | n/a | 6.48 | (0.47) | 6.50 | (0.70) | 3.36 | (0.92) | 6.01 | n/a | 9.26 | n/a | 6.58 | (0.07) |
| $Na_2O$ | 7.74 | n/a | 3.63 | (0.16) | 2.90 | n/a | 3.48 | (0.08) | 3.51 | (0.19) | 4.55 | (0.34) | 3.76 | n/a | 2.85 | n/a | 3.73 | (0.15) |
| $K_2O$ | 5.03 | n/a | 1.04 | (0.14) | 0.94 | n/a | 0.94 | (0.06) | 1.00 | (0.14) | 2.43 | (0.60) | 1.38 | n/a | 0.91 | n/a | 1.09 | (0.01) |
| $P_2O_5$ | 0.06 | n/a | 0.43 | (0.05 | 0.38 | n/a | 0.39 | (0.02) | 0.42 | (0.04) | 1.39 | (0.28) | 0.54 | n/a | 0.39 | n/a | 0.45 | (0.00) |
| $H_2O(d)$ | 1.22 | n/a | 0.30 | (0.05) | 0.70 | n/a | 0.18 | (0.08) | 0.26 | (0.12) | 0.76 | (0.65) | 0.53 | n/a | 0.62 | n/a | 0.18 | (0.06) |
| n | n/a | | 8 | | 1 | | 5 | | 13 | | 6 | | 1 | | 1 | | 7 | |

Notes:

Data from Hoodoo Mountain reprinted with permission from the Bulletin of Volcanology from Edwards et al. (2002). Data from the Iskut River volcanic field reprinted with permission from The Canadian Mineralogist from Russell and Hauksdottir (2000). All analyses are normaized to 100% on a water-free basis. Standard deviation in parentheses; n - number of analyses; $H_2O(d)$ - water by difference.

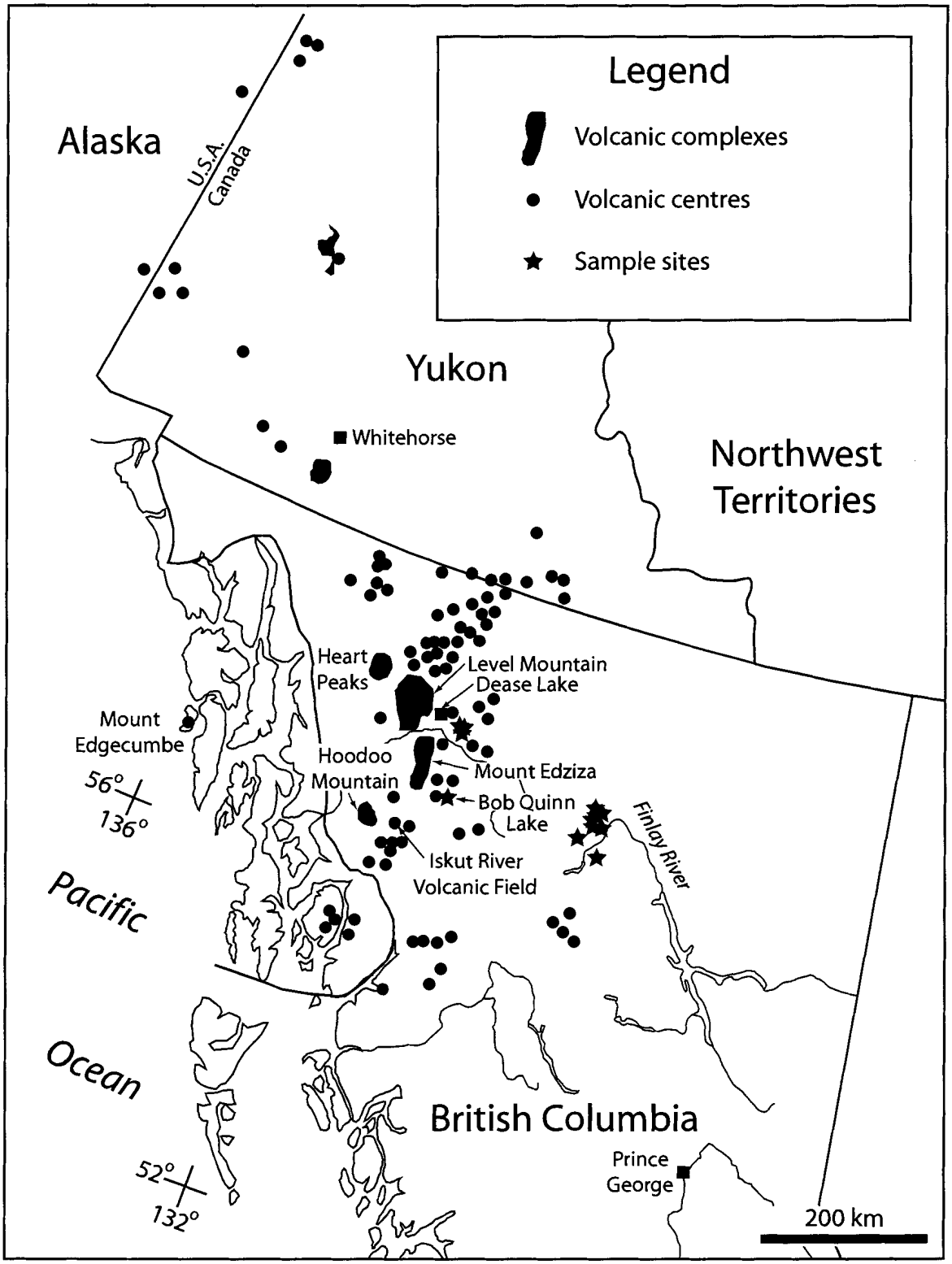


Figure 3.1. Location of volcanic centres and complexes forming the northern Cordilleran volcanic province and sample sites. Modified with permission from Edwards and Russell (2000).

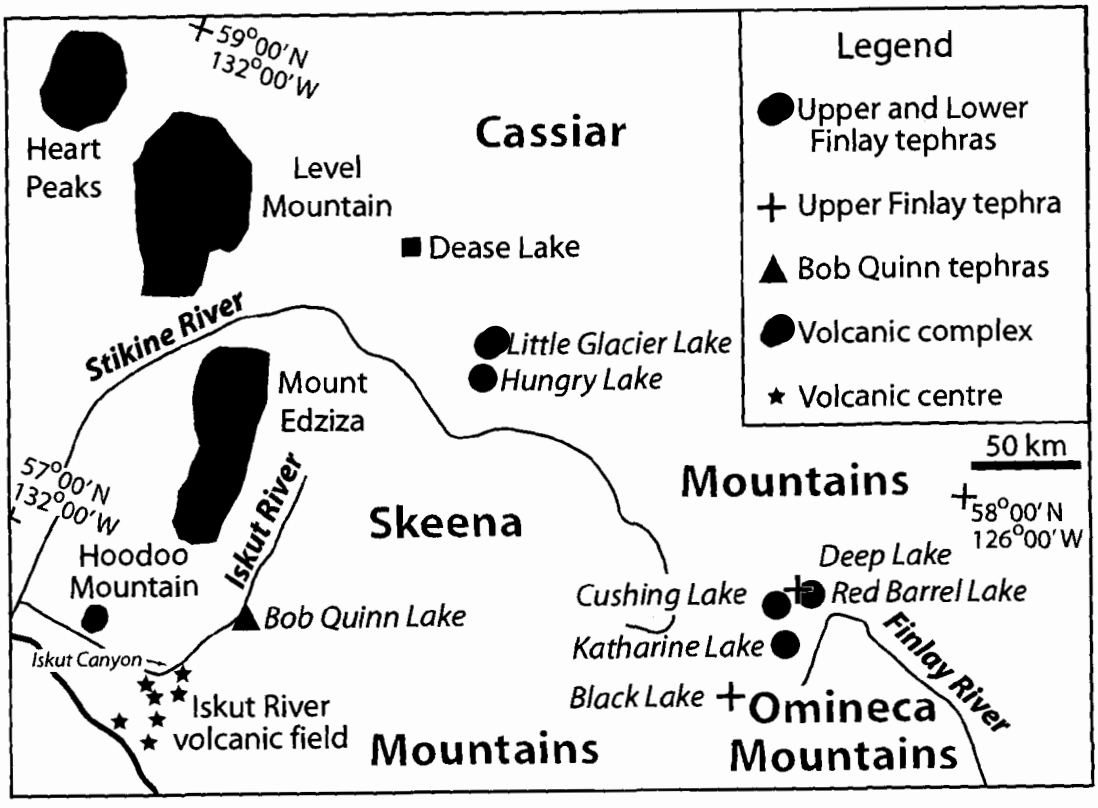


Figure 3.2. Map of part of northern British Columbia showing locations of large volcanic centres, sampled lakes, and occurrences of the Finlay and Bob Quinn tephras.

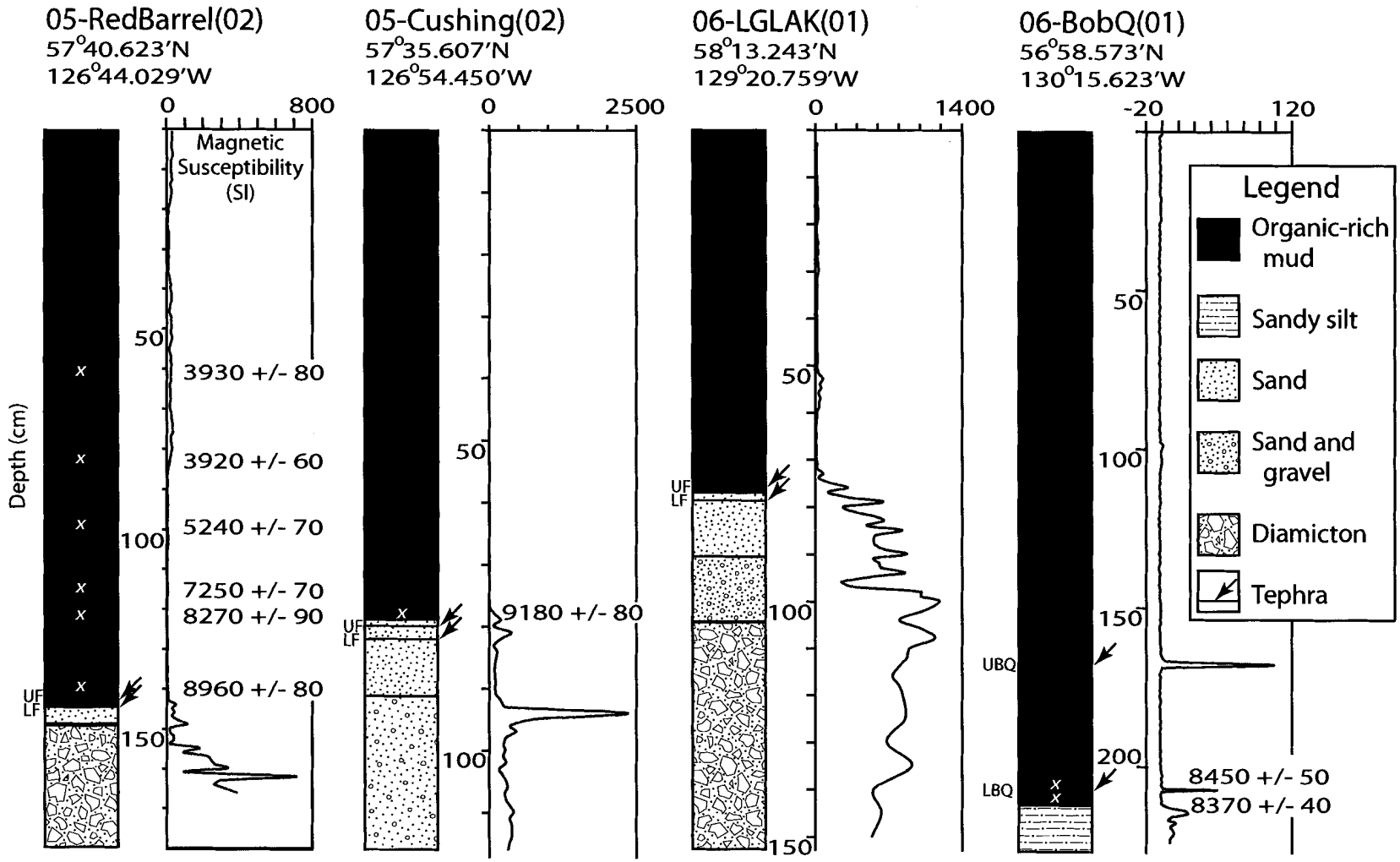


Figure 3.3. Stratigraphic and magnetic susceptibility logs and radiocarbon ages for cores collected from Red Barrel, Cushing, Little Glacier, and Bob Quinn lakes. UF-upper Finlay tephra, LF-lower Finlay tephra, UBQ-upper Bob Quinn tephra, LBQ-lower Bob Quinn tephra.

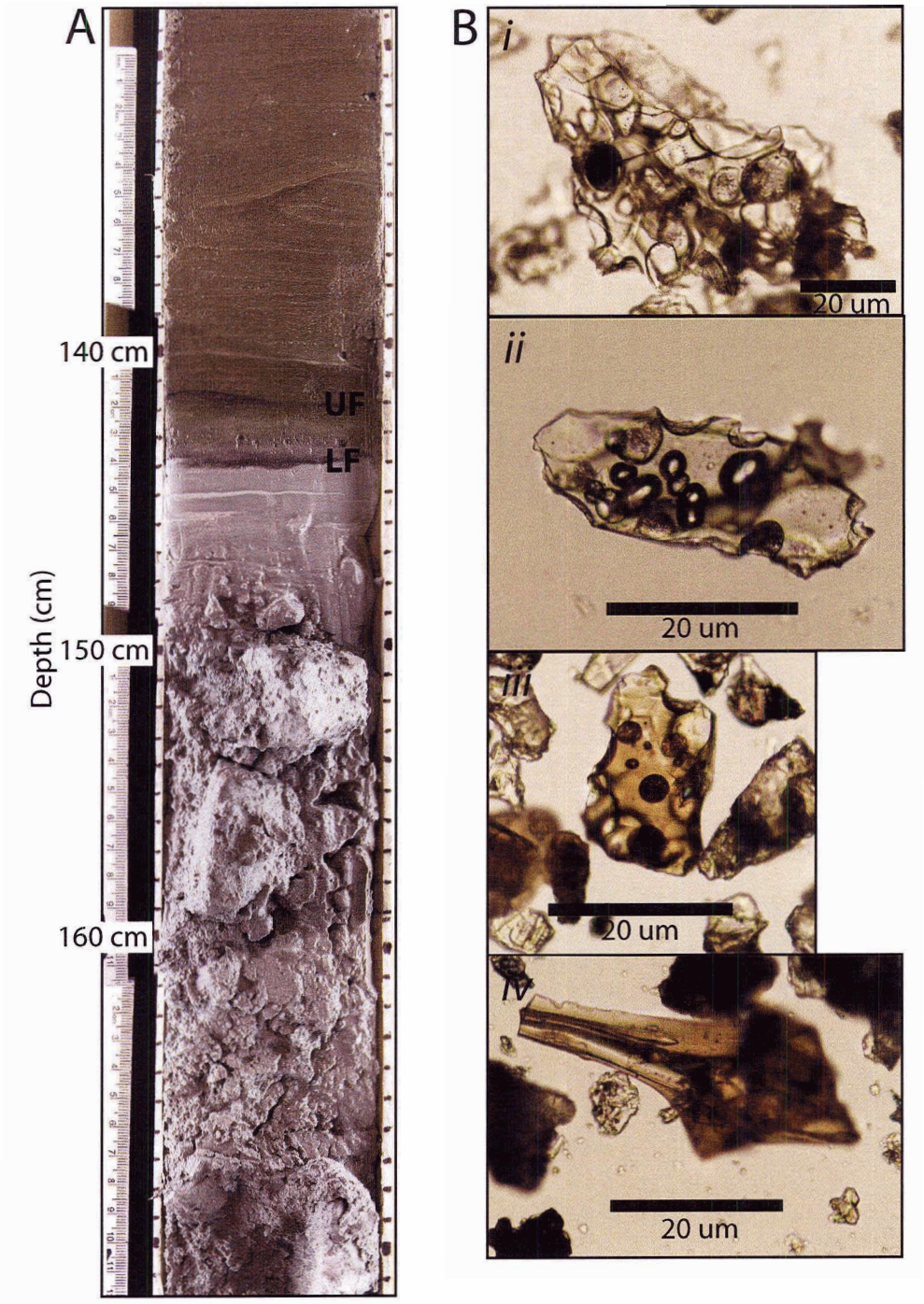


Figure 3.4. A) Sediments from Red Barrel Lake showing the upper (UF) and lower (LF) Finlay tephras. B) Glass shards from the upper (*i, ii*) and lower (*iii, iv*) Finlay tephras. Shards are dominantly blocky with spherical vesicles, but needle-shaped shards with lineated, lensoid vesicles are also present.

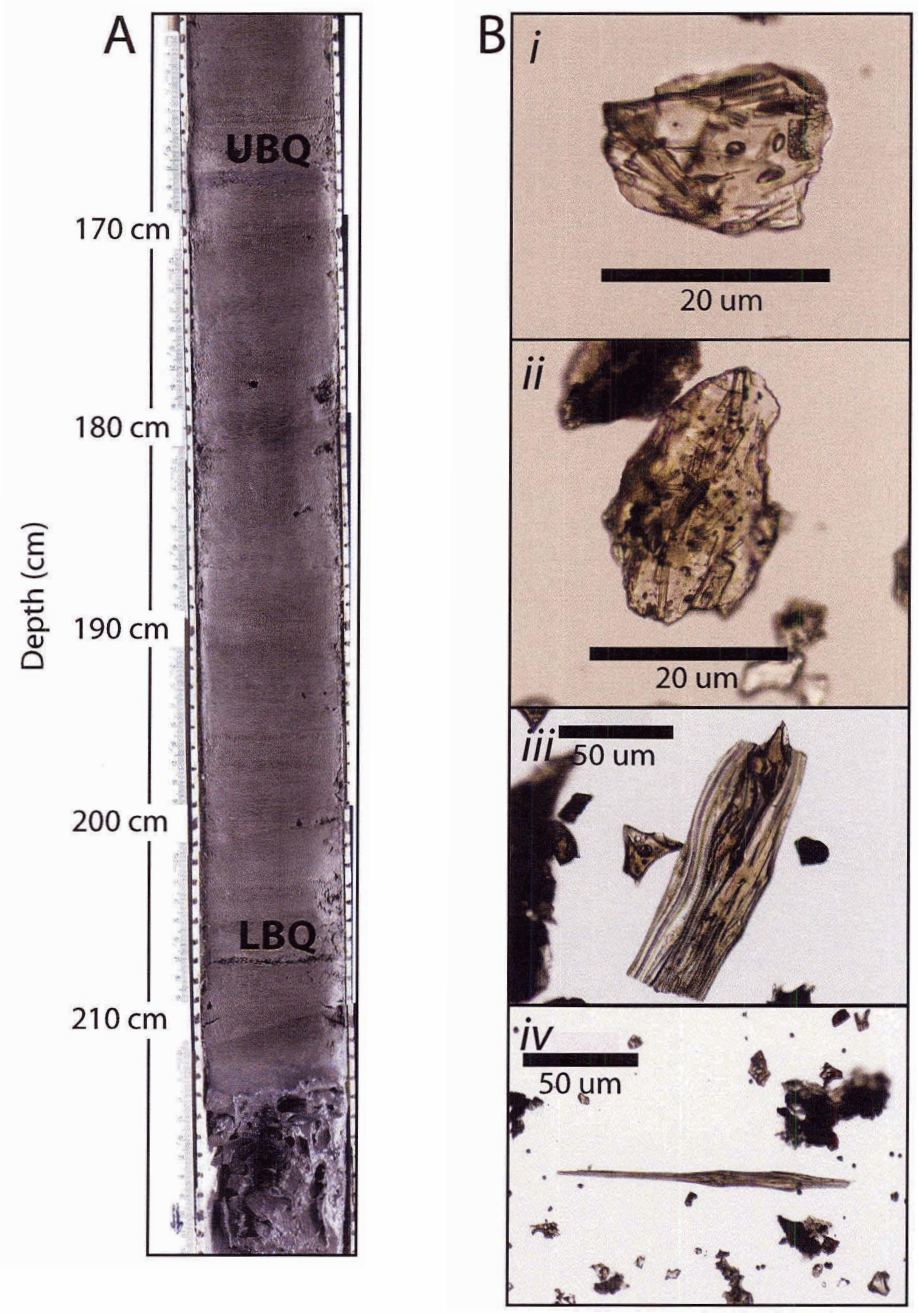


Figure 3.5. A) Sediments from Bob Quinn Lake showing the upper (UBQ) and lower (LBQ) tephras. B) Glass shards from the upper (*i, ii*) and lower (*iii, iv*) Bob Quinn tephra. Shards in the upper tephra are dominantly blocky with spherical vesicles. Shards in the lower tephra are dominantly elongate and needle-shaped with lineated, lensoid vesicles.

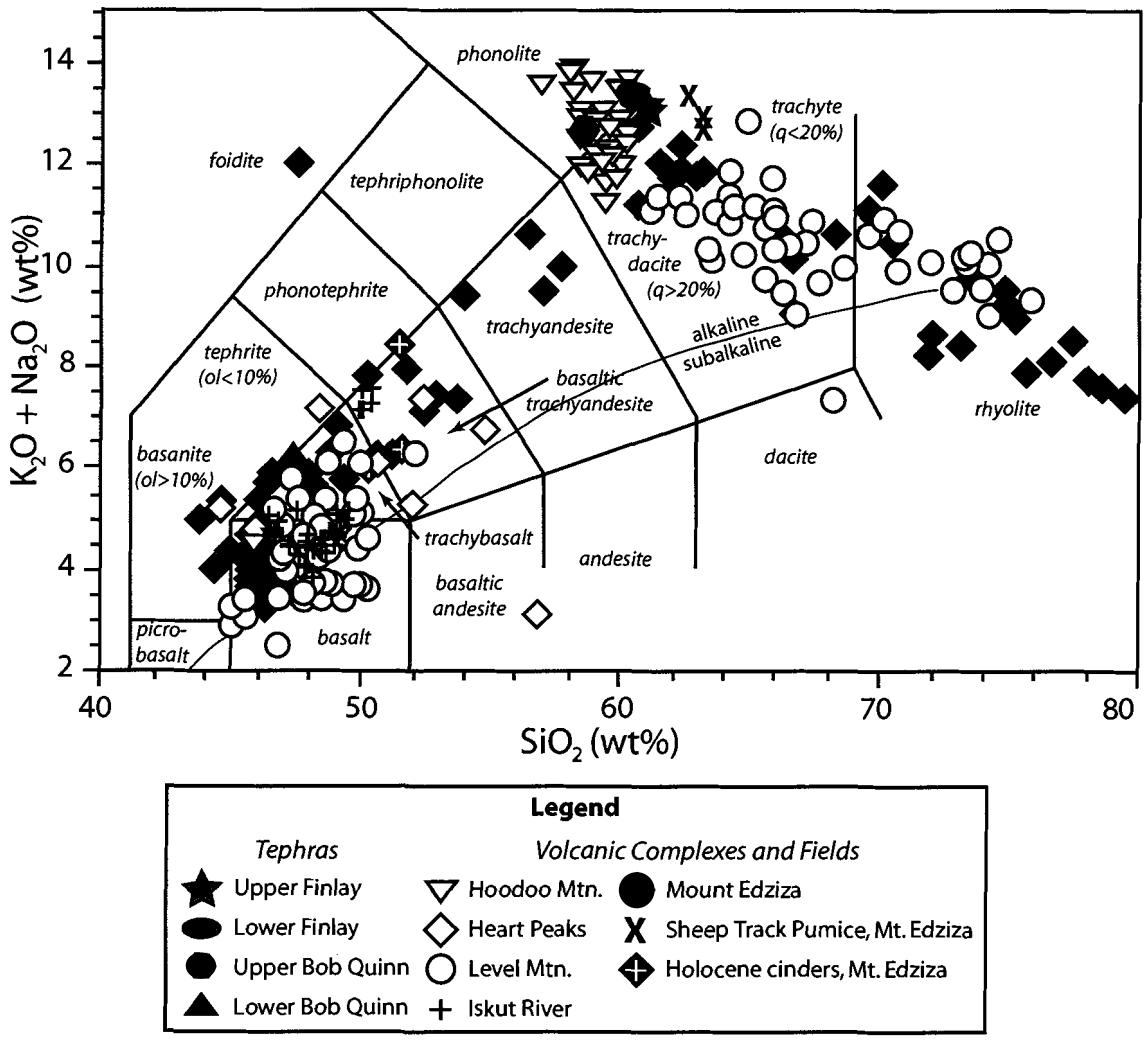


Figure 3.6. Plot of $K_2O + Na_2O$ vs. $SiO_2$ (LeBas et al., 1986) for average values of the Finlay and Bob Quinn tephras and rocks from several volcanic complexes in northwest British Columbia. Modified with permission from Edwards and Russell (2000).

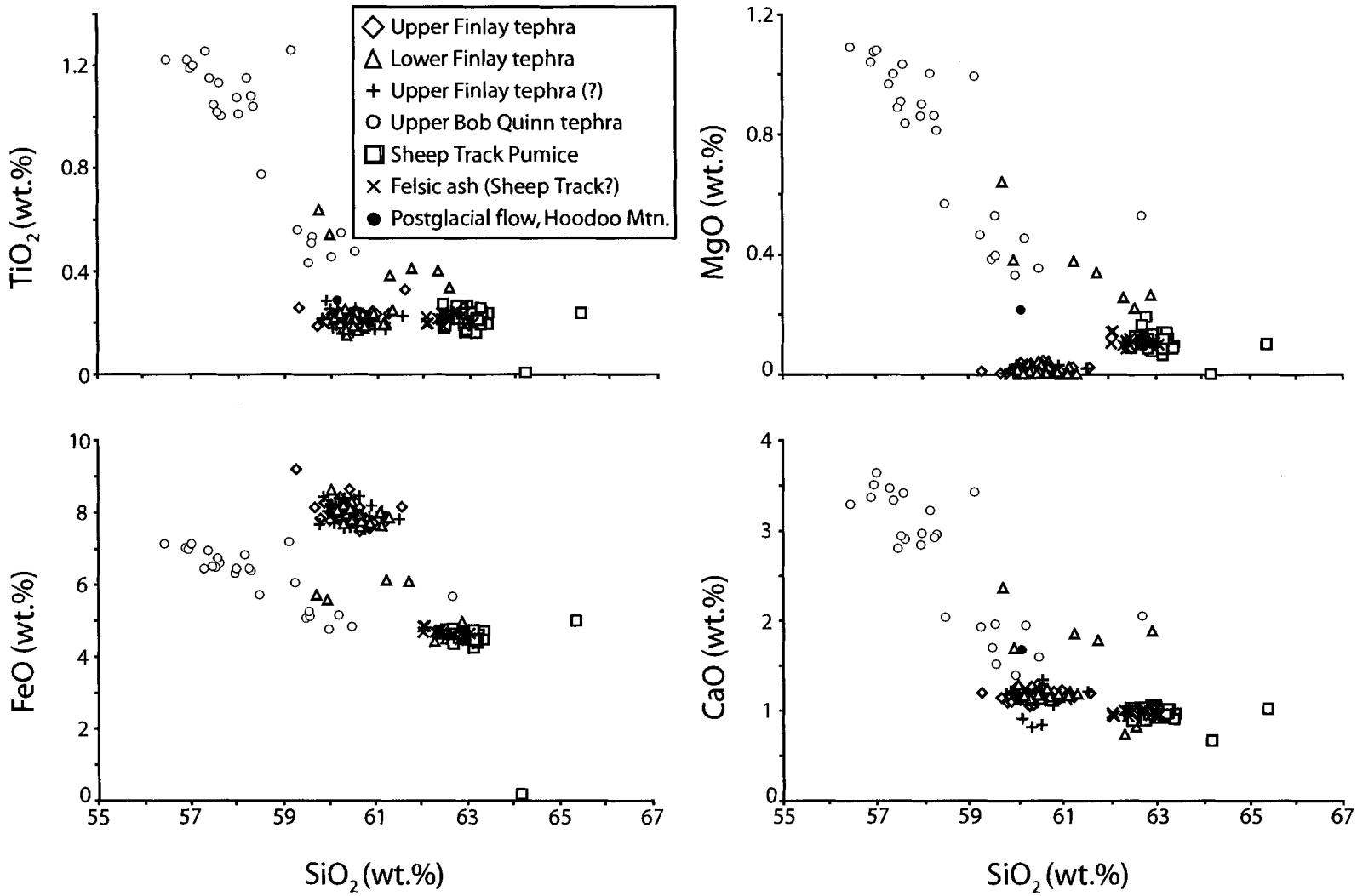


Figure 3.7. Oxide variation diagrams showing compositions of the Finlay and upper Bob Quinn tephras, Sheep Track Pumice (Mount Edziza), and a postglacial phonolitic flow on Hoodoo Mountain. Hoodoo Mountain data from Edwards et al. (2002).

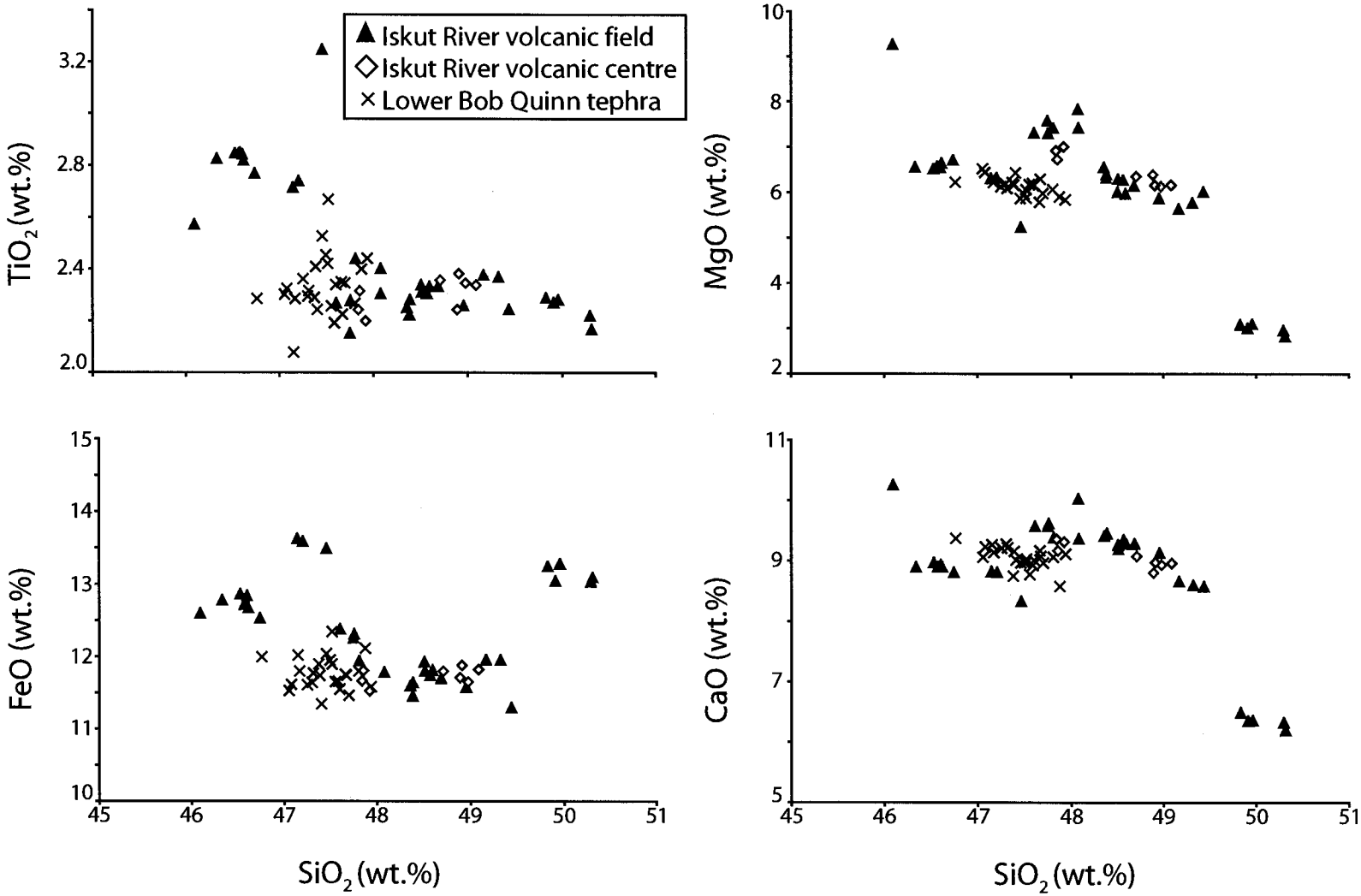


Figure 3.8. Oxide variation diagrams showing the compositions of the lower Bob Quinn tephra and rocks from the Iskut River volcanic field, including the Iskut River volcanic centre. Iskut River data from Russell and Hauksdóttir (2000).

# CHAPTER 4:

## Conclusions

The Finlay moraines of northern British Columbia are late-glacial in age, bracketed by a radiocarbon age of 9230 ± 50 $^{14}$C yr BP and cosmogenic surface exposure ages of about 13,000 $^{14}$C yr BP. They record a regional advance of alpine glaciers during terminal deglaciation of the Canadian Cordillera, which likely coincided with Younger Dryas cooling documented in north-coastal British Columbia. Lateral meltwater channels crosscut late-glacial moraines and record interaction between advancing alpine glaciers and the decaying Cordilleran Ice Sheet, which occupied trunk valleys in the study area. Comparison of the Finlay advance to other, probably correlative, late-glacial advances, such as the Crowfoot advance in the southern Canadian Rocky Mountains, demonstrates variable glacier responses to late-glacial climate change in western North America. The style of deglaciation in the Finlay River area was a significant factor in preserving large alpine glaciers at intermediate and high elevations. These remnant glaciers later advanced when regional equilibrium line fell to 1650-1750 m asl. Differing temperature and precipitation gradients, differing rates and magnitudes of late-glacial climatic change, and the effects of remnant ice masses on local atmospheric circulation also contributed to the complexity of documented late-glacial glacier advances in western North America.

Two, early Holocene phonolitic tephras occur in sediment cores retrieved from lakes nearly 200 km apart in the Finlay River and Dease Lake areas. They lie at the transition from deglacial sediments to postglacial organic-rich mud in the cores. The Finlay tephras are new chronostratigraphic markers for northwest British Columbia.

Their probable source is Hoodoo Mountain, a large volcano of the northern Cordilleran volcanic province. However, Mount Edziza, Level Mountain, and Hearth Peaks cannot be excluded as sources. Two other tephras occur in sediments retrieved from Bob Quinn Lake. The lower Bob Quinn tephra is basaltic and was deposited ca. 8400 $^{14}$C yr ago by an eruption in the Iskut River volcanic field. The upper Bob Quinn tephra is phonolitic and may originate from Mount Edziza or Hoodoo Mountain. Although the tephra is early Holocene, its exact age is unknown. The Bob Quinn tephras serve as valuable late Quaternary marker horizons in the Iskut River area.

Future studies in the region should include efforts to better date the Finlay moraines and the timing of ice sheet retreat in northern British Columbia, and attempts to recover new paleoclimatic records. Bednarski's (1999, 2000, 2001) cosmogenic surface exposure ages from the northern Rocky Mountains provide the first estimates of the time of deglaciation at the eastern margin of the Cordilleran Ice Sheet. More cosmogenic and radiocarbon ages are needed to establish the timing and regional pattern of ice retreat in northern British Columbia. Additional paleoclimatic data from north-coastal British Columbia and northwestern Alberta are needed to evaluate existing late glacial climate records and to improve understanding of late Pleistocene-Holocene climate change in this large, poorly studied region.

More sediment cores from lakes in northern British Columbia will better constrain the age and distribution of the tephras identified in this study and may identify the source vents for the eruptions that produced them. It is likely that additional tephras will be found.

# REFERENCES


Alley, R.B. 2000. The Younger Dryas cold interval as viewed form central Greenland. Quaternary Science Reviews, **19**: 213-226.

Armstrong, J.E. 1981. Post-Vashon Wiconsin glaciation, Fraser Lowland, British Columbia. Geological Survey of Canada, Bulletin 322.

Barrie, J.V., and Conway, K.W. 1999. Late Quaternary glaciation and postglacial stratigraphy of the northern Pacific margin of Canada. Quaternary Research, **51**: 113-123.

Bednarski, J.M. 1999. Preliminary report on mapping surficial geology of Trutch map area, northeastern British Columbia. *In* Current Research 1999-A. Geological Survey of Canada Paper. pp. 35-43.

Bednarski, J.M. 2000. Surficial geology, Trutch, British Columbia. Geological Survey of Canada, Open File 3885.

Bednarski, J.M. 2001. Drift composition and surficial geology of the Trutch map area (94G), northeastern British Columbia. Geological Survey of Canada, Open File 3815.

Begét, J.E., and Motyka, R.J. 1998. New dates on late Pleistocene dacitic tephra from the Mount Edgecumbe volcanic field, southeastern Alaska. Quaternary Research, **49**: 123-125.

Björck, S., Kromer, B., Johnsen, S., Bennike, O., Hammarlund, D., Lemdahl, G., Possnert, G., Rasumussen, T., Wohlfarth, B., Hammer, C., and Spurk, M. 1996. Synchronized terrestrial-atmospheric deglacial records around the North Atlantic. Science, **274**: 1155-1160.

Blaise, B., Clague, J.J., and Mathewes, R.W. 1990. Time of maximum Late Wisconsin glaciation, west coast of Canada. Quaternary Research, **34**: 282-295.

Bobrowsky, P., and Rutter, N.W. 1992. The Quaternary geologic history of the Canadian Rocky Mountains. Géographie physique et Quaternaire, **46**: 5-50.

Bond, J. 2004. Late Wisconsinan McConnell glaciation of the Whitehorse map area (105D), Yukon. *In* Yukon Exploration Geology 2003. Edited by D.S. Emond and L.L. Lewis. Yukon Geological Survey, pp. 73-88.

Bond, J.D., and Kennedy, K.E. 2005. Late Wisconsinan McConnell ice-flow and sediment distribution patterns in the Pelly Mountains, Yukon. *In* Yukon Exploration Geology 2004. Edited by D.S. Emond, L.L. Lewis, and G.D. Bradshaw. Yukon Geological Survey, pp. 67-82.

Briner, J.P., Kaufman, D.S., Werner, A., Caffee, M., Levy, L., Manley, W.F., Kaplan, M.R., and Finkel, R.C. 2002. Glacier readvance during the late glacial (Younger Dryas?) in the Ahklun Mountains, southwestern Alaska. Geology, **30**: 679-682.

Broecker, W.S. 2003. Does the trigger for abrupt climate change reside in the ocean or in the atmosphere? Science, **300**: 1519-1522.

Broecker, W.S. 2006. Was the Younger Dryas triggered by a flood? Science, **312**: 1146-1148.

Broecker, W.S., Kennett, J.P., Flower, B.P., Teller, J.T., Trumbore, S., Bonani, G., and Wolfli, W. 1989. Routing of meltwater from the Laurentide Ice Sheet during the Younger Dryas cold episode. Nature, **341**: 318-321.

Casey, J.J. 1980. Geology of the Heart Peaks Volcanic Centre, northwestern British Columbia. M.Sc. thesis, Department of Geology, University of Alberta, Edmonton, Alberta.

Clague, J.J. 1981. Late Quaternary geology and geochronology of British Columbia. Part 2: Summary and discussion of radiocarbon-dated Quaternary history. Geological Survey of Canada, Paper 80-35.

Clague, J.J. 1985. Deglaciation of the Prince Rupert – Kitimat area, British Columbia. Canadian Journal of Earth Sciences, **22**: 256-265.

Clague, J.J. 1989. Quaternary geology of the Canadian Cordillera. *In* Quaternary Geology of Canada and Greenland. Edited by R.J. Fulton. Geological Survey of Canada, Geology of Canada, no. 1, pp. 15-96.

Clague, J.J., and James, T.S. 2002. History and isostatic effects of the last ice sheet in southern British Columbia. Quaternary Science Reviews, **21**: 71-87.

Clague, J.J., Evans, S.G., Rampton, V.N., and Woodsworth, G.J. 1995. Improved age estimates for the White River and Bridge River tephras, western Canada. Canadian Journal of Earth Sciences, **32**: 1172-1179.

Clague, J.J., Mathewes, R.W., Guilbault, J.-P., Hutchinson, I., and Ricketts, B.D. 1997. Pre-Younger Dryas resurgence of the southwestern margin of the Cordilleran ice sheet, British Columbia, Canada. Boreas, **26**: 261-278.

Clark, P.U., Marshall, S.J., Clarke, G.K.C., Hostetler, S.W., Licciardi, J.M., and Teller, J.T. 2001. Freshwater forcing of abrupt climate change during the last glaciation. Science, **293**: 283-287.

Clark, P.U., Pisias, N.G., Stocker, T.F., and Weaver, A.J. 2002. The role of the thermohaline circulation in abrupt climate change. Nature, **415**: 863-869.

Edwards, B.R. 1997. Field, kinetic and thermodynamic studies of magmatic assimilation in the northern Cordilleran volcanic province, northwestern British Columbia. Ph.D. thesis, Department of Earth and Ocean Sciences, University of British Columbia, Vancouver, British Columbia.

Edwards, B.R., and Russell, J.K. 1999. Northern Cordilleran volcanic province: A northern Basin and Range? Geology, **27**: 243-246.

Edwards, B.R., and Russell, J.K. 2000. Distribution, nature, and origin of Neogene-Quaternary magmatism in the northern Cordilleran volcanic province, Canada. Geological Society of America Bulletin, **122**: 1280-1295.

Edwards, B.R., Russell, J.K., Anderson, R.G., Villeneuve, J., and Hastings, N. 1999. Punctuated, peralkaline, subglacial volcanism at Hoodoo Mountain volcano, northwestern British Columbia, Canada. Abstracts, American Geophysical Union, Fall Meeting, San Francisco, California, V12A-02.

Edwards, B.R., Anderson, R.G., Russell, J.K., Hastings, N.L., and Guo, Y.T. 2000. The Quaternary Hoodoo Mountain Volcanic Complex and Paleozoic and Mesozoic basement rocks, parts of Hoodoo Mountain (NTS 104B/14) and Craig River (104B/11) map areas, northwestern British Columbia. Geological Survey of Canada, Open File Map 3721, scale 1:20,000.

Edwards, B.R., Russell, J.K., and Anderson, R.G. 2002. Subglacial, phonolitic volcanism at Hoodoo Mountain volcano, northern Canadian Cordillera. Bulletin of Volcanology, **64**: 254-272.

Engstrom, D.R., Hansen, B.C.S., and Wright, H.E., Jr. 1990. A possible Younger Dryas record in southeastern Alaska. Science, **250**: 1383-1385.

Environment Canada. 2002. National climate data and information archive [online]. Available from http://www.climate.weatheroffice.ec.gc.ca [Cited 9 September 2006].

Fanning, A.F., and Weaver, A.J. 1997. Temporal-geographical meltwater influences on the North Atlantic Conveyor: implications for the Younger Dryas. Paleoceanography, **12**: 307-320.

Friele, P.A., and Clague, J.J. 2002a. Younger Dryas readvance in Squamish river valley, southern Coast mountains, British Columbia. Quaternary Science Reviews, **21**: 1925-1933.

Friele, P.A., and Clague, J.J. 2002b. Readvance of glaciers in the British Columbia Coast Mountains at the end of the last glaciation. Quaternary International, **87**: 45-58.

Fulton, R.J. 1967. Deglaciation studies in Kamloops region, an area of moderate relief, British Columbia. Geological Survey of Canada, Bulletin 154.

Fulton, R.J. 1991. A conceptual model for growth and decay of the Cordilleran ice sheet. Géographie physique et Quaternaire, **45**: 281-286.

Gosse, J.C., Evenson, E.B., Klein, J., Lawn, B., and Middleton, R. 1995. Precise cosmogenic $^{10}$Be measurements in western North America: Support for a global Younger Dryas cooling event. Geology, **23**: 877-880.

Hamilton, T.S. 1981. Late Cenozoic alkaline volcanics of the Level Mountain Range, northwestern British Columbia: geology, petrology, and palaeomagnetism. Ph.D. thesis, Department of Geology, University of Alberta, Edmonton, Alberta.

Hamilton, T.S. 1991. Level Mountain. *In* Volcanoes of North America. *Edited by* C.A. Wood and J. Kienle. Cambridge University Press, New York, pp. 121-123.

Hansen, B.C.S., and Engstrom, D.R. 1996. Vegetation history of Pleasant Island, southeastern Alaska, since 13,000 yr BP. Quaternary Science Reviews, **46**: 161-175.

Hendy, I.L., Kennett, J.P., Roark, E.B., and Ingram, B.L. 2002. Apparent synchroneity of submillennial scale climate events between Greenland and Santa Barbara Basin, California from 30-10 ka. Quaternary Science Reviews, **21**: 1167-1184.

Hetherington, R., and Reid, R.G.B. 2003. Malacological insights into the marine ecology and changing climate of the late Pleistocene – early Holocene Queen Charlotte Islands archipelago, western Canada, and implications for early peoples. Canadian Journal of Zoology, **81**: 626-661.

Heusser, C.J. 1960. Late Pleistocene environments of North Pacific North America. American Geographical Society, Special Publication 35.

Hu, F.S., Brubaker, L.B., and Anderson, P.M. 1995. Postglacial vegetation and climate change in the northern Bristol Bay region, southwestern Alaska. Quaternary Research, **43**: 382-392.

Hu, F.S., Lee, B.Y., Kaufman, D.S., Yoneji, S., Nelson, D.M., and Henne, P.D. 2002. Response of tundra ecosystem in southwestern Alaska to Younger-Dryas climatic oscillation. Global Change Biology, **8**: 1156-1163.

Hughes, O.L. 1990. Surficial geology and geomorphology, Aishihik Lake, Yukon Territory. Geological Survey of Canada, Paper 87-29.

Jackson, L.E., Jr., Ward, B., Duk-Rodkin, A., and Hughes, O.L. 1991. The last Cordilleran Ice Sheet in southern Yukon Territory. Géographie physique et Quaternaire, **45**: 341-354.

Kennedy, K.E., and Bond, J.D. 2004. Evidence for a late-McConnell readvance of the Cassiar Lobe in Seagull Creek, Pelly Mountains, central Yukon. *In* Yukon Exploration Geology 2003. Edited by D.S. Emond and L.L. Lewis. Yukon Geological Survey, pp. 121-128.

Kovanen, D.J., and Easterbrook, D.J. 2001. Late Pleistocene, post-Vashon, alpine glaciation of the Nooksack drainage, North Cascades, Washington. Geological Society of America Bulletin, **113**: 274-288.

Lacourse, T. 2005. Late Quaternary dynamics of forest vegetation on northern Vancouver Island, British Columbia, Canada. Quaternary Science Reviews, **24**: 105-121.

LeBas, M.J., LeMaitre, R.W., Streckeisen, A., and Zanettin, B. 1986. A chemical classification of volcanic rocks based on the total alkali-silica diagram. Journal of Petrology, **27**: 745-750.

Lehman, S.L., and Keigwin, L.D. 1992. Sudden changes in North Atlantic circulation during the last glaciation. Nature, **356**: 757-762.

Lerbekmo, J.F., and Campbell, F.A. 1969. Distribution composition and source of White River ash, Yukon Territory. Canadian Journal of Earth Sciences, **6**: 109-116.

Lerbekmo, J.F., Westgate, J.A., Smith, D.G.W., and Denton, G.H. 1975. New data on the character and history of the White River volcanic eruption, Alaska. *In* Quaternary Studies. Edited by Suggate, R.P., and Cresswell, M.M. The Royal Society of New Zealand, Wellington, pp. 203-209.

Licciardi, J.M., Clark, P.U., Brook, E.J., Elmore, D., and Sharma, P. 2004. Variable responses of western U.S. glaciers during the last deglaciation. Geology, **32**: 81-84.

Mangan, M.T., Waythomas, C.F., Miller, T.P., and Trusdell, F.A. 2003. Emmons Lake Volcanic Center, Alaska Peninsula: Source of the Late Wisconsin Dawson tephra, Yukon Territory, Canada. Canadian Journal of Earth Sciences, **40**: 925-936.

Mann, D.H., and Hamilton, T.D. 1995. Late Pleistocene and Holocene paleoenvironments of the north Pacific coast. Quaternary Science Reviews, **14**: 449-471.

Mathewes, R.W. 1993. Evidence for Younger Dryas – age cooling on the North Pacific coast of America. Quaternary Science Reviews, **12**: 321-331.

Mathewes, R.W., Heusser, L.E., and Patterson, R.T. 1993. Evidence for a Younger Dryas – like event on the British Columbia coast. Geology, **21**: 101-104.

Mathews, W.H. 1980. Retreat of the last ice sheets in northeastern British Columbia and adjacent Alberta. Geological Survey of Canada, Bulletin 331.

Mathews, W.H. 1986. Physiographic map of the Canadian Cordillera. Geological Survey of Canada, Map 1701A, scale 1:5 million.

Mayewski, P.A., Meeker, L.D., Whitlow, S., Twickler, M.S., Morrison, M.C., Alley, R.B., Bloomfield, P., and Taylor, K. 1993. The atmosphere during the Younger Dryas. Science, **261**: 195-197.

McCuaig, S.J., and Roberts, M.C. 2002. Topographically-independent ice flow in northwestern British Columbia: Implications for Cordilleran Ice Sheet reconstruction. Journal of Quaternary Science, **17**: 341-348.

McKenzie, G.D. 1970. Some properties and age of volcanic ash in Glacier Bay National Monument. Arctic, **23**: 46-49.

Meidinger, D., and Pojar, J. 1991. Ecosystems of British Columbia. British Columbia Ministry of Forests, Victoria, British Columbia.

Meissner, K.J., and Clark, P.U. 2006. Impact of floods versus routing events on the thermohaline circulation. Geophysical Research Letters, **33**: Art. No. L15704.

Menounos, B., and Reasoner, M. A. 1997. Evidence for cirque glaciation in the Colorado Front Range during the Younger Dryas Chronozone. Quaternary Research, **48**: 38-47.

Mikolajewicz, U., Crowley, T.J., Schiller, A., and Voss, R. 1997. Modelling teleconnections between the North Atlantic and North Pacific during the Younger Dryas. Nature, **387**: 384-387.

Osborn, G., and Gerloff, L. 1997. Latest Pleistocene and early Holocene fluctuations of glaciers in the Canadian and northern American Rockies. Quaternary International, **38/39**: 7-19.

Osborn, G.D, Robinson, B.J., and Luckman, B.H. 2001. Holocene and latest Pleistocene fluctuations of Stutfield Glacier, Canadian Rockies. Canadian Journal of Earth Sciences, **38**: 1141-1155.

Owen, L.A., Finkel, R.C., Minnich, R.A., and Perez, A.E. 2003. Extreme southwestern margin of the late Quaternary glaciation in North America: Timing and controls. Geology, **31**: 729-732.

Patterson, R.T., Guilbault, J.P., Thomson, R.E., and Luternauer, J.L. 1995. Foraminiferal evidence of Younger Dryas age cooling on the British Columbia shelf. Géographie physique et Quaternaire, **49**: 409-427.

Peltier, W.R., Vettoretti, G., and Stastna, M. 2006. Atlantic meridional overturning and climate response to Arctic Ocean freshening. Geophysical Research Letters, **33**: Art. No. L06713.

Peteet, D. (Editor). 1995. Global Younger Dryas? Quaternary Science Reviews, **14**.

Peteet, D.M., and Mann, D.H. 1994. Late-glacial vegetational, tephra, and climatic history of southwestern Kodiak Island, Alaska. Ecoscience, **1**: 255-267.

Porter, S. C. 1975. Equilibrium line altitudes of late Quaternary glaciers in the Southern Alps, New Zealand. Quaternary Research, **5**: 27-47.

Preece, S.J., Westgate, J.A., and Gorton, M.P. 1992. Compositional variation and provenance of late Cenozoic distal tephra beds, Fairbanks area, Alaska. Quaternary International, **13/14**: 97-101.

Preece, S.J., Westgate, J.A., Stemper, B.A., and Péwé, T.L. 1999. Tephrochronology of late Cenozoic loess at Fairbanks, central Alaska. Geological Society of America Bulletin, **111**: 71-90.

Read, P.B., Brown, R.L., Psutka, J.F., Moore, J.M., Journeay, M., Lane, L.S., and Orchard, M.J. 1989. Geology of parts of Snippaker Creek (104B/10), Forrest Kerr Creek (104B/15), Bob Quinn Lake (104B/16), Iskut River (104G/1) and More Creek (104G/2). Geological Survey of Canada, Open File 2094.

Reasoner, M.A. 1993. Equipment and procedure improvements for a lightweight, inexpensive, percussion core sampling system. Paleolimnology, **8**: 273-281.

Reasoner, M.A., Osborn, G., and Rutter, N.W. 1994. Age of the Crowfoot advance in the Canadian Rocky Mountains: A glacial event coeval with the Younger Dryas oscillation. Geology, **22**: 439-442.

Reimer P.J., Baillie, M.G.L., Bard, E., Bayliss, A., Beck, J.W., Bertrand, C., Blackwell, P.G., Buck, C.E., Burr, G., Cutler, K.B., Damon, P.E., Edwards, R.L., Fairbanks, R.G., Friedrich, M., Guilderson, T.P., Hughen, K.A., Kromer, B., McCormac, F.G., Manning, S., Bronk Ramsey, C., Reimer, R.W., Remmele, S., Southon, J.R., Stuiver, M., Talamo, S., Taylor, F.W., van der Plicht, J., and Weyhenmeyer, C.E. 2004. IntCal04 terrestrial radiocarbon age calibration, 0 – 26 cal kyr BP. Radiocarbon, **46**: 1029-1058.

Richter, D.H., Preece, S.J., McGimsey, R.G., and Westgate, J.A. 1995. Mount Churchill, Alaska – Source of the late Holocene White River ash. Canadian Journal of Earth Sciences, **32**: 741-748.

Riedel, J.L., Clague, J.J., Scott, K.M., and Swanson, T. 2003. Late Fraser alpine glacier activity in the North Cascades, Washington. Geological Society of America, Abstracts with Programs Vol. 35, pp. 216.

Riehle, J.R., Mann, D.H., Peteet, D.M., Engstrom, D.R., Brew, D.A., and Meyer, C.E. 1992. The Mount Edgecumbe tephra deposits, a marker horizon in southeastern Alaska near the Pleistocene-Holocene boundary. Quaternary Research, **37**: 183-202.

Roots, E.F. 1954. Geology and mineral deposits of Aiken Lake map-area, British Columbia. Geological Survey of Canada, Memoir 274.

Russell, J.K., and Hauksdóttir, S. 2000. Estimates of crustal assimilation in Quaternary lavas from the northern Cordillera, British Columbia. The Canadian Mineralogist, **39**: 275-297.

Ryder, J.M., and Maynard, D., 1991. The Cordilleran Ice Sheet in northern British Columbia. Géographie physique et Quaternaire, **45**: 355-363.

Saunders, I.R., Clague, J.J., and Roberts, M.C. 1987. Deglaciation of Chilliwack River valley, British Columbia. Canadian Journal of Earth Sciences, **24**: 915-923.

Souch, C. 1989. New radiocarbon dates for early deglaciation from the southeastern Coast Mountains of British Columbia. Canadian Journal of Earth Sciences, **26**: 2169-2171.

Souther, J.G. 1992. The Late Cenozoic Mount Edziza Volcanic Complex, British Columbia. Geological Survey of Canada, Memoir 420.

Souther, J.G., and Yorath, C.J. 1991. Neogene assemblages. *In* Geology of the Cordilleran Orogen, Canada. *Edited by* Gabrielse, H., and Yorath, C.J. Geological Survey of Canada, Geology of Canada, no. 4, pp. 373-401.

Steig, E.J., Brook, E.J., White, J.W.C., Sucher, C.M., Bender, M.L., Lehman, S.J., Morse, D.L., Waddington, E.D., and Clow, G.D. 1998. Synchronous climate changes in Antarctica and the North Atlantic. Science, **282**: 92-95.

Stumpf, A.J., Broster, B.E., and Levson, V.M. 2000. Multiphase flow of the late Wisconsinan Cordilleran ice sheet in western Canada. Geological Society of America Bulletin, **112**: 1850-1863.

Tallman, A.M. 1975. Glacial and periglacial geomorphology of the Fourth of July Creek valley, Atlin region, Cassiar district, northwestern British Columbia. Ph.D. thesis, Michigan State University, East Lansing, Michigan.

Tarasov, L., and Peltier, W.R. 2005. Arctic freshwater forcing of the Younger Dryas cold reversal. Nature, **435**: 662-665.

Tarasov, L., and Peltier, W.R. 2006. A calibrated deglacial drainage chronology for the North American continent: Evidence of an Arctic trigger for the Younger Dryas. Quaternary Science Reviews, **25**: 659-688.

Teller, J.T., Leverington, D.W., and Mann, J.D. 2002. Freshwater outbursts to the oceans from glacial Lake Agassiz and their role in climate change during the last deglaciation. Quaternary Science Reviews, **21**: 879-887.

Teller, J.T., Boyd, M., Yang, Z., Kor, P.S.G., and Fard, A.M. 2005. Alternative routing of Lake Agassiz overflow during the Younger Dryas: New dates, paleotopography, and a re-evaluation. Quaternary Science Reviews, **24**: 1890-1905.

Villeneuve, M.E., Whalen, J.B., Edwards, B.R., and Anderson, R.G. 1998. Time-scales of episodic magmatism in the Canadian Cordillera as determined by 40Ar-39Ar geochronology. Geological Association of Canada – Mineralogical Association of Canada, Annual Meeting, Program with Abstracts, Quebec City, Quebec, A192.

Watson, K. de P., and Mathews, W.H. 1944. The Tuya-Teslin area, northern British Columbia. British Columbia Department of Mines, Bulletin 19.

Westgate, J.A., Preece, S.J., Kotler, E., and Hall, S. 2000. Dawson tephra: A prominent stratigraphic marker of Late Wisconsinan age in west-central Yukon, Canada. Canadian Journal of Earth Sciences, **37**: 621-627.

Yehle, L.A. 1974. Reconnaissance engineering geology of Sitka and vicinity, Alaska, with emphasis on evaluation of earthquake and other geologic hazards. United States Geological Survey, Open File Report 74-53

# APPENDIX A:

## Map of glacial landforms and deposits (See CD inside back cover)

### Instructions

The appended compact disc (CD) contains an Adobe PDF file that contains a hillshaded digital elevation model (DEM) map of glacial landforms and deposits in the Finlay River area. The map is part of NTS 94/E. The file can be viewed using the program Adobe Acrobat. The hillshaded map was produced with permission using digital elevation data from the Province of British Columbia, Base Mapping and Geomatic Services Branch.

# APPENDIX B:

## Equilibrium line altitude reconstructions

I estimated equilibrium line altitudes of former alpine glaciers in the Finlay River area using the accumulation area ratio (AAR) method of Porter (1975) and assuming an accumulation area ratio of 0.60. An accumulation area ratio of 0.60 means that the accumulation area of the glaciers that constructed the late-glacial moraines was 60% of the total glacier area.

The margins of three former alpine glaciers that did not coalesce with trunk valley ice were estimated from lateral and terminal moraines and trimlines. The former glacier surfaces were reconstructed by drawing contour lines perpendicular to the lateral moraines and trimlines. The hypsometry of reconstructed glacier surfaces was calculated in a GIS, and the equilibrium line altitudes were then estimated using the accumulation area ratio of 0.60. The reconstructions indicate that the regional equilibrium line altitude was 1650-1750 m asl at the time the late-glacial moraines were constructed.

Little Ice Age equilibrium line altitudes were calculated using the same procedure. For Little Ice Age glaciers, however, the ground surface was used to approximate the former glacier surfaces, which is reasonable given the position of Little Ice Age moraines near present-day glacier margins. The equilibrium line altitude during the Little Ice Age was determined to be 1900-1950 m asl.

# APPENDIX C:

## Lake sediment core data

# Appendix C: Legend

Organic-rich mud

Sandy silt

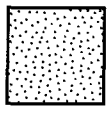

Sand

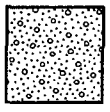

Sand and gravel

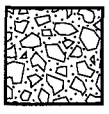

Diamicton

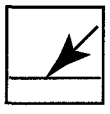

Tephra

| | |
|---|---|
| UF | Upper Finlay tephra |
| LF | Lower Finlay tephra |
| UBQ | Upper Bob Quinn tephra |
| LBQ | Lower Bob Quinn tephra |

## Black Lake
Core: 05-Black(01)
Location: 57°13.686'N, 127°03.115'W

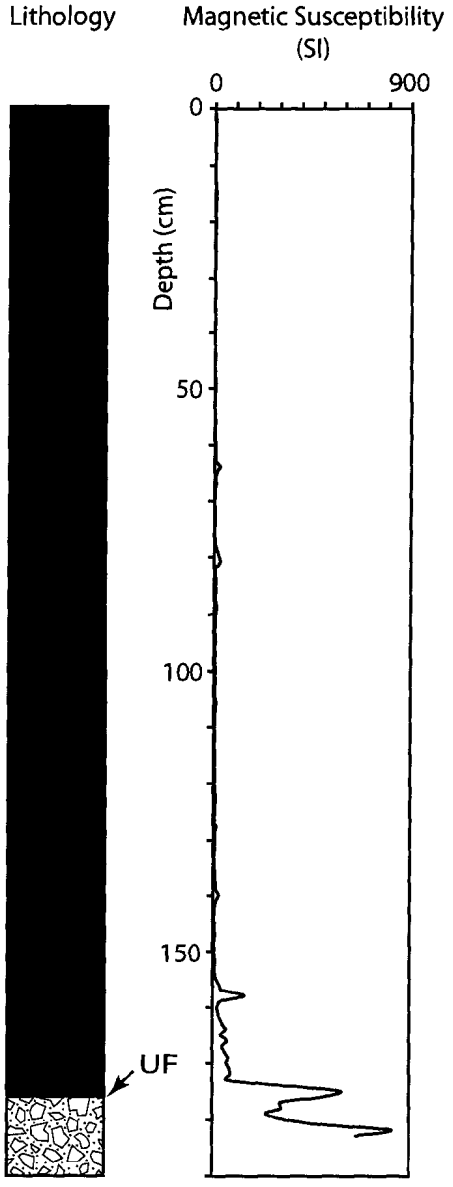

## Bob Quinn Lake
Core: 06-BobQ(01)
Location: 56°58.573' N, 130°15.623' W

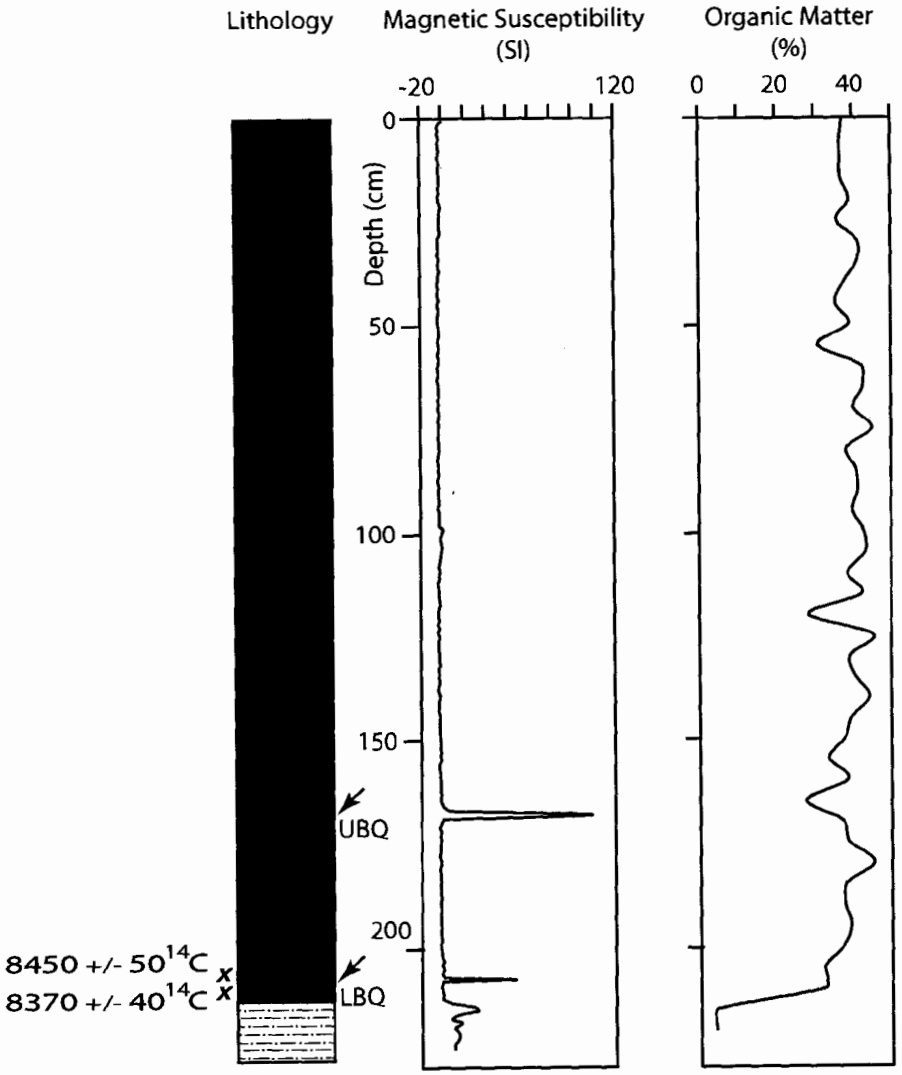

## Bronlund Lake

Core: 05-Bron(01)

Location: 57°25.463' N, 126°35.460' W

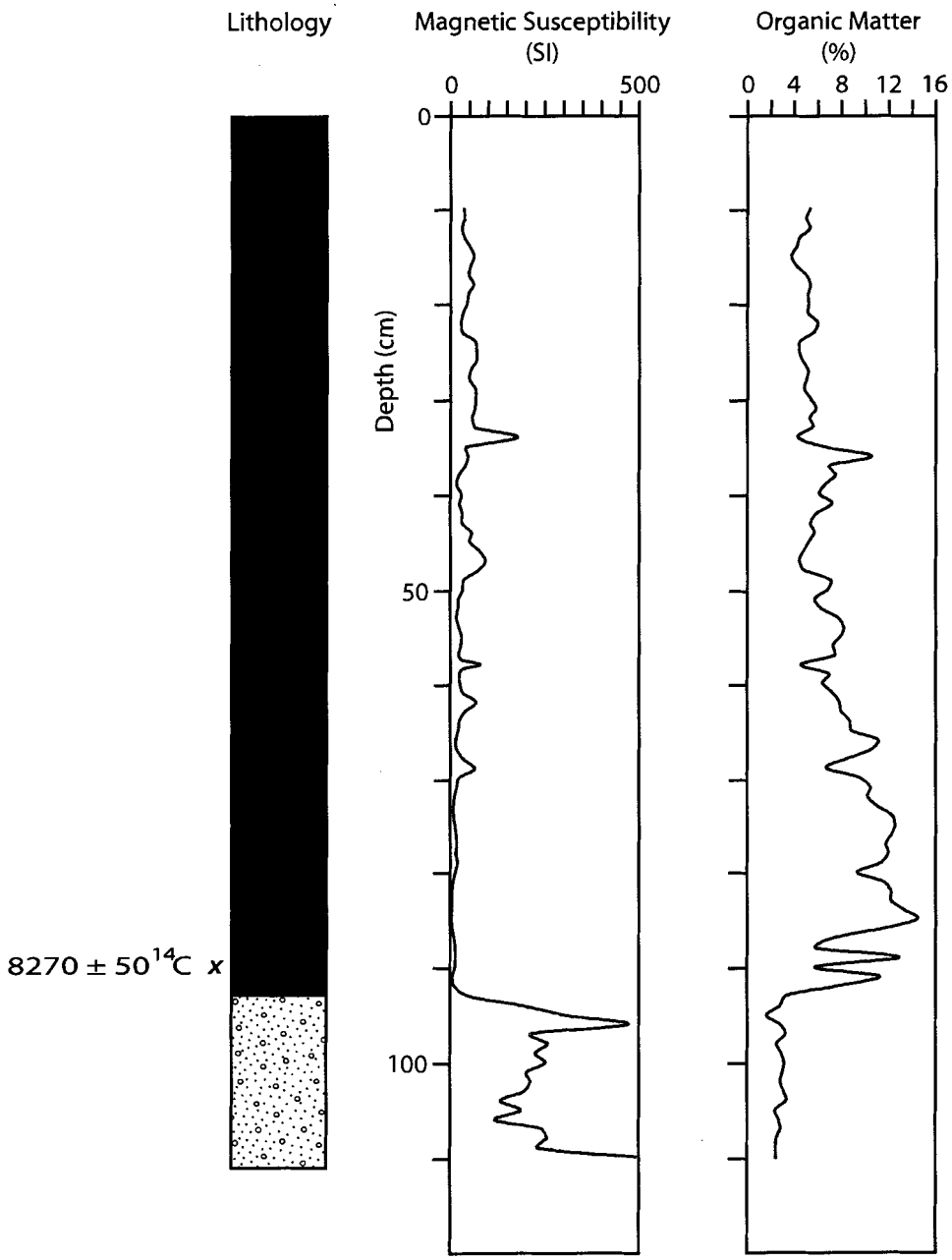

## Cushing Lake
Core: 05-Cushing(01)
Location: 57° 35.541' N, 126° 54.566' W

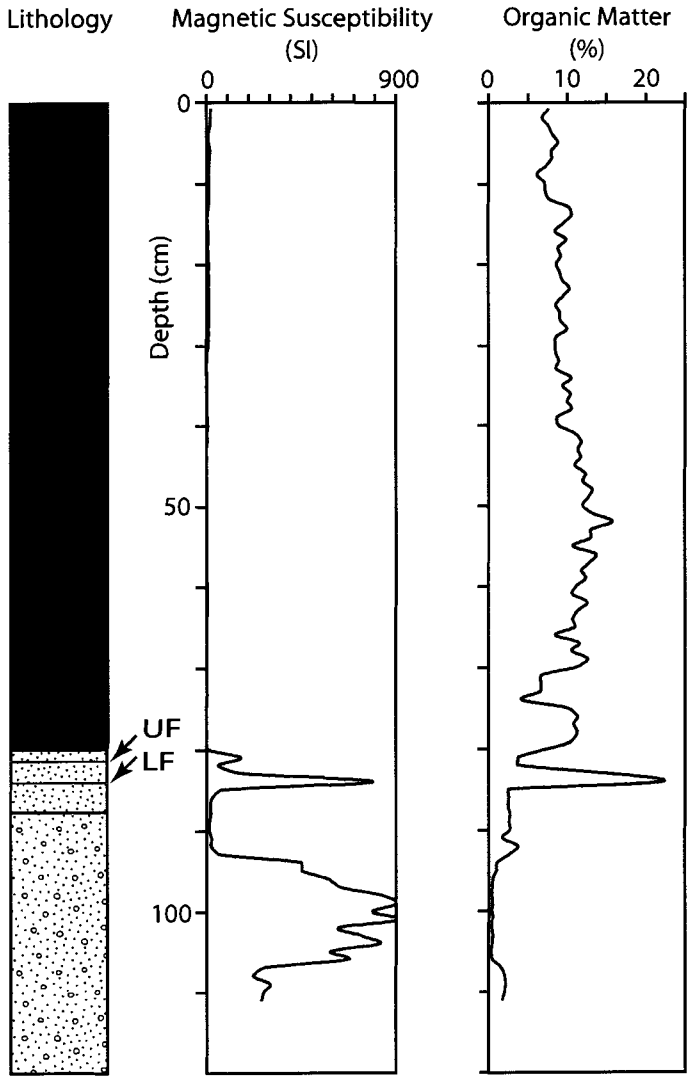

## Cushing Lake
Core: 05-Cushing(02)
Location: 57°35.607' N, 126°54.450' W

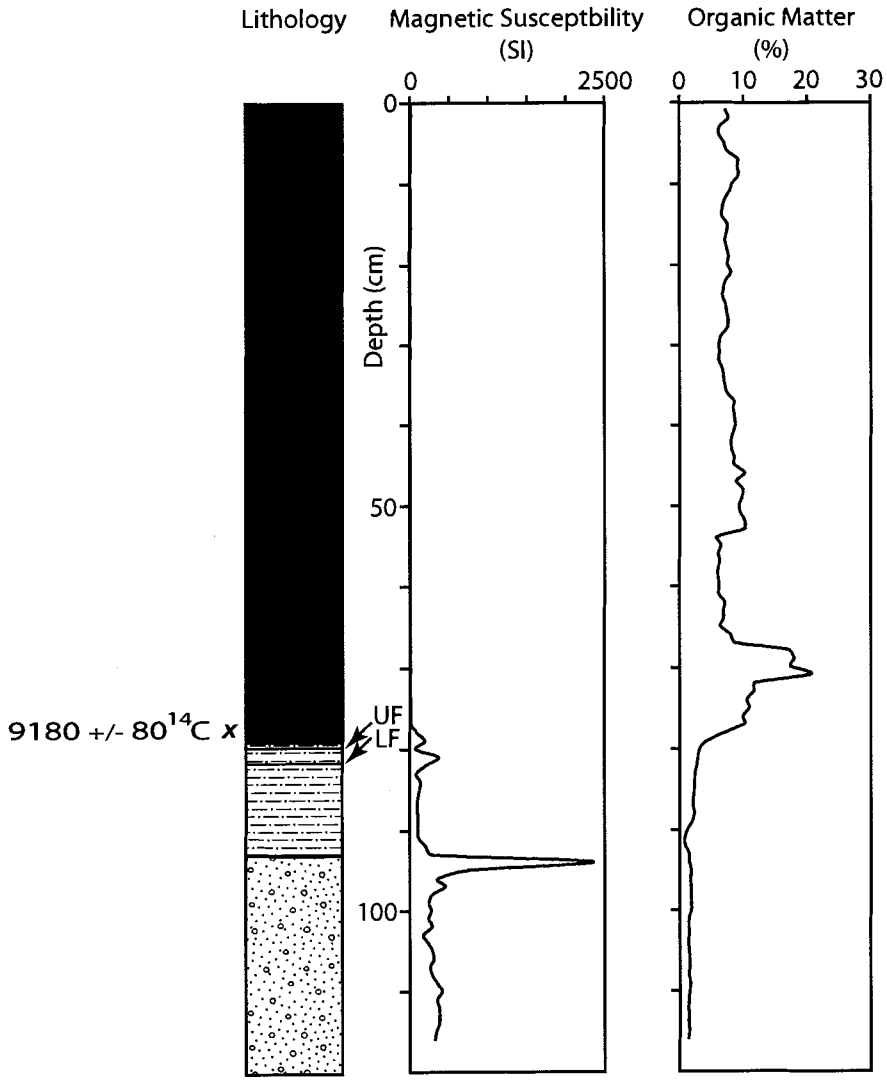

## Deep Lake
Core: 05-Deep(01)
Location: 57°40.943′ N, 126°46.372′ W

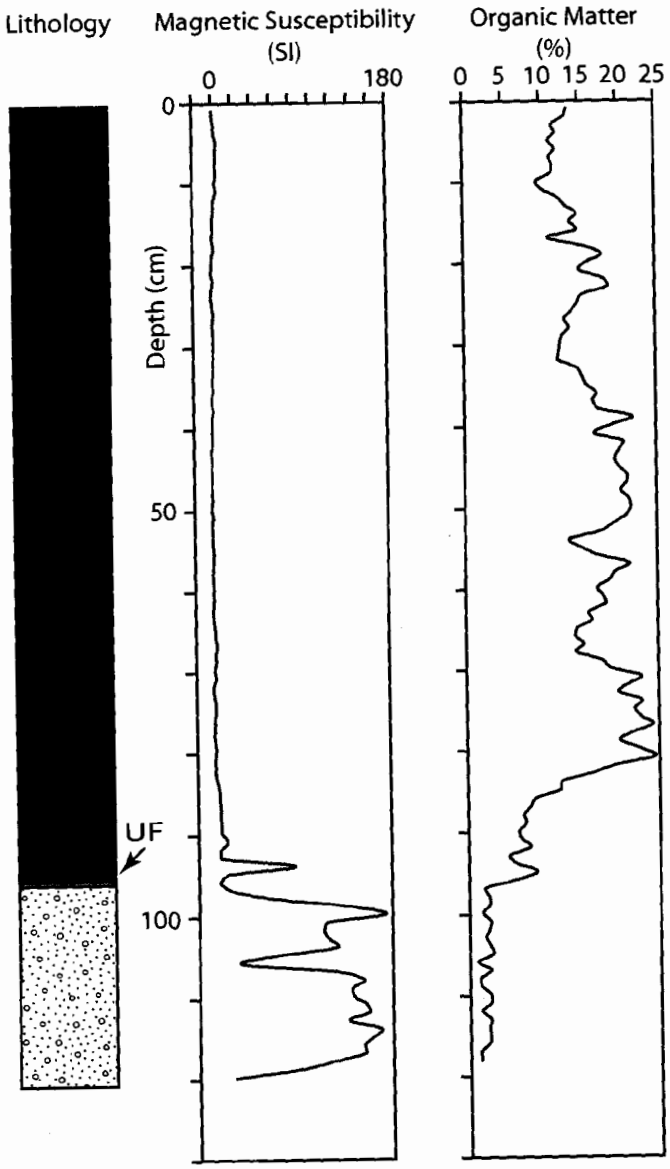

## Hungry Lake
Core: 06-Hungry(01)
Location: 58° 04.325' N, 129° 18.970' W

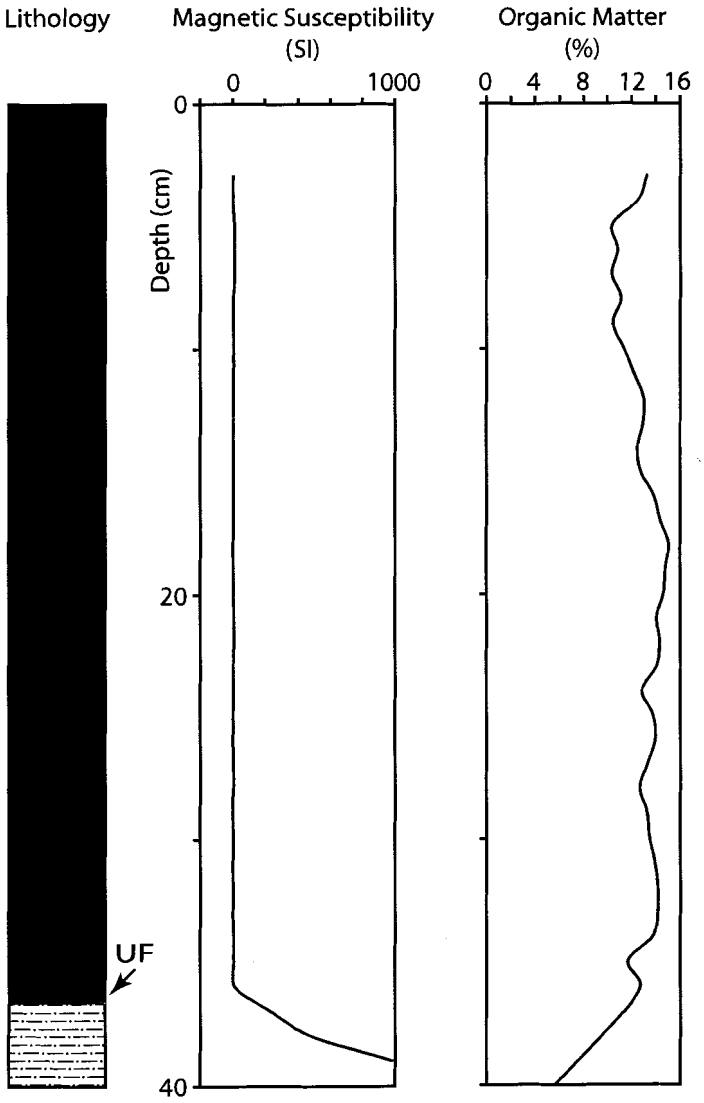

## Hungry Lake
Core: 06-Hungry(02)
Location: 58° 04.325' N, 129° 18.970' W

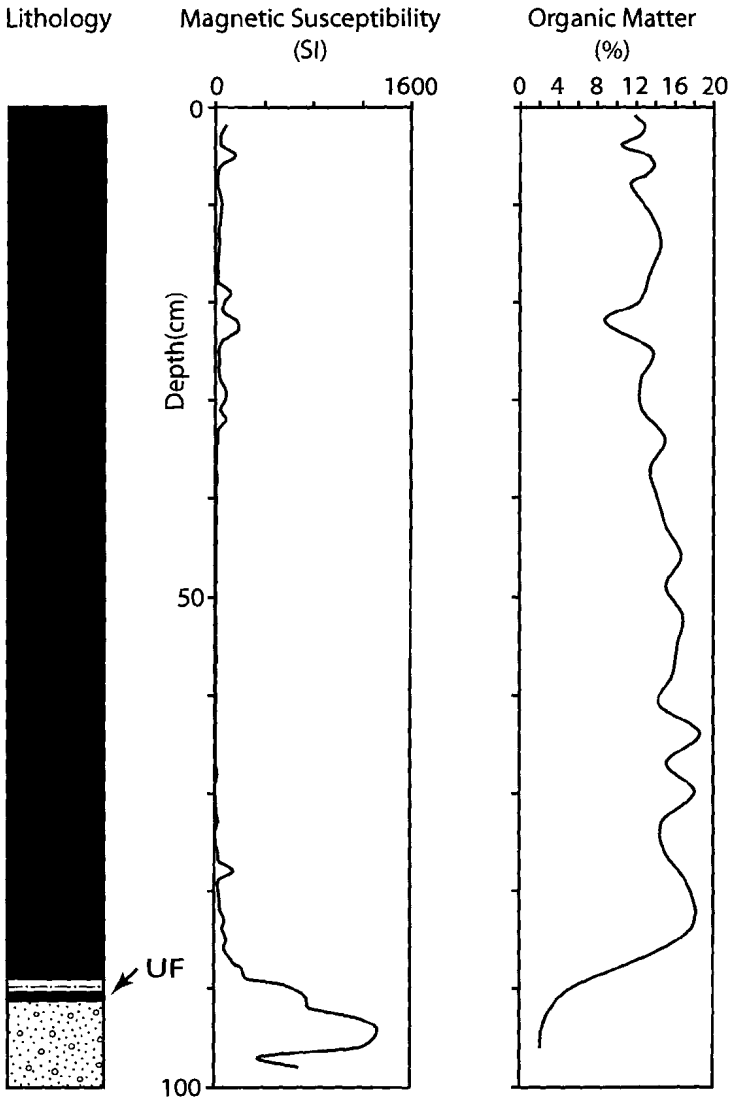

## Katharine Lake
Core: 05-Kath(01)
Location: 57°26.643′ N, 126°48.582′ W

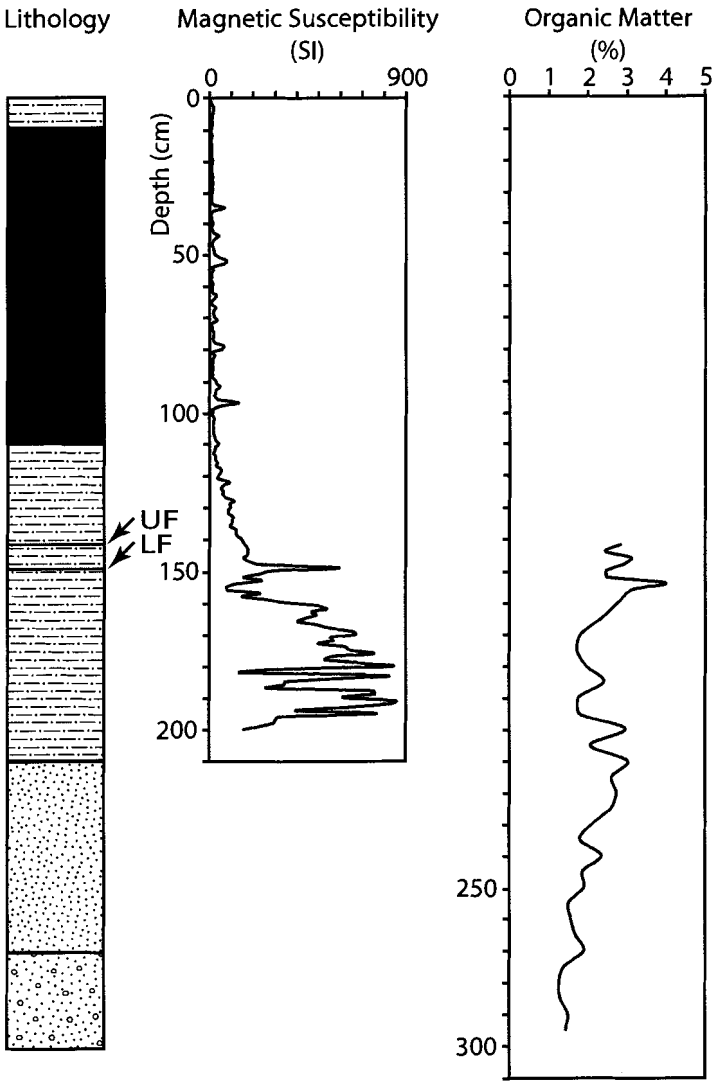

## Little Glacier Lake
Core: 06-LGLAK(01)
Location: 58° 13.243' N, 129° 20.759' W

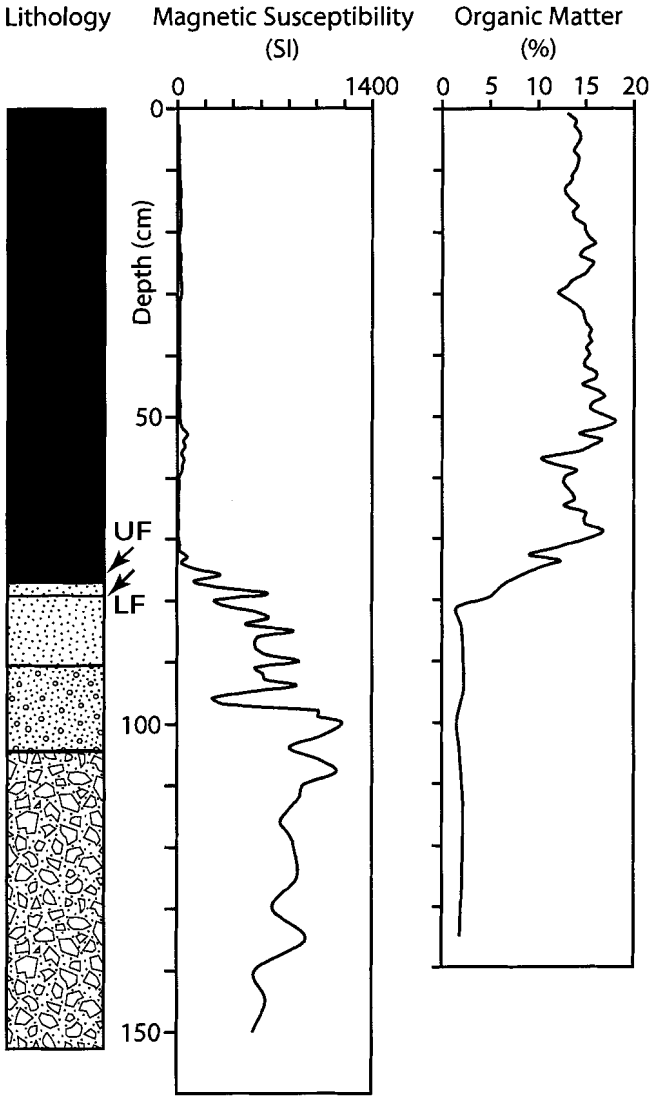

## Red Barrel Lake

Core: 05-RedBarrel(02)

Location: 57°40.623' N, 126°44.029' W

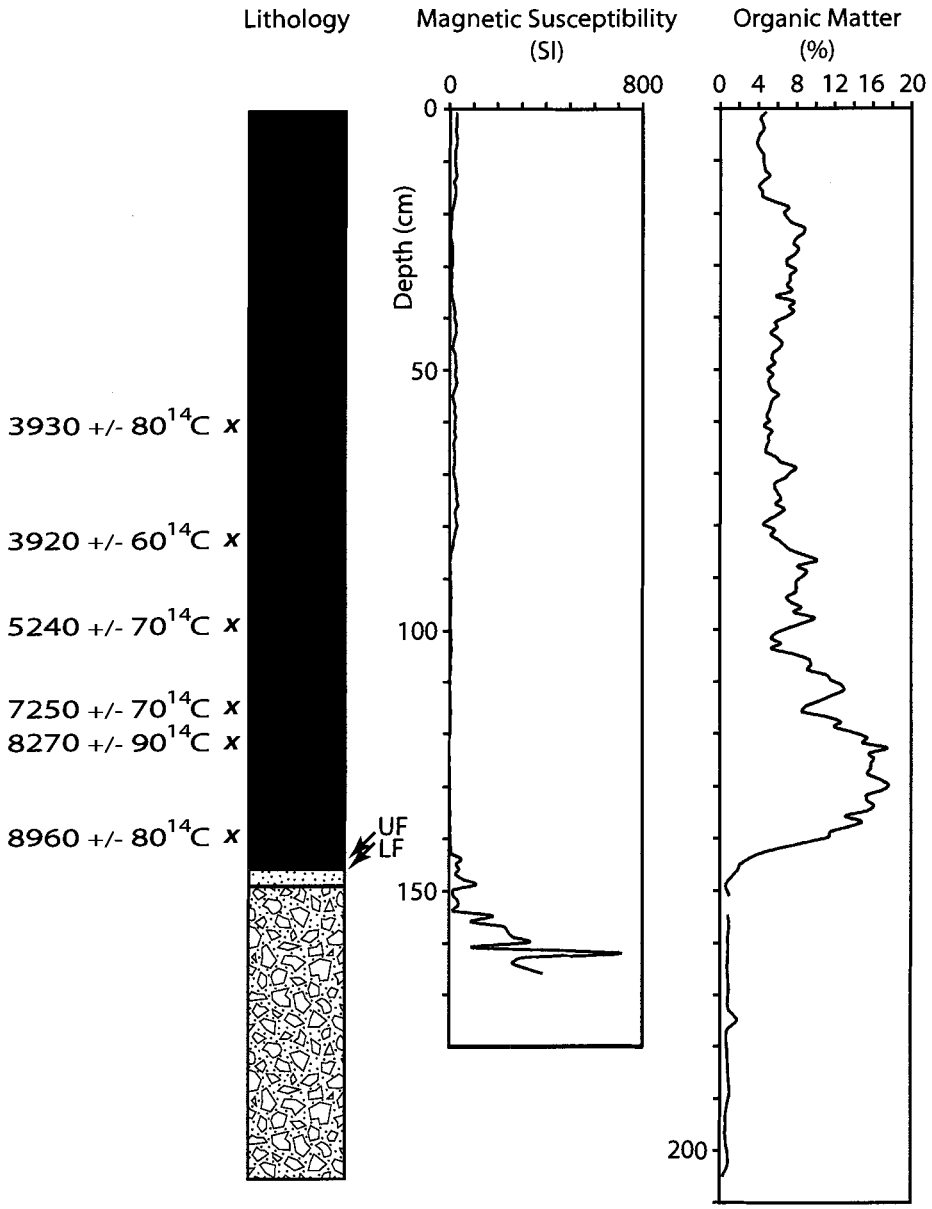

## Sandwich Lake
Core: 05-Sand(01)
Location: 57°01.565'N, 126°29.747'W

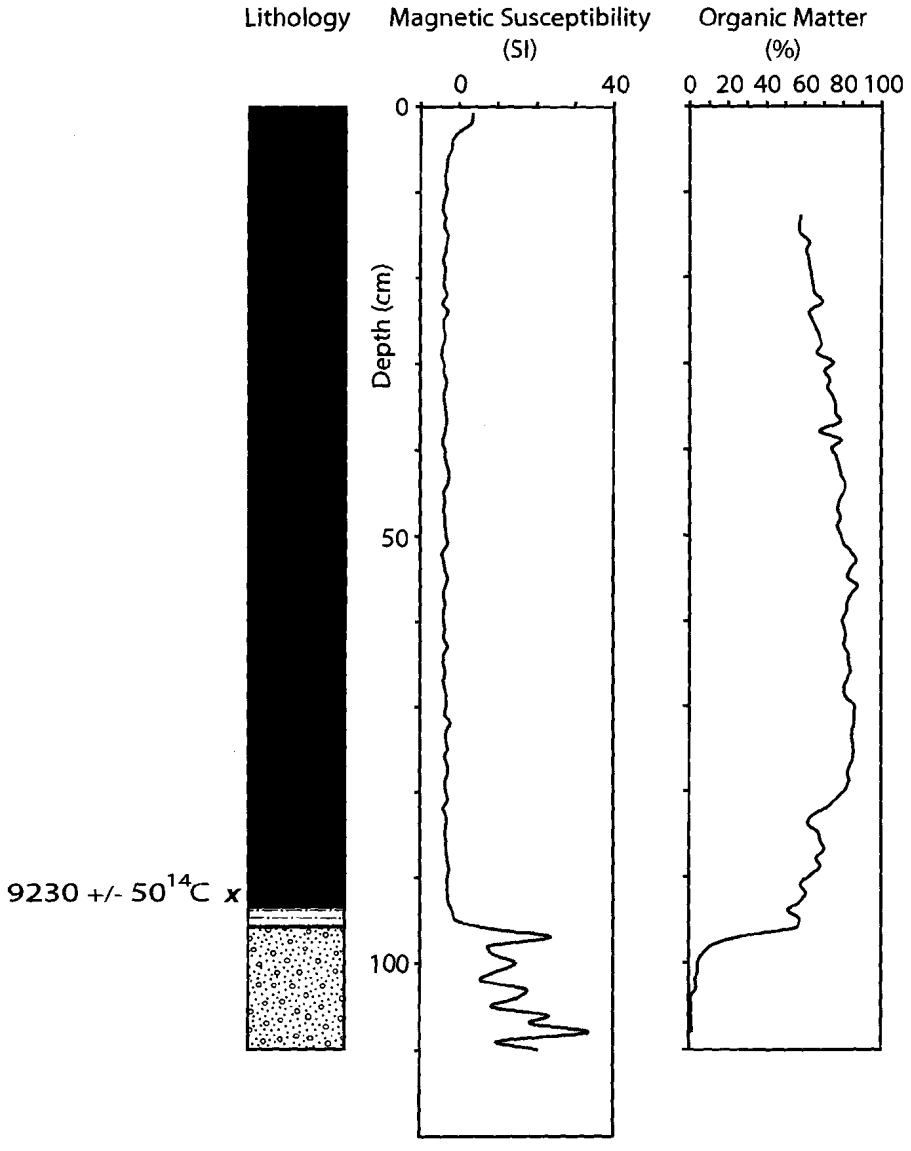

## Sandwich Lake
Core: 05-Sand(02)
Location: 57°01.555' N, 126°29.753' W

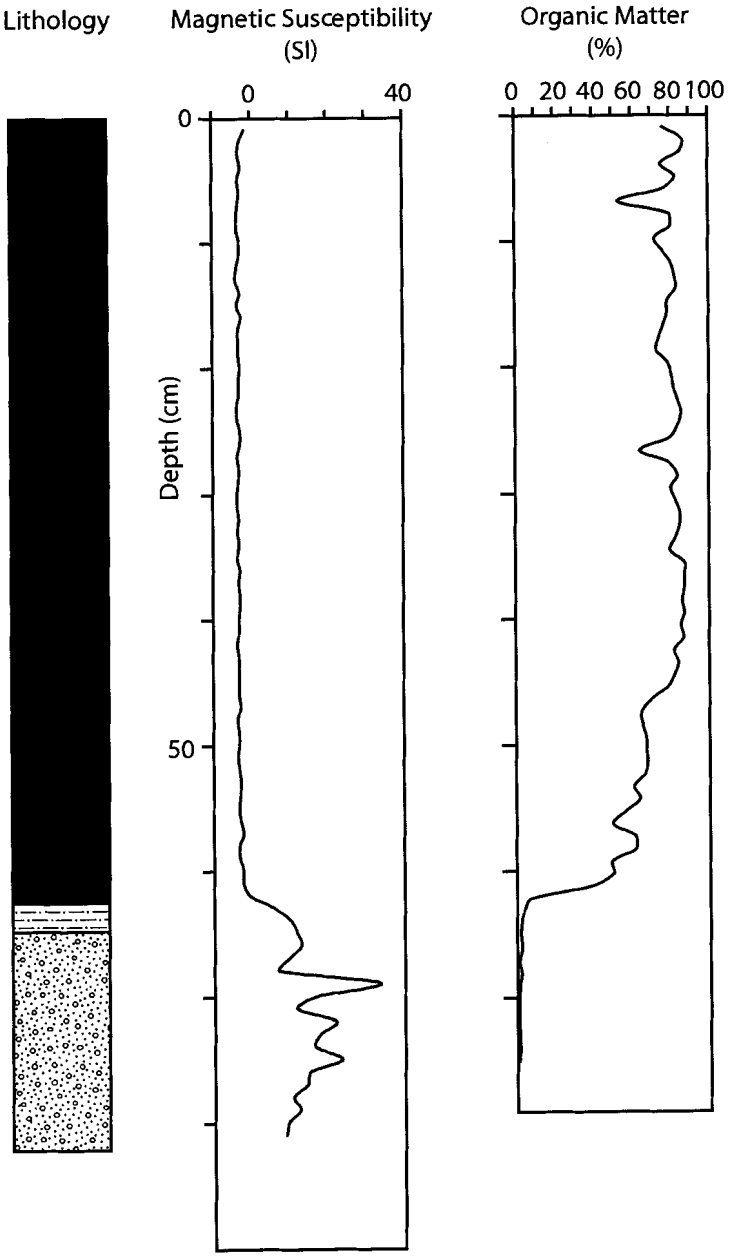

## Sister Lake

Core: 06-Sister(01)

Location: 58°07.568' N, 129°20.506' W

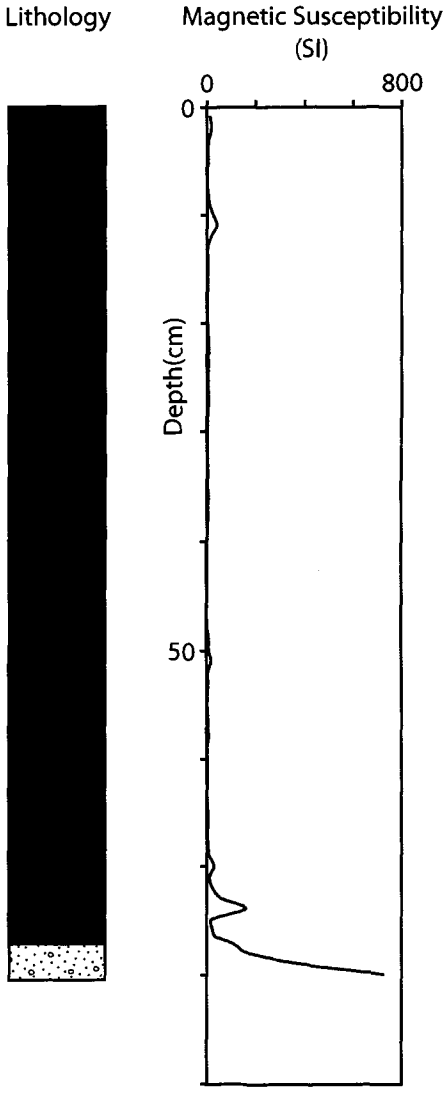

# APPENDIX D:

## Microprobe data

Table B1. Major element composition of glass shards in the lower Finlay tephra from core 05-RedBarrel(02).

| Anaylysis number | Sample number | $SiO_2$ | $TiO_2$ | $Al_2O_3$ | FeO(t) | MnO | CaO | MgO | $Na_2O$ | $K_2O$ | Total |
|---|---|---|---|---|---|---|---|---|---|---|---|
| 32 | UA1144_1 | 61.571 | 0.676 | 19.240 | 5.784 | 0.125 | 2.242 | 0.668 | 3.725 | 4.748 | 98.779 |
| 33 | UA1144_2 | 56.465 | 1.461 | 19.149 | 7.429 | 0.187 | 5.396 | 1.971 | 4.106 | 3.154 | 99.318 |
| 34 | UA1144_3 | 63.302 | 0.255 | 20.198 | 3.920 | 0.131 | 1.103 | 0.223 | 6.328 | 4.365 | 99.825 |
| 38 | UA1144_7 | 63.272 | 0.811 | 18.712 | 6.080 | 0.135 | 2.313 | 0.595 | 2.082 | 3.515 | 97.515 |
| 39 | UA1144_8 | 59.871 | 0.840 | 19.078 | 6.254 | 0.150 | 2.799 | 0.859 | 3.632 | 4.924 | 98.407 |
| 40 | UA1144_9 | 59.500 | 0.900 | 18.831 | 6.151 | 0.153 | 2.541 | 0.922 | 3.637 | 5.084 | 97.719 |
| 41 | UA1144_10 | 61.260 | 0.744 | 19.468 | 5.752 | 0.172 | 2.251 | 0.619 | 3.771 | 5.149 | 99.186 |
| 42 | UA1144_11 | 63.913 | 0.755 | 19.063 | 6.277 | 0.155 | 2.324 | 0.594 | 1.049 | 3.059 | 97.189 |
| 44 | UA1144_13 | 62.970 | 0.207 | 17.504 | 8.076 | 0.199 | 1.251 | 0.006 | 3.654 | 4.539 | 98.406 |
| 45 | UA1144_14 | 57.375 | 1.278 | 17.890 | 8.607 | 0.178 | 4.443 | 1.490 | 3.065 | 3.570 | 97.896 |
| 49 | UA1144_18 | 60.861 | 0.704 | 19.034 | 5.385 | 0.146 | 2.280 | 0.703 | 4.658 | 5.008 | 98.779 |
| 50 | UA1144_19 | 67.188 | 0.437 | 18.249 | 1.527 | 0.059 | 2.603 | 0.072 | 2.629 | 5.321 | 98.085 |
| 51 | UA1144_20 | 63.343 | 0.094 | 19.960 | 0.794 | 0.028 | 1.366 | 0.041 | 6.726 | 5.363 | 97.715 |
| 52 | UA1144_21 | 64.665 | 0.132 | 19.387 | 1.642 | 0.079 | 1.332 | 0.119 | 5.332 | 5.661 | 98.349 |
| 190 | UA1144_23 | 60.469 | 0.767 | 18.870 | 6.212 | 0.101 | 2.639 | 0.790 | 5.109 | 4.784 | 99.741 |
| 191 | UA1144_24 | 63.994 | 0.015 | 21.115 | 1.403 | 0.014 | 1.564 | 0.058 | 5.840 | 5.436 | 99.439 |
| 192 | UA1144_25 | 64.342 | 0.090 | 20.707 | 1.642 | 0.039 | 1.607 | 0.128 | 6.238 | 5.336 | 100.129 |
| 193 | UA1144_26 | 60.150 | 0.617 | 19.352 | 5.874 | 0.144 | 2.275 | 0.644 | 4.667 | 4.744 | 98.467 |
| *35 | UA1144_4 | 61.578 | 0.501 | 16.913 | 5.007 | 0.134 | 1.416 | 0.270 | 0.480 | 2.826 | 89.125 |
| *36 | UA1144_5 | 60.597 | 0.731 | 17.868 | 5.665 | 0.149 | 2.064 | 0.587 | 3.154 | 4.567 | 95.382 |
| *37 | UA1144_6 | 61.349 | 0.816 | 18.238 | 6.167 | 0.133 | 2.291 | 0.598 | 1.808 | 3.455 | 94.855 |
| *43 | UA1144_12 | 61.906 | 0.838 | 18.248 | 6.373 | 0.152 | 2.375 | 0.606 | 0.621 | 2.004 | 93.123 |
| *48 | UA1144_17 | 62.174 | 0.501 | 17.054 | 5.619 | 0.096 | 1.208 | 0.302 | 1.307 | 4.871 | 93.132 |

* Indicates analyses that were excluded from average major element calculations on the basis of their low total weight percents or differing oxide values.

Table B2. Major element composition of glass shards in the lower Finlay tephra from core 06-LGLAK(01).

| Anaylysis number | Sample number | $SiO_2$ | $TiO_2$ | $Al_2O_3$ | FeO(t) | MnO | CaO | MgO | $Na_2O$ | $K_2O$ | Total |
|---|---|---|---|---|---|---|---|---|---|---|---|
| 269 | UA1165_1 | 60.940 | 0.220 | 16.831 | 7.931 | 0.221 | 1.138 | - | 5.683 | 4.710 | 97.674 |
| 270 | UA1165_2 | 60.689 | 0.199 | 16.619 | 8.053 | 0.216 | 1.167 | 0.040 | 5.799 | 4.745 | 97.527 |
| 271 | UA1165_3 | 60.554 | 0.193 | 16.137 | 7.823 | 0.200 | 1.183 | 0.022 | 5.736 | 4.774 | 96.622 |
| 272 | UA1165_4 | 60.873 | 0.192 | 16.627 | 8.449 | 0.206 | 1.123 | 0.018 | 5.807 | 4.842 | 98.137 |
| 274 | UA1165_6 | 60.496 | 0.213 | 16.841 | 8.455 | 0.161 | 1.171 | - | 5.682 | 4.785 | 97.804 |
| 275 | UA1165_7 | 60.395 | 0.182 | 16.736 | 8.324 | 0.196 | 1.159 | - | 5.727 | 4.789 | 97.508 |
| 276 | UA1165_8 | 61.300 | 0.230 | 16.820 | 8.010 | 0.205 | 1.176 | 0.006 | 5.760 | 4.742 | 98.249 |
| 277 | UA1165_9 | 61.303 | 0.203 | 16.934 | 8.082 | 0.181 | 1.112 | 0.022 | 5.815 | 4.865 | 98.517 |
| 278 | UA1165_10 | 60.893 | 0.248 | 16.920 | 8.312 | 0.235 | 1.117 | 0.003 | 5.993 | 4.756 | 98.477 |
| 279 | UA1165_11 | 60.646 | 0.188 | 16.552 | 7.967 | 0.194 | 1.202 | 0.009 | 5.864 | 4.963 | 97.585 |
| 280 | UA1165_12 | 61.149 | 0.188 | 16.364 | 8.263 | 0.186 | 1.155 | - | 5.604 | 4.818 | 97.727 |
| 281 | UA1165_13 | 61.175 | 0.147 | 16.940 | 8.061 | 0.178 | 1.133 | - | 6.244 | 4.894 | 98.772 |
| 283 | UA1165_15 | 61.442 | 0.175 | 17.038 | 7.956 | 0.197 | 1.192 | 0.005 | 6.063 | 4.627 | 98.695 |
| 284 | UA1165_16 | 61.096 | 0.170 | 16.864 | 8.307 | 0.186 | 1.196 | 0.001 | 6.176 | 4.825 | 98.821 |
| 285 | UA1165_17 | 61.803 | 0.191 | 16.675 | 8.181 | 0.216 | 1.187 | 0.013 | 6.158 | 4.771 | 99.195 |
| 286 | UA1165_18 | 61.785 | 0.184 | 16.836 | 8.154 | 0.218 | 1.162 | 0.022 | 6.040 | 4.836 | 99.237 |
| 287 | UA1165_19 | 61.133 | 0.189 | 16.624 | 8.315 | 0.199 | 1.184 | 0.011 | 6.002 | 5.043 | 98.700 |
| 288 | UA1165_20 | 61.166 | 0.227 | 16.711 | 8.269 | 0.199 | 1.238 | 0.001 | 5.836 | 4.746 | 98.393 |
| *273 | UA1165_5 | 60.697 | 0.477 | 19.325 | 5.066 | 0.139 | 1.718 | 0.491 | 5.329 | 5.288 | 98.530 |
| *282 | UA1165_14 | 63.285 | 0.133 | 19.184 | 3.461 | 0.107 | 0.906 | 0.062 | 5.925 | 5.649 | 98.712 |

* Indicates analyses that were excluded from average major element calculations on the basis of their low total weight percents or differing oxide values.

- Inidcates analyses with values below detection.

Table B3. Major element composition of glass shards in the lower Finlay tephra from core 05-Cushing(01).

| Anaylysis number | Sample number | $SiO_2$ | $TiO_2$ | $Al_2O_3$ | FeO(t) | MnO | CaO | MgO | $Na_2O$ | $K_2O$ | Total |
|---|---|---|---|---|---|---|---|---|---|---|---|
| 328 | UA1168_1 | 61.242 | 0.193 | 17.032 | 8.416 | 0.267 | 1.210 | - | 6.039 | 4.834 | 99.233 |
| 329 | UA1168_2 | 60.702 | 0.220 | 16.061 | 8.623 | 0.258 | 1.231 | 0.040 | 6.075 | 4.587 | 97.797 |
| 330 | UA1168_3 | 61.090 | 0.234 | 16.894 | 8.216 | 0.202 | 1.204 | - | 5.859 | 4.771 | 98.470 |
| 331 | UA1168_4 | 60.199 | 0.212 | 16.320 | 8.935 | 0.217 | 1.275 | 0.012 | 5.859 | 4.780 | 97.809 |
| 333 | UA1168_6 | 61.480 | 0.167 | 16.460 | 8.426 | 0.223 | 1.182 | 0.028 | 6.007 | 5.034 | 99.007 |
| 335 | UA1168_8 | 61.042 | 0.169 | 16.910 | 8.573 | 0.207 | 1.135 | 0.007 | 5.863 | 4.854 | 98.760 |
| 336 | UA1168_9 | 59.654 | 0.626 | 18.754 | 5.904 | 0.089 | 2.330 | 0.628 | 4.979 | 4.786 | 97.750 |
| 337 | UA1168_10 | 60.767 | 0.238 | 16.379 | 8.056 | 0.164 | 1.162 | - | 5.242 | 4.939 | 96.947 |
| 338 | UA1168_11 | 60.475 | 0.537 | 17.996 | 5.817 | 0.134 | 1.687 | 0.376 | 5.673 | 5.695 | 98.390 |
| 339 | UA1168_12 | 61.163 | 0.208 | 16.696 | 8.139 | 0.208 | 1.195 | 0.012 | 6.053 | 4.867 | 98.541 |
| 340 | UA1168_13 | 63.866 | 0.256 | 16.784 | 5.224 | 0.090 | 1.894 | 0.261 | 5.142 | 5.798 | 99.315 |
| 341 | UA1168_14 | 60.614 | 0.181 | 16.761 | 8.386 | 0.229 | 1.167 | - | 5.684 | 4.856 | 97.878 |
| 342 | UA1168_15 | 60.586 | 0.231 | 16.590 | 8.392 | 0.226 | 1.163 | - | 6.075 | 4.862 | 98.125 |
| 343 | UA1168_16 | 61.775 | 0.378 | 17.455 | 6.390 | 0.185 | 1.847 | 0.372 | 4.662 | 5.812 | 98.876 |
| 344 | UA1168_17 | 62.460 | 0.406 | 17.008 | 6.378 | 0.169 | 1.779 | 0.336 | 4.827 | 5.759 | 99.122 |
| 345 | UA1168_18 | 62.630 | 0.328 | 18.783 | 4.666 | 0.112 | 0.817 | 0.215 | 4.629 | 5.961 | 98.141 |
| 346 | UA1168_19 | 63.018 | 0.398 | 18.992 | 4.645 | 0.132 | 0.738 | 0.253 | 4.941 | 5.900 | 99.017 |
| *332 | UA1168_5 | 54.811 | 1.867 | 16.813 | 10.070 | 0.172 | 5.277 | 2.154 | 4.789 | 3.471 | 99.424 |
| *334 | UA1168_7 | 63.682 | 0.139 | 19.204 | 2.120 | 0.065 | 0.858 | 0.132 | 5.505 | 6.612 | 98.317 |
| *347 | UA1168_20 | 67.376 | - | 19.335 | 0.460 | 0.008 | 0.942 | - | 6.196 | 5.715 | 100.032 |

* Indicates analyses that were excluded from average major element calculations on the basis of their low total weight percents or differing oxide values.

- Inidcates analyses with values below detection.

Table B4. Major element composition of glass shards in the upper Finlay tephra from core 05-RedBarrel(02).

| Anaylysis number | Sample number | $SiO_2$ | $TiO_2$ | $Al_2O_3$ | FeO(t) | MnO | CaO | MgO | $Na_2O$ | $K_2O$ | Total |
|---|---|---|---|---|---|---|---|---|---|---|---|
| 12 | UA1143_1 | 60.378 | 0.203 | 16.666 | 8.256 | 0.197 | 1.209 | 0.018 | 8.399 | 4.705 | 100.031 |
| 13 | UA1143_2 | 61.879 | 0.238 | 17.026 | 8.256 | 0.261 | 1.218 | 0.035 | 4.194 | 4.468 | 97.575 |
| 14 | UA1143_3 | 62.068 | 0.227 | 17.022 | 8.576 | 0.216 | 1.265 | 0.027 | 3.607 | 4.394 | 97.402 |
| 15 | UA1143_4 | 61.990 | 0.222 | 16.801 | 8.437 | 0.243 | 1.221 | 0.021 | 3.855 | 4.273 | 97.063 |
| 16 | UA1143_5 | 62.862 | 0.240 | 17.411 | 8.805 | 0.231 | 1.304 | 0.013 | 2.578 | 4.222 | 97.666 |
| 17 | UA1143_6 | 62.822 | 0.260 | 17.215 | 8.493 | 0.280 | 1.222 | 0.033 | 3.887 | 4.345 | 98.557 |
| 18 | UA1143_7 | 62.451 | 0.255 | 17.174 | 8.414 | 0.260 | 1.161 | - | 4.043 | 4.398 | 98.156 |
| 19 | UA1143_8 | 61.874 | 0.200 | 16.831 | 8.413 | 0.230 | 1.235 | 0.006 | 4.062 | 4.505 | 97.356 |
| 20 | UA1143_9 | 62.333 | 0.249 | 17.007 | 8.286 | 0.256 | 1.298 | 0.015 | 4.118 | 4.402 | 97.964 |
| 21 | UA1143_10 | 63.089 | 0.228 | 17.195 | 8.255 | 0.179 | 1.224 | - | 3.889 | 4.387 | 98.446 |
| 22 | UA1143_11 | 62.475 | 0.274 | 16.819 | 8.589 | 0.252 | 1.260 | 0.003 | 3.943 | 4.400 | 98.015 |
| 25 | UA1143_14 | 62.520 | 0.247 | 17.171 | 8.353 | 0.239 | 1.199 | 0.005 | 3.643 | 4.470 | 97.847 |
| 26 | UA1143_15 | 62.843 | 0.260 | 17.119 | 8.269 | 0.226 | 1.271 | 0.015 | 3.861 | 4.304 | 98.168 |
| 27 | UA1143_16 | 62.899 | 0.272 | 17.167 | 8.556 | 0.200 | 1.066 | 0.023 | 4.200 | 4.431 | 98.814 |
| 28 | UA1143_17 | 62.165 | 0.282 | 17.037 | 8.445 | 0.232 | 1.062 | - | 3.918 | 4.364 | 97.505 |
| 29 | UA1143_18 | 63.118 | 0.215 | 17.247 | 8.757 | 0.223 | 1.228 | 0.005 | 4.289 | 4.394 | 99.476 |
| 30 | UA1143_19 | 63.391 | 0.196 | 17.382 | 8.161 | 0.203 | 1.296 | 0.024 | 3.848 | 4.407 | 98.908 |
| 31 | UA1143_20 | 61.852 | 0.216 | 16.674 | 8.416 | 0.196 | 1.304 | 0.013 | 4.076 | 4.368 | 97.115 |
| 185 | UA1143_21 | 60.523 | 0.221 | 16.286 | 8.921 | 0.250 | 1.312 | 0.026 | 5.562 | 4.708 | 97.809 |
| 186 | UA1143_22 | 61.421 | 0.199 | 16.659 | 8.613 | 0.228 | 1.174 | - | 5.807 | 4.816 | 98.917 |
| 187 | UA1143_23 | 60.980 | 0.219 | 16.633 | 8.951 | 0.222 | 1.252 | 0.014 | 5.938 | 4.887 | 99.096 |
| 188 | UA1143_24 | 60.659 | 0.196 | 16.581 | 8.156 | 0.206 | 1.254 | 0.005 | 5.266 | 4.755 | 97.078 |
| *23 | UA1143_12 | 60.987 | 0.256 | 17.141 | 7.862 | 0.185 | 1.158 | 0.023 | 1.344 | 2.830 | 91.786 |
| *24 | UA1143_13 | 60.582 | 0.233 | 16.460 | 7.669 | 0.219 | 1.126 | 0.046 | 1.600 | 3.165 | 91.100 |

* Indicates analyses that were excluded from average major element calculations on the basis of their low total weight percents or differing oxide values.
- Inidcates analyses with values below detection.

Table B5. Major element composition of glass shards in the upper Finlay tephra from core 06-LGLAK(01).

| Anaylysis number | Sample number | $SiO_2$ | $TiO_2$ | $Al_2O_3$ | FeO(t) | MnO | CaO | MgO | $Na_2O$ | $K_2O$ | Total |
|---|---|---|---|---|---|---|---|---|---|---|---|
| 243 | UA1164_1 | 60.266 | 0.177 | 16.782 | 7.687 | 0.176 | 1.141 | 0.012 | 5.762 | 4.907 | 96.910 |
| 244 | UA1164_2 | 59.907 | 0.211 | 16.017 | 8.851 | 0.191 | 1.264 | 0.016 | 5.544 | 4.802 | 96.803 |
| 245 | UA1164_3 | 60.318 | 0.173 | 16.857 | 7.890 | 0.222 | 1.112 | 0.043 | 5.822 | 4.666 | 97.103 |
| 246 | UA1164_4 | 60.333 | 0.200 | 16.636 | 8.119 | 0.209 | 1.230 | 0.037 | 6.163 | 4.829 | 97.756 |
| 247 | UA1164_5 | 60.808 | 0.190 | 16.761 | 8.191 | 0.182 | 1.166 | 0.030 | 5.901 | 4.669 | 97.898 |
| 248 | UA1164_6 | 59.820 | 0.213 | 16.413 | 8.377 | 0.237 | 1.136 | 0.005 | 5.781 | 4.853 | 96.835 |
| 249 | UA1164_7 | 59.877 | 0.182 | 16.686 | 8.298 | 0.189 | 1.103 | 0.016 | 6.000 | 4.769 | 97.120 |
| 250 | UA1164_8 | 60.672 | 0.230 | 16.808 | 8.122 | 0.198 | 1.130 | 0.021 | 6.329 | 4.898 | 98.408 |
| 251 | UA1164_9 | 59.956 | 0.201 | 16.529 | 8.383 | 0.214 | 1.078 | - | 5.759 | 4.810 | 96.930 |
| 252 | UA1164_10 | 60.433 | 0.227 | 16.551 | 8.381 | 0.219 | 1.096 | 0.012 | 5.605 | 4.759 | 97.283 |
| 253 | UA1164_11 | 60.162 | 0.164 | 16.888 | 7.965 | 0.184 | 1.037 | 0.005 | 5.997 | 4.861 | 97.263 |
| 254 | UA1164_12 | 59.475 | 0.203 | 16.567 | 8.048 | 0.203 | 1.069 | - | 6.340 | 4.844 | 96.749 |
| 255 | UA1164_13 | 60.316 | 0.200 | 16.296 | 8.164 | 0.226 | 1.055 | 0.019 | 6.141 | 4.990 | 97.407 |
| 256 | UA1164_14 | 60.494 | 0.184 | 16.724 | 8.458 | 0.210 | 1.156 | 0.033 | 5.732 | 4.886 | 97.877 |
| 257 | UA1164_15 | 60.790 | 0.190 | 16.762 | 8.170 | 0.237 | 1.168 | 0.006 | 5.669 | 4.779 | 97.771 |
| 258 | UA1164_16 | 60.114 | 0.205 | 16.702 | 8.011 | 0.255 | 1.183 | - | 5.410 | 4.739 | 96.619 |
| 259 | UA1164_17 | 60.437 | 0.226 | 16.829 | 8.177 | 0.210 | 1.099 | - | 5.604 | 4.777 | 97.359 |
| 260 | UA1164_18 | 59.794 | 0.181 | 16.783 | 8.171 | 0.186 | 1.093 | 0.017 | 5.616 | 4.752 | 96.593 |
| 261 | UA1164_19 | 60.874 | 0.226 | 16.588 | 7.953 | 0.243 | 1.130 | 0.021 | 5.433 | 4.700 | 97.168 |
| 262 | UA1164_20 | 60.116 | 0.205 | 16.613 | 7.989 | 0.200 | 1.131 | - | 5.785 | 4.784 | 96.823 |

- Inidcates analyses with values below detection.

Table B6. Major element composition of glass shards in the upper Finlay tephra from core 05-Cushing(01).

| Anaylysis number | Sample number | $SiO_2$ | $TiO_2$ | $Al_2O_3$ | FeO(t) | MnO | CaO | MgO | $Na_2O$ | $K_2O$ | Total |
|---|---|---|---|---|---|---|---|---|---|---|---|
| 354 | UA1169_1 | 61.540 | 0.240 | 16.985 | 7.897 | 0.182 | 1.119 | 0.012 | 5.821 | 4.839 | 98.635 |
| 355 | UA1169_2 | 60.891 | 0.205 | 16.835 | 8.315 | 0.211 | 1.177 | - | 5.746 | 5.011 | 98.391 |
| 356 | UA1169_3 | 61.083 | 0.203 | 17.003 | 8.429 | 0.216 | 1.158 | 0.022 | 5.979 | 5.058 | 99.151 |
| 357 | UA1169_4 | 61.423 | 0.225 | 16.694 | 8.375 | 0.229 | 1.176 | - | 6.027 | 4.891 | 99.040 |
| 358 | UA1169_5 | 60.626 | 0.210 | 16.706 | 8.113 | 0.211 | 1.181 | 0.029 | 5.754 | 4.877 | 97.707 |
| 359 | UA1169_6 | 61.292 | 0.214 | 17.256 | 8.423 | 0.221 | 1.151 | 0.003 | 5.836 | 4.841 | 99.237 |
| 360 | UA1169_7 | 60.822 | 0.228 | 16.806 | 8.623 | 0.211 | 1.252 | 0.010 | 6.039 | 4.870 | 98.861 |
| 361 | UA1169_8 | 61.010 | 0.190 | 16.781 | 7.880 | 0.191 | 1.130 | 0.020 | 5.802 | 4.966 | 97.970 |
| 362 | UA1169_9 | 60.605 | 0.224 | 16.573 | 8.758 | 0.223 | 1.178 | 0.031 | 5.824 | 4.760 | 98.176 |
| 363 | UA1169_10 | 61.234 | 0.171 | 16.563 | 8.631 | 0.165 | 1.273 | 0.006 | 6.019 | 4.907 | 98.969 |
| 364 | UA1169_11 | 61.112 | 0.227 | 16.697 | 7.984 | 0.226 | 1.218 | 0.007 | 5.626 | 4.784 | 97.881 |
| 365 | UA1169_12 | 61.358 | 0.203 | 16.738 | 8.283 | 0.246 | 1.253 | - | 5.774 | 4.989 | 98.844 |
| 366 | UA1169_13 | 61.009 | 0.184 | 17.164 | 8.604 | 0.252 | 1.153 | - | 6.275 | 4.937 | 99.578 |
| 367 | UA1169_14 | 61.109 | 0.244 | 16.758 | 8.596 | 0.205 | 1.193 | 0.027 | 5.917 | 4.836 | 98.885 |
| 368 | UA1169_15 | 61.477 | 0.201 | 17.248 | 8.776 | 0.230 | 1.114 | 0.011 | 6.028 | 5.034 | 100.119 |
| 369 | UA1169_16 | 61.192 | 0.197 | 16.766 | 8.206 | 0.246 | 1.098 | 0.002 | 6.093 | 4.869 | 98.669 |
| 370 | UA1169_17 | 60.761 | 0.192 | 16.874 | 8.549 | 0.210 | 1.057 | - | 5.811 | 4.908 | 98.362 |
| 371 | UA1169_18 | 63.134 | 0.330 | 15.975 | 8.650 | 0.243 | 1.209 | 0.020 | 5.692 | 4.905 | 100.158 |
| 372 | UA1169_19 | 61.046 | 0.185 | 16.629 | 8.441 | 0.199 | 1.072 | - | 6.048 | 4.945 | 98.565 |
| 373 | UA1169_20 | 59.678 | 0.251 | 16.563 | 9.561 | 0.210 | 1.191 | 0.008 | 5.892 | 4.883 | 98.237 |

- Inidcates analyses with values below detection.

Table B7. Major element composition of glass shards in the upper Finlay tephra from core 06-Hungry(02).

| Anaylysis number | Sample number | $SiO_2$ | $TiO_2$ | $Al_2O_3$ | FeO(t) | MnO | CaO | MgO | $Na_2O$ | $K_2O$ | Total |
|---|---|---|---|---|---|---|---|---|---|---|---|
| 289 | UA1166_1 | 61.377 | 0.213 | 17.122 | 7.976 | 0.229 | 1.150 | 0.019 | 6.179 | 4.849 | 99.114 |
| 290 | UA1166_2 | 61.341 | 0.166 | 17.070 | 8.238 | 0.241 | 1.176 | 0.012 | 6.003 | 4.658 | 98.905 |
| 291 | UA1166_3 | 61.529 | 0.214 | 16.678 | 7.931 | 0.221 | 1.151 | 0.008 | 6.076 | 4.867 | 98.675 |
| 292 | UA1166_4 | 61.216 | 0.201 | 16.466 | 8.017 | 0.211 | 1.121 | 0.009 | 6.121 | 4.761 | 98.123 |
| 293 | UA1166_5 | 60.525 | 0.150 | 16.873 | 8.314 | 0.238 | 1.137 | 0.005 | 5.919 | 4.865 | 98.026 |
| 294 | UA1166_6 | 61.783 | 0.160 | 17.077 | 8.021 | 0.256 | 1.142 | 0.011 | 6.252 | 4.840 | 99.542 |
| 295 | UA1166_7 | 61.213 | 0.249 | 16.904 | 8.107 | 0.162 | 1.148 | - | 6.462 | 4.830 | 99.075 |
| 296 | UA1166_8 | 61.196 | 0.177 | 16.835 | 8.177 | 0.187 | 1.149 | 0.027 | 6.105 | 4.735 | 98.588 |
| 297 | UA1166_9 | 60.572 | 0.215 | 16.452 | 8.458 | 0.286 | 1.123 | 0.001 | 5.738 | 4.974 | 97.819 |
| 298 | UA1166_10 | 59.988 | 0.278 | 16.394 | 8.731 | 0.218 | 1.204 | 0.013 | 6.002 | 4.842 | 97.670 |
| 299 | UA1166_11 | 61.153 | 0.170 | 16.986 | 8.462 | 0.198 | 1.195 | - | 5.876 | 4.812 | 98.852 |
| 300 | UA1166_12 | 60.889 | 0.211 | 16.589 | 8.623 | 0.238 | 1.175 | - | 6.160 | 4.951 | 98.836 |
| 301 | UA1166_13 | 60.645 | 0.208 | 16.669 | 8.541 | 0.197 | 1.182 | 0.018 | 6.081 | 4.875 | 98.416 |
| 302 | UA1166_14 | 60.300 | 0.225 | 16.555 | 8.512 | 0.234 | 1.191 | 0.004 | 6.102 | 4.722 | 97.845 |
| 303 | UA1166_15 | 61.155 | 0.217 | 16.523 | 8.029 | 0.226 | 1.188 | 0.016 | 5.436 | 4.346 | 97.136 |
| 304 | UA1166_16 | 61.087 | 0.178 | 16.698 | 8.067 | 0.215 | 1.199 | - | 6.043 | 4.907 | 98.394 |
| 305 | UA1166_17 | 61.023 | 0.251 | 16.669 | 8.147 | 0.202 | 1.201 | - | 5.952 | 4.897 | 98.342 |
| 306 | UA1166_18 | 61.032 | 0.199 | 16.882 | 8.344 | 0.207 | 1.190 | 0.018 | 5.864 | 4.881 | 98.617 |
| 307 | UA1166_19 | 61.529 | 0.195 | 16.981 | 7.883 | 0.188 | 1.115 | 0.005 | 6.048 | 4.827 | 98.771 |

- Inidcates analyses with values below detection.

Table B8. Major element composition of glass shards in the upper Finlay tephra from core 06-Hungry(01).

| Anaylysis number | Sample number | $SiO_2$ | $TiO_2$ | $Al_2O_3$ | FeO(t) | MnO | CaO | MgO | $Na_2O$ | $K_2O$ | Total |
|---|---|---|---|---|---|---|---|---|---|---|---|
| 308 | UA1167_1 | 62.054 | 0.178 | 17.230 | 8.541 | 0.181 | 1.230 | 0.030 | 6.427 | 4.808 | 100.679 |
| 309 | UA1167_2 | 61.052 | 0.212 | 16.954 | 8.100 | 0.200 | 1.195 | - | 6.676 | 4.875 | 99.264 |
| 310 | UA1167_3 | 60.483 | 0.166 | 16.901 | 8.408 | 0.214 | 1.160 | 0.027 | 5.075 | 4.758 | 97.192 |
| 311 | UA1167_4 | 60.611 | 0.222 | 16.507 | 8.423 | 0.216 | 1.199 | - | 5.838 | 4.788 | 97.804 |
| 312 | UA1167_5 | 60.829 | 0.203 | 16.774 | 8.742 | 0.246 | 0.819 | - | 5.945 | 4.788 | 98.346 |
| 313 | UA1167_6 | 61.726 | 0.242 | 16.817 | 8.685 | 0.217 | 0.924 | 0.014 | 6.462 | 4.845 | 99.932 |
| 314 | UA1167_7 | 61.430 | 0.238 | 16.648 | 8.772 | 0.208 | 0.849 | - | 5.997 | 4.821 | 98.963 |
| 315 | UA1167_8 | 61.114 | 0.199 | 17.043 | 8.186 | 0.285 | 1.115 | - | 5.393 | 4.814 | 98.149 |
| 316 | UA1167_9 | 60.887 | 0.191 | 16.632 | 8.186 | 0.196 | 1.133 | - | 5.401 | 4.720 | 97.346 |
| 317 | UA1167_10 | 60.937 | 0.236 | 16.683 | 8.728 | 0.215 | 1.144 | 0.025 | 5.678 | 4.747 | 98.393 |
| 318 | UA1167_11 | 61.250 | 0.251 | 16.972 | 8.479 | 0.204 | 1.143 | - | 6.372 | 4.785 | 99.456 |
| 319 | UA1167_12 | 61.176 | 0.167 | 16.640 | 8.303 | 0.175 | 1.109 | 0.009 | 5.415 | 4.804 | 97.798 |
| 320 | UA1167_13 | 61.039 | 0.211 | 16.856 | 8.784 | 0.229 | 1.147 | - | 5.895 | 4.749 | 98.910 |
| 321 | UA1167_14 | 61.157 | 0.217 | 16.926 | 8.556 | 0.211 | 1.140 | - | 5.971 | 4.998 | 99.176 |
| 322 | UA1167_15 | 61.251 | 0.196 | 16.991 | 7.838 | 0.168 | 1.055 | - | 6.024 | 4.706 | 98.229 |
| 323 | UA1167_16 | 61.770 | 0.224 | 16.842 | 8.093 | 0.206 | 1.162 | 0.003 | 5.976 | 4.898 | 99.174 |
| 324 | UA1167_17 | 60.768 | 0.191 | 16.708 | 7.955 | 0.235 | 1.153 | - | 5.877 | 4.879 | 97.766 |
| 325 | UA1167_18 | 61.182 | 0.225 | 16.909 | 8.339 | 0.266 | 1.204 | 0.022 | 5.881 | 4.794 | 98.822 |
| 326 | UA1167_19 | 61.275 | 0.230 | 16.677 | 8.829 | 0.226 | 1.169 | 0.009 | 5.505 | 4.834 | 98.754 |
| 327 | UA1167_20 | 61.549 | 0.234 | 17.153 | 8.091 | 0.169 | 1.348 | 0.020 | 5.859 | 4.738 | 99.161 |

- Inidcates analyses with values below detection.

Table B9. Major element composition of glass shards in the lower Bob Quinn tephra from core 06-BobQ(01).

| Anaylysis number | Sample number | $SiO_2$ | $TiO_2$ | $Al_2O_3$ | FeO(t) | MnO | CaO | MgO | $Na_2O$ | $K_2O$ | Total |
|---|---|---|---|---|---|---|---|---|---|---|---|
| 223 | UA1163_1 | 47.627 | 2.166 | 17.263 | 12.066 | 0.187 | 8.823 | 6.122 | 3.568 | 0.877 | 98.699 |
| 224 | UA1163_2 | 48.151 | 2.219 | 17.184 | 12.264 | 0.164 | 9.052 | 6.275 | 3.478 | 0.879 | 99.666 |
| 225 | UA1163_3 | 47.864 | 2.236 | 17.398 | 11.842 | 0.177 | 8.989 | 6.411 | 3.675 | 0.925 | 99.517 |
| 226 | UA1163_4 | 48.000 | 2.331 | 17.317 | 11.931 | 0.155 | 8.909 | 5.938 | 3.587 | 1.060 | 99.228 |
| 227 | UA1163_5 | 47.769 | 2.239 | 17.420 | 12.106 | 0.165 | 8.704 | 6.122 | 3.572 | 0.969 | 99.066 |
| 228 | UA1163_6 | 47.277 | 2.333 | 17.404 | 12.012 | 0.128 | 9.099 | 6.048 | 3.499 | 0.894 | 98.694 |
| 229 | UA1163_7 | 47.365 | 2.288 | 17.201 | 12.000 | 0.156 | 9.004 | 6.478 | 3.714 | 0.988 | 99.194 |
| 230 | UA1163_8 | 47.277 | 2.256 | 17.204 | 12.277 | 0.156 | 8.623 | 6.125 | 3.573 | 0.923 | 98.414 |
| 231 | UA1163_9 | 46.244 | 2.232 | 17.216 | 12.264 | 0.188 | 9.150 | 6.078 | 3.314 | 0.937 | 97.623 |
| 232 | UA1163_10 | 47.243 | 2.484 | 16.546 | 12.396 | 0.222 | 8.815 | 5.763 | 3.615 | 1.065 | 98.149 |
| 233 | UA1163_11 | 47.805 | 2.366 | 16.678 | 12.509 | 0.168 | 8.458 | 5.817 | 3.618 | 1.038 | 98.457 |
| 234 | UA1163_12 | 47.751 | 2.402 | 16.935 | 12.363 | 0.221 | 8.961 | 6.014 | 3.539 | 0.937 | 99.123 |
| 235 | UA1163_13 | 47.985 | 2.448 | 17.169 | 12.485 | 0.191 | 8.955 | 5.949 | 3.516 | 0.978 | 99.676 |
| 236 | UA1163_14 | 47.594 | 2.300 | 17.063 | 12.245 | 0.176 | 9.155 | 6.041 | 3.623 | 0.980 | 99.177 |
| 237 | UA1163_15 | 47.884 | 2.243 | 16.979 | 12.221 | 0.217 | 8.966 | 5.997 | 3.394 | 0.961 | 98.862 |
| 238 | UA1163_16 | 47.552 | 2.387 | 16.965 | 12.180 | 0.187 | 9.077 | 6.104 | 3.531 | 0.993 | 98.976 |
| 239 | UA1163_17 | 47.501 | 2.305 | 17.212 | 11.919 | 0.146 | 8.881 | 6.062 | 3.511 | 0.888 | 98.425 |
| 240 | UA1163_18 | 47.513 | 2.276 | 17.057 | 12.091 | 0.164 | 9.202 | 6.140 | 3.612 | 0.976 | 99.031 |
| 241 | UA1163_19 | 47.887 | 2.331 | 17.020 | 12.211 | 0.165 | 9.099 | 5.737 | 3.604 | 1.017 | 99.071 |
| 242 | UA1163_20 | 47.254 | 2.304 | 17.351 | 12.053 | 0.160 | 9.148 | 6.380 | 3.480 | 0.886 | 99.016 |
| 420 | UA1163_21 | 47.114 | 2.051 | 16.908 | 12.423 | 0.198 | 9.146 | 6.218 | 3.545 | 0.949 | 98.552 |
| 421 | UA1163_22 | 47.380 | 2.626 | 16.206 | 12.728 | 0.134 | 8.844 | 5.785 | 3.570 | 1.057 | 98.330 |
| 422 | UA1163_23 | 48.238 | 2.426 | 16.900 | 12.054 | 0.158 | 9.053 | 5.798 | 3.621 | 0.966 | 99.214 |

Table B10. Major element composition of glass shards in the upper Bob Quinn tephra from core 06-BobQ(01).

| Anaylysis number | Sample number | $SiO_2$ | $TiO_2$ | $Al_2O_3$ | FeO(t) | MnO | CaO | MgO | $Na_2O$ | $K_2O$ | Total |
|---|---|---|---|---|---|---|---|---|---|---|---|
| 203 | UA1162_1 | 60.199 | 0.560 | 18.312 | 6.372 | 0.135 | 1.940 | 0.466 | 5.939 | 5.111 | 99.034 |
| 204 | UA1162_2 | 57.808 | 1.129 | 17.934 | 7.042 | 0.149 | 3.158 | 0.982 | 4.706 | 4.480 | 97.388 |
| 205 | UA1162_3 | 58.513 | 1.070 | 18.190 | 6.613 | 0.110 | 2.832 | 0.857 | 5.782 | 4.495 | 98.462 |
| 206 | UA1162_4 | 57.436 | 0.986 | 18.334 | 6.821 | 0.139 | 2.856 | 0.821 | 5.436 | 4.517 | 97.346 |
| 207 | UA1162_5 | 57.997 | 1.012 | 18.506 | 6.775 | 0.160 | 2.925 | 0.904 | 5.463 | 4.712 | 98.454 |
| 208 | UA1162_6 | 58.647 | 1.032 | 18.199 | 6.655 | 0.107 | 2.939 | 0.807 | 5.313 | 4.607 | 98.306 |
| 209 | UA1162_7 | 58.269 | 1.001 | 18.230 | 6.716 | 0.125 | 2.944 | 0.893 | 5.333 | 4.688 | 98.199 |
| 210 | UA1162_8 | 58.517 | 1.070 | 18.401 | 6.714 | 0.133 | 2.897 | 0.854 | 5.154 | 4.506 | 98.246 |
| 211 | UA1162_9 | 60.460 | 0.434 | 19.079 | 5.352 | 0.116 | 1.711 | 0.384 | 5.853 | 5.692 | 99.081 |
| 212 | UA1162_10 | 57.156 | 1.210 | 18.079 | 7.303 | 0.160 | 3.335 | 1.031 | 5.368 | 4.520 | 98.162 |
| 213 | UA1162_11 | 57.313 | 1.111 | 17.790 | 6.944 | 0.120 | 3.357 | 1.015 | 5.217 | 4.434 | 97.301 |
| 214 | UA1162_12 | 57.093 | 1.219 | 18.196 | 7.476 | 0.178 | 3.284 | 1.087 | 5.744 | 4.414 | 98.691 |
| 215 | UA1162_13 | 60.856 | 0.472 | 18.638 | 5.048 | 0.139 | 1.587 | 0.351 | 5.527 | 5.581 | 98.199 |
| 216 | UA1162_14 | 57.395 | 1.180 | 18.147 | 7.287 | 0.115 | 3.486 | 1.069 | 5.520 | 4.203 | 98.402 |
| 217 | UA1162_15 | 56.935 | 1.182 | 17.794 | 7.373 | 0.126 | 3.580 | 1.064 | 5.405 | 4.078 | 97.537 |
| 218 | UA1162_16 | 60.590 | 0.453 | 18.414 | 4.998 | 0.136 | 1.395 | 0.328 | 6.139 | 5.856 | 98.309 |
| 219 | UA1162_17 | 59.939 | 0.528 | 18.620 | 5.349 | 0.098 | 1.513 | 0.393 | 5.983 | 5.573 | 97.996 |
| 220 | UA1162_18 | 57.148 | 1.235 | 17.864 | 6.667 | 0.152 | 3.419 | 0.952 | 5.451 | 4.512 | 97.400 |
| 221 | UA1162_19 | 57.863 | 1.145 | 18.026 | 7.254 | 0.177 | 3.315 | 0.998 | 5.266 | 4.552 | 98.596 |
| 222 | UA1162_20 | 60.335 | 0.543 | 18.451 | 5.365 | 0.137 | 1.927 | 0.447 | 5.548 | 5.053 | 97.806 |
| 424 | UA1162_21 | 58.189 | 1.045 | 18.316 | 6.827 | 0.127 | 2.804 | 0.887 | 5.778 | 4.795 | 98.768 |
| 425 | UA1162_22 | 58.065 | 1.222 | 18.215 | 7.315 | 0.151 | 3.321 | 0.963 | 3.216 | 4.460 | 96.928 |
| 426 | UA1162_23 | 61.113 | 0.592 | 18.461 | 5.741 | 0.136 | 1.982 | 0.507 | 2.830 | 5.019 | 96.381 |

Table B11. Major element composition of Sheep Track Pumice, Mount Edziza.

| Anaylysis number | Sample number | $SiO_2$ | $TiO_2$ | $Al_2O_3$ | FeO(t) | MnO | CaO | MgO | $Na_2O$ | $K_2O$ | Total |
|---|---|---|---|---|---|---|---|---|---|---|---|
| 132 | UA1155_1 | 64.135 | 0.180 | 18.704 | 5.032 | 0.151 | 1.051 | 0.091 | 5.563 | 5.430 | 100.337 |
| 133 | UA1155_2 | 64.057 | 0.212 | 18.572 | 4.901 | 0.146 | 1.012 | 0.122 | 5.468 | 5.347 | 99.837 |
| 134 | UA1155_3 | 63.426 | 0.272 | 18.459 | 4.948 | 0.149 | 0.961 | 0.101 | 5.694 | 5.169 | 99.179 |
| 135 | UA1155_4 | 64.021 | 0.235 | 18.312 | 4.947 | 0.146 | 0.972 | 0.093 | 5.010 | 5.151 | 98.887 |
| 136 | UA1155_5 | 63.757 | 0.237 | 18.646 | 4.822 | 0.155 | 1.069 | 0.114 | 5.025 | 5.288 | 99.113 |
| 137 | UA1155_6 | 63.837 | 0.238 | 18.400 | 4.942 | 0.188 | 1.014 | 0.118 | 5.328 | 5.341 | 99.406 |
| 138 | UA1155_7 | 63.649 | 0.192 | 18.512 | 4.842 | 0.117 | 1.005 | 0.113 | 4.987 | 5.324 | 98.741 |
| 139 | UA1155_8 | 64.024 | 0.195 | 18.570 | 4.933 | 0.167 | 1.010 | 0.101 | 5.113 | 5.145 | 99.258 |
| 140 | UA1155_9 | 64.231 | 0.189 | 18.797 | 4.965 | 0.141 | 0.911 | 0.089 | 5.776 | 5.240 | 100.339 |
| 141 | UA1155_10 | 63.917 | 0.227 | 18.561 | 5.052 | 0.161 | 1.010 | 0.127 | 5.480 | 5.288 | 99.823 |
| 142 | UA1155_11 | 63.801 | 0.235 | 18.348 | 4.835 | 0.151 | 1.022 | 0.118 | 5.322 | 4.758 | 98.590 |
| 144 | UA1155_13 | 63.820 | 0.196 | 18.371 | 4.827 | 0.126 | 1.068 | 0.093 | 5.339 | 5.361 | 99.201 |
| 145 | UA1155_14 | 63.970 | 0.262 | 18.708 | 5.063 | 0.115 | 0.939 | 0.100 | 5.206 | 5.445 | 99.808 |
| 146 | UA1155_15 | 64.458 | 0.189 | 18.531 | 4.941 | 0.136 | 0.979 | 0.095 | 5.357 | 5.175 | 99.861 |
| 147 | UA1155_16 | 63.875 | 0.212 | 18.750 | 4.878 | 0.091 | 0.974 | 0.112 | 5.321 | 5.399 | 99.612 |
| 149 | UA1155_18 | 65.254 | 0.163 | 18.999 | 4.901 | 0.109 | 0.972 | 0.084 | 5.559 | 5.334 | 101.375 |
| 150 | UA1155_19 | 64.612 | 0.215 | 18.766 | 4.897 | 0.118 | 0.959 | 0.126 | 5.449 | 5.297 | 100.439 |
| 151 | UA1155_20 | 64.177 | 0.224 | 18.588 | 4.883 | 0.100 | 1.055 | 0.114 | 5.284 | 5.223 | 99.648 |
| *143 | UA1155_12 | 62.948 | 0.211 | 17.971 | 4.539 | 0.161 | 0.987 | 0.108 | 4.707 | 5.243 | 96.875 |
| *148 | UA1155_17 | 64.947 | 0.231 | 18.925 | 5.156 | 0.111 | 1.010 | 0.098 | 2.491 | 5.448 | 98.417 |

* Indicates analyses that were excluded from average major element calculations on the basis of their low total weight percents or differing oxide values.

Table B12. Major element composition of Sheep Track Pumice on flank of Tenana Cone, Mount Edziza.

| Anaylysis number | Sample number | $SiO_2$ | $TiO_2$ | $Al_2O_3$ | FeO(t) | MnO | CaO | MgO | $Na_2O$ | $K_2O$ | Total |
|---|---|---|---|---|---|---|---|---|---|---|---|
| 165 | UA1156_1 | 62.956 | 0.188 | 18.262 | 4.626 | 0.142 | 0.900 | 0.083 | 4.896 | 5.215 | 97.268 |
| 167 | UA1156_3 | 63.070 | 0.226 | 18.386 | 4.414 | 0.150 | 0.916 | 0.062 | 5.231 | 5.176 | 97.631 |
| 168 | UA1156_4 | 62.722 | 0.258 | 18.131 | 4.799 | 0.106 | 0.913 | 0.129 | 5.080 | 5.351 | 97.489 |
| 169 | UA1156_5 | 63.101 | 0.232 | 18.283 | 4.664 | 0.064 | 0.967 | 0.091 | 5.117 | 5.413 | 97.932 |
| 170 | UA1156_6 | 62.382 | 0.154 | 18.152 | 4.658 | 0.123 | 0.983 | 0.108 | 4.935 | 5.230 | 96.725 |
| 171 | UA1156_7 | 63.030 | 0.251 | 18.371 | 4.689 | 0.159 | 0.936 | 0.115 | 5.216 | 5.311 | 98.078 |
| 172 | UA1156_8 | 62.689 | 0.200 | 18.304 | 4.685 | 0.133 | 0.968 | 0.082 | 5.012 | 5.169 | 97.242 |
| 174 | UA1156_10 | 63.052 | 0.210 | 18.201 | 4.739 | 0.153 | 0.928 | 0.082 | 4.966 | 5.420 | 97.751 |
| 175 | UA1156_11 | 62.546 | 0.249 | 18.313 | 4.667 | 0.121 | 0.938 | 0.187 | 5.021 | 5.410 | 97.452 |
| 176 | UA1156_12 | 63.090 | 0.193 | 17.894 | 4.918 | 0.150 | 0.991 | 0.136 | 5.056 | 5.322 | 97.750 |
| 177 | UA1156_13 | 62.760 | 0.168 | 18.304 | 4.722 | 0.129 | 1.019 | 0.074 | 5.097 | 5.291 | 97.564 |
| 178 | UA1156_14 | 62.960 | 0.192 | 18.287 | 4.695 | 0.142 | 0.998 | 0.096 | 5.260 | 5.264 | 97.894 |
| 179 | UA1156_15 | 63.030 | 0.187 | 18.223 | 4.655 | 0.139 | 0.966 | 0.127 | 5.042 | 5.161 | 97.530 |
| 180 | UA1156_16 | 62.419 | 0.259 | 18.410 | 4.521 | 0.134 | 1.023 | 0.160 | 5.209 | 5.166 | 97.301 |
| 181 | UA1156_17 | 62.817 | 0.250 | 18.278 | 4.535 | 0.098 | 1.002 | 0.134 | 5.130 | 4.911 | 97.155 |
| 182 | UA1156_18 | 62.741 | 0.202 | 18.185 | 4.602 | 0.123 | 0.949 | 0.114 | 5.036 | 5.213 | 97.165 |
| 183 | UA1156_19 | 62.172 | 0.209 | 18.166 | 4.777 | 0.114 | 0.882 | 0.107 | 5.059 | 5.436 | 96.922 |
| 184 | UA1156_20 | 62.926 | 0.231 | 18.307 | 4.718 | 0.125 | 0.955 | 0.084 | 5.348 | 5.168 | 97.862 |
| *166 | UA1156_2 | 64.339 | 0.003 | 19.224 | 0.227 | 0.014 | 0.671 | 0.000 | 6.893 | 5.725 | 97.096 |
| *173 | UA1156_9 | 60.273 | 0.227 | 17.681 | 4.586 | 0.110 | 0.864 | 0.096 | 5.073 | 5.224 | 94.134 |

* Indicates analyses that were excluded from average major element calculations on the basis of their low total weight percents or differing oxide values.

Table B13. Major element composition of white ash (Sheep Track Pumice?) beneath till, south side of Buck Ridge, Mount Edziza.

| Anaylysis number | Sample number | $SiO_2$ | $TiO_2$ | $Al_2O_3$ | FeO(t) | MnO | CaO | MgO | $Na_2O$ | $K_2O$ | Total |
|---|---|---|---|---|---|---|---|---|---|---|---|
| 380 | UA1157_1 | 62.944 | 0.218 | 18.345 | 5.095 | 0.134 | 0.980 | 0.139 | 5.516 | 5.686 | 99.057 |
| 381 | UA1157_2 | 63.211 | 0.194 | 18.185 | 5.119 | 0.127 | 0.948 | 0.142 | 5.791 | 5.580 | 99.297 |
| 382 | UA1157_3 | 63.355 | 0.243 | 18.223 | 4.848 | 0.121 | 0.992 | 0.115 | 5.360 | 5.479 | 98.736 |
| 383 | UA1157_4 | 63.840 | 0.236 | 18.421 | 4.968 | 0.085 | 0.954 | 0.110 | 5.763 | 5.468 | 99.845 |
| 384 | UA1157_5 | 63.704 | 0.184 | 18.652 | 5.016 | 0.152 | 0.980 | 0.098 | 5.534 | 5.342 | 99.662 |
| 385 | UA1157_6 | 64.035 | 0.230 | 18.617 | 4.862 | 0.183 | 1.036 | 0.101 | 5.536 | 5.132 | 99.732 |
| 386 | UA1157_7 | 64.049 | 0.228 | 18.804 | 4.945 | 0.122 | 0.996 | 0.119 | 5.586 | 5.300 | 100.149 |
| 387 | UA1157_8 | 63.621 | 0.184 | 18.179 | 4.857 | 0.131 | 1.047 | 0.095 | 5.400 | 5.357 | 98.871 |
| 388 | UA1157_9 | 63.172 | 0.193 | 18.410 | 4.945 | 0.138 | 0.962 | 0.102 | 5.785 | 5.585 | 99.292 |
| 389 | UA1157_10 | 63.905 | 0.232 | 18.695 | 4.967 | 0.135 | 1.022 | 0.108 | 5.364 | 5.516 | 99.944 |
| 390 | UA1157_11 | 64.196 | 0.231 | 18.485 | 4.761 | 0.125 | 0.962 | 0.104 | 5.599 | 5.246 | 99.709 |
| 391 | UA1157_12 | 63.873 | 0.214 | 18.436 | 4.976 | 0.099 | 1.021 | 0.097 | 5.751 | 5.553 | 100.020 |
| 392 | UA1157_13 | 63.892 | 0.194 | 18.290 | 4.882 | 0.167 | 0.961 | 0.097 | 5.201 | 5.398 | 99.082 |
| 393 | UA1157_14 | 63.873 | 0.211 | 18.496 | 4.929 | 0.134 | 1.014 | 0.085 | 5.734 | 5.437 | 99.913 |
| 394 | UA1157_15 | 64.196 | 0.198 | 18.407 | 4.861 | 0.153 | 0.948 | 0.104 | 5.514 | 5.188 | 99.569 |

Table B14. Major element composition of Holocene scoria on the west flank of Williams Cone, Mount Edziza.

| Anaylysis number | Sample number | $SiO_2$ | $TiO_2$ | $Al_2O_3$ | FeO(t) | MnO | CaO | MgO | $Na_2O$ | $K_2O$ | Total |
|---|---|---|---|---|---|---|---|---|---|---|---|
| 66 | UA1149_1 | 51.525 | 2.482 | 15.975 | 11.682 | 0.232 | 7.018 | 3.247 | 4.198 | 2.504 | 98.863 |
| 67 | UA1149_2 | 51.616 | 2.566 | 16.132 | 11.579 | 0.186 | 6.955 | 3.136 | 4.093 | 2.446 | 98.709 |
| 70 | UA1149_5 | 51.572 | 2.521 | 16.135 | 11.542 | 0.173 | 7.106 | 3.135 | 3.964 | 2.529 | 98.677 |
| 71 | UA1149_6 | 52.173 | 2.519 | 15.957 | 12.057 | 0.221 | 7.123 | 3.238 | 3.889 | 2.447 | 99.624 |
| 72 | UA1149_7 | 52.056 | 2.315 | 15.759 | 11.745 | 0.181 | 7.159 | 3.170 | 4.090 | 2.541 | 99.016 |
| 73 | UA1149_8 | 51.952 | 2.460 | 16.000 | 11.473 | 0.179 | 7.120 | 3.172 | 4.248 | 2.556 | 99.160 |
| 74 | UA1149_9 | 51.102 | 2.538 | 15.938 | 11.649 | 0.200 | 7.089 | 3.077 | 4.261 | 2.522 | 98.376 |
| 75 | UA1149_10 | 51.835 | 2.519 | 16.009 | 11.637 | 0.183 | 7.100 | 3.296 | 4.245 | 2.339 | 99.163 |
| 76 | UA1149_11 | 51.822 | 2.522 | 16.110 | 11.840 | 0.158 | 7.101 | 3.252 | 4.156 | 2.465 | 99.426 |
| 77 | UA1149_12 | 51.695 | 2.525 | 16.071 | 11.580 | 0.227 | 7.226 | 3.244 | 4.147 | 2.474 | 99.189 |
| 78 | UA1149_13 | 51.743 | 2.552 | 16.019 | 11.880 | 0.152 | 7.290 | 3.228 | 3.461 | 2.583 | 98.908 |
| 80 | UA1149_15 | 51.834 | 2.298 | 16.306 | 11.782 | 0.165 | 7.069 | 3.255 | 4.432 | 2.433 | 99.574 |
| 81 | UA1149_16 | 51.717 | 2.433 | 16.045 | 11.725 | 0.176 | 6.890 | 3.299 | 4.118 | 2.550 | 98.953 |
| 82 | UA1149_17 | 51.757 | 2.586 | 16.038 | 11.974 | 0.195 | 7.157 | 3.254 | 3.969 | 2.556 | 99.486 |
| 83 | UA1149_18 | 51.741 | 2.284 | 16.315 | 11.781 | 0.189 | 7.041 | 3.283 | 4.085 | 2.522 | 99.241 |
| 84 | UA1149_19 | 51.555 | 2.285 | 16.105 | 11.886 | 0.159 | 7.205 | 3.279 | 4.197 | 2.456 | 99.127 |
| 85 | UA1149_20 | 52.182 | 2.602 | 15.898 | 11.222 | 0.163 | 6.611 | 2.788 | 4.247 | 2.925 | 98.638 |
| *68 | UA1149_3 | 63.734 | 0.331 | 19.685 | 2.345 | 0.070 | 1.585 | 0.118 | 5.471 | 5.250 | 98.589 |
| *69 | UA1149_4 | 62.293 | 0.126 | 21.859 | 1.599 | 0.078 | 3.185 | 0.067 | 6.150 | 3.946 | 99.303 |
| *79 | UA1149_14 | 3.959 | 0.309 | 1.992 | 0.584 | 0.030 | 0.701 | 0.286 | 3.440 | 2.185 | 13.486 |

* Indicates analyses that were excluded from average major element calculations on the basis of their low total weight percents or differing oxide values.

Table B15. Major element composition of Holocene scoria from englacial cinders, Mount Edziza ice cap.

| Anaylysis number | Sample number | $SiO_2$ | $TiO_2$ | $Al_2O_3$ | FeO(t) | MnO | CaO | MgO | $Na_2O$ | $K_2O$ | Total |
|---|---|---|---|---|---|---|---|---|---|---|---|
| 92 | UA1150_1 | 48.724 | 2.863 | 15.381 | 13.475 | 0.163 | 9.258 | 4.871 | 3.818 | 1.348 | 99.901 |
| 93 | UA1150_2 | 48.481 | 2.832 | 15.422 | 13.618 | 0.227 | 9.330 | 4.883 | 3.886 | 1.354 | 100.033 |
| 94 | UA1150_3 | 50.879 | 2.752 | 15.566 | 13.040 | 0.147 | 7.771 | 3.711 | 4.124 | 2.063 | 100.053 |
| 95 | UA1150_4 | 50.893 | 2.693 | 15.536 | 12.567 | 0.144 | 7.335 | 3.351 | 4.034 | 2.390 | 98.943 |
| 96 | UA1150_5 | 50.318 | 2.845 | 15.643 | 12.910 | 0.126 | 7.722 | 3.440 | 3.982 | 2.176 | 99.162 |
| 97 | UA1150_6 | 50.288 | 2.765 | 15.752 | 12.710 | 0.178 | 7.505 | 3.465 | 4.186 | 2.248 | 99.097 |
| 98 | UA1150_7 | 50.552 | 2.672 | 15.501 | 12.744 | 0.181 | 7.628 | 3.428 | 4.022 | 2.154 | 98.882 |
| 99 | UA1150_8 | 50.744 | 2.728 | 15.338 | 12.904 | 0.172 | 6.823 | 3.168 | 4.015 | 2.372 | 98.264 |
| 100 | UA1150_9 | 50.818 | 2.887 | 15.625 | 13.036 | 0.236 | 7.348 | 3.218 | 4.225 | 2.464 | 99.857 |
| 101 | UA1150_10 | 49.799 | 2.682 | 15.534 | 13.304 | 0.157 | 8.012 | 3.702 | 4.051 | 1.961 | 99.202 |
| 102 | UA1150_11 | 49.852 | 2.710 | 15.754 | 12.624 | 0.158 | 8.112 | 3.707 | 3.960 | 1.894 | 98.771 |
| 103 | UA1150_12 | 48.166 | 2.693 | 15.593 | 13.245 | 0.216 | 9.385 | 4.743 | 3.439 | 1.325 | 98.805 |
| 104 | UA1150_13 | 47.593 | 2.780 | 15.411 | 13.229 | 0.174 | 9.314 | 4.752 | 3.459 | 1.250 | 97.962 |
| 105 | UA1150_14 | 51.093 | 2.888 | 15.367 | 12.630 | 0.188 | 7.225 | 3.194 | 3.942 | 2.424 | 98.951 |
| 106 | UA1150_15 | 51.327 | 2.760 | 15.566 | 12.963 | 0.221 | 7.129 | 3.315 | 4.213 | 2.306 | 99.800 |
| 107 | UA1150_16 | 50.865 | 2.819 | 15.498 | 12.690 | 0.203 | 7.878 | 3.406 | 4.031 | 2.302 | 99.692 |
| 108 | UA1150_17 | 50.556 | 2.767 | 15.515 | 12.970 | 0.204 | 7.752 | 3.619 | 3.891 | 2.181 | 99.455 |
| 109 | UA1150_18 | 51.185 | 2.839 | 15.670 | 12.562 | 0.175 | 7.251 | 3.228 | 4.063 | 2.386 | 99.359 |
| 110 | UA1150_19 | 50.869 | 2.668 | 15.705 | 12.690 | 0.201 | 7.289 | 3.389 | 4.184 | 2.332 | 99.327 |
| 111 | UA1150_20 | 50.805 | 2.847 | 15.201 | 13.039 | 0.187 | 7.805 | 3.605 | 3.821 | 2.139 | 99.449 |

Table B16. Major element composition of Holocene scoria overlying tundra, north end of Mount Edziza ice cap.

| Anaylysis number | Sample number | $SiO_2$ | $TiO_2$ | $Al_2O_3$ | FeO(t) | MnO | CaO | MgO | $Na_2O$ | $K_2O$ | Total |
|---|---|---|---|---|---|---|---|---|---|---|---|
| 112 | UA1153_1 | 51.894 | 2.580 | 16.185 | 12.337 | 0.187 | 6.993 | 3.272 | 3.991 | 2.489 | 99.928 |
| 113 | UA1153_2 | 51.394 | 2.732 | 16.171 | 11.981 | 0.197 | 7.218 | 3.343 | 4.234 | 2.340 | 99.610 |
| 114 | UA1153_3 | 51.333 | 2.734 | 15.978 | 11.972 | 0.198 | 7.216 | 3.147 | 4.213 | 2.402 | 99.193 |
| 115 | UA1153_4 | 51.466 | 2.618 | 16.135 | 12.093 | 0.199 | 7.279 | 3.276 | 3.913 | 2.211 | 99.190 |
| 116 | UA1153_5 | 51.694 | 2.666 | 16.098 | 11.653 | 0.175 | 6.992 | 3.211 | 4.050 | 2.412 | 98.951 |
| 117 | UA1153_6 | 51.783 | 2.716 | 16.263 | 12.026 | 0.179 | 7.121 | 3.272 | 4.074 | 2.370 | 99.804 |
| 118 | UA1153_7 | 51.279 | 2.701 | 16.087 | 11.992 | 0.222 | 7.211 | 3.398 | 4.031 | 2.254 | 99.175 |
| 119 | UA1153_8 | 52.411 | 2.609 | 16.319 | 12.209 | 0.155 | 7.101 | 3.354 | 4.183 | 2.503 | 100.844 |
| 120 | UA1153_9 | 50.939 | 2.700 | 16.193 | 11.686 | 0.154 | 7.133 | 3.042 | 4.231 | 2.295 | 98.373 |
| 121 | UA1153_10 | 51.663 | 2.652 | 16.121 | 11.977 | 0.146 | 7.027 | 3.038 | 4.108 | 2.440 | 99.172 |
| 122 | UA1153_11 | 51.172 | 2.723 | 15.575 | 12.423 | 0.165 | 7.279 | 3.397 | 4.108 | 2.391 | 99.233 |
| 123 | UA1153_12 | 51.218 | 2.660 | 15.992 | 11.791 | 0.204 | 7.154 | 3.322 | 3.820 | 2.444 | 98.605 |
| 124 | UA1153_13 | 51.646 | 2.569 | 15.945 | 11.858 | 0.225 | 7.221 | 3.218 | 3.723 | 2.335 | 98.740 |
| 125 | UA1153_14 | 50.582 | 2.727 | 15.436 | 12.159 | 0.218 | 7.246 | 3.247 | 3.879 | 2.315 | 97.809 |
| 126 | UA1153_15 | 51.712 | 2.532 | 15.649 | 11.629 | 0.203 | 7.024 | 3.279 | 4.076 | 2.457 | 98.561 |
| 127 | UA1153_16 | 51.201 | 2.753 | 16.266 | 12.150 | 0.181 | 7.443 | 3.374 | 4.151 | 2.348 | 99.867 |
| 128 | UA1153_17 | 51.835 | 2.618 | 16.169 | 12.281 | 0.177 | 7.092 | 3.252 | 4.342 | 2.480 | 100.246 |
| 129 | UA1153_18 | 52.326 | 2.602 | 16.100 | 12.116 | 0.208 | 7.157 | 3.217 | 4.355 | 2.344 | 100.425 |
| 130 | UA1153_19 | 51.308 | 2.682 | 16.127 | 12.341 | 0.190 | 7.325 | 3.359 | 3.776 | 2.471 | 99.579 |
| 131 | UA1153_20 | 51.818 | 2.694 | 16.009 | 11.697 | 0.205 | 6.924 | 3.162 | 3.968 | 2.305 | 98.782 |

Table B17. Major element composition of glass shards in Old Crow tephra standard.

| Anaylysis number | Sample number | $SiO_2$ | $TiO_2$ | $Al_2O_3$ | FeO(t) | MnO | CaO | MgO | $Na_2O$ | $K_2O$ | Total |
|---|---|---|---|---|---|---|---|---|---|---|---|
| 9 | Old Crow std | 72.619 | 0.249 | 12.870 | 1.586 | 0.070 | 1.403 | 0.242 | 3.463 | 3.632 | 96.134 |
| 10 | Old Crow std | 71.733 | 0.319 | 12.521 | 1.678 | 0.088 | 1.333 | 0.266 | 1.901 | 3.522 | 93.361 |
| 11 | Old Crow std | 74.271 | 0.267 | 12.793 | 1.687 | 0.061 | 1.357 | 0.237 | 1.869 | 3.340 | 95.882 |
| 86 | UT1434_OldCrow_std_1 | 73.290 | 0.287 | 13.091 | 1.715 | 0.026 | 1.438 | 0.238 | 2.579 | 3.680 | 96.344 |
| 87 | UT1434_OldCrow_std_2 | 73.888 | 0.304 | 13.000 | 1.767 | 0.052 | 1.342 | 0.284 | 2.637 | 3.686 | 96.960 |
| 88 | UT1434_OldCrow_std_3 | 73.955 | 0.244 | 13.085 | 1.771 | 0.051 | 1.416 | 0.225 | 2.621 | 3.516 | 96.884 |
| 89 | UT1434_OldCrow_std_4 | 73.466 | 0.265 | 12.943 | 1.752 | 0.058 | 1.201 | 0.243 | 2.435 | 3.636 | 95.999 |
| 90 | UT1434_OldCrow_std_5 | 72.914 | 0.274 | 12.996 | 1.781 | 0.075 | 1.447 | 0.287 | 2.502 | 3.773 | 96.049 |
| 91 | UT1434_OldCrow_std_6 | 73.795 | 0.287 | 12.996 | 1.731 | 0.011 | 1.375 | 0.289 | 2.514 | 3.518 | 96.516 |
| 159 | UT1434_OldCrow_std_7 | 73.451 | 0.277 | 12.821 | 1.623 | 0.070 | 1.313 | 0.260 | 2.479 | 3.528 | 95.822 |
| 160 | UT1434_OldCrow_std_8 | 73.653 | 0.284 | 12.764 | 1.756 | 0.054 | 1.328 | 0.279 | 2.441 | 3.625 | 96.184 |
| 161 | UT1434_OldCrow_std_9 | 74.516 | 0.289 | 13.173 | 1.815 | 0.074 | 1.428 | 0.248 | 2.814 | 3.734 | 98.091 |
| 162 | UT1434_OldCrow_std_10 | 72.705 | 0.253 | 12.919 | 1.734 | 0.049 | 1.296 | 0.247 | 2.373 | 3.667 | 95.243 |
| 163 | UT1434_OldCrow_std_11 | 72.098 | 0.286 | 12.524 | 1.706 | 0.051 | 1.320 | 0.244 | 1.586 | 3.456 | 93.271 |
| 164 | UT1434_OldCrow_std_12 | 73.334 | 0.212 | 12.110 | 1.436 | 0.059 | 1.070 | 0.177 | 2.097 | 3.727 | 94.222 |
| 194 | UT1434_OldCrow_std_13 | 72.660 | 0.294 | 12.791 | 1.654 | 0.067 | 1.370 | 0.242 | 2.403 | 3.574 | 95.055 |
| 195 | UT1434_OldCrow_std_14 | 73.173 | 0.273 | 12.995 | 1.840 | 0.051 | 1.459 | 0.243 | 2.591 | 3.605 | 96.230 |
| 196 | UT1434_OldCrow_std_15 | 72.357 | 0.286 | 12.632 | 1.542 | 0.055 | 1.108 | 0.252 | 2.101 | 3.556 | 93.889 |
| 197 | UT1434_OldCrow_std_16 | 72.236 | 0.248 | 12.569 | 1.687 | 0.070 | 1.146 | 0.286 | 1.951 | 3.546 | 93.739 |
| 198 | UT1434_OldCrow_std_17 | 72.144 | 0.267 | 12.523 | 1.651 | 0.078 | 1.097 | 0.274 | 2.780 | 3.274 | 94.088 |
| 199 | UT1434_OldCrow_std_18 | 72.354 | 0.256 | 12.645 | 1.750 | 0.081 | 1.095 | 0.256 | 2.897 | 3.450 | 94.784 |
| 263 | UT1434_OldCrow_std_19 | 71.250 | 0.295 | 12.564 | 1.678 | 0.042 | 1.349 | 0.239 | 2.025 | 3.594 | 93.036 |
| 264 | UT1434_OldCrow_std_20 | 72.741 | 0.321 | 12.649 | 1.648 | 0.056 | 1.361 | 0.251 | 2.547 | 3.709 | 95.283 |
| 265 | UT1434_OldCrow_std_21 | 71.482 | 0.238 | 12.592 | 1.689 | 0.080 | 1.262 | 0.241 | 2.011 | 3.480 | 93.075 |
| 266 | UT1434_OldCrow_std_22 | 72.080 | 0.267 | 12.388 | 1.705 | 0.066 | 1.327 | 0.253 | 2.181 | 3.569 | 93.836 |
| 267 | UT1434_OldCrow_std_23 | 73.073 | 0.274 | 12.896 | 1.693 | 0.044 | 1.249 | 0.275 | 2.528 | 3.515 | 95.547 |
| 268 | UT1434_OldCrow_std_24 | 71.567 | 0.273 | 12.727 | 1.613 | 0.013 | 1.295 | 0.267 | 2.226 | 3.423 | 93.404 |

Table B17 (cont.). Major element composition of glass shards in Old Crow tephra standard.

| Anaylysis number | Sample number | $SiO_2$ | $TiO_2$ | $Al_2O_3$ | FeO(t) | MnO | CaO | MgO | $Na_2O$ | $K_2O$ | Total |
|---|---|---|---|---|---|---|---|---|---|---|---|
| 348 | UT1434_OldCrow_std_25 | 73.969 | 0.255 | 13.016 | 1.759 | 0.018 | 1.422 | 0.302 | 3.389 | 3.607 | 97.737 |
| 349 | UT1434_OldCrow_std_26 | 71.918 | 0.287 | 12.508 | 1.768 | 0.064 | 1.382 | 0.279 | 2.427 | 3.439 | 94.072 |
| 350 | UT1434_OldCrow_std_27 | 73.697 | 0.291 | 12.974 | 1.84 | 0.089 | 1.382 | 0.277 | 2.775 | 3.551 | 96.876 |
| 351 | UT1434_OldCrow_std_28 | 72.214 | 0.283 | 12.868 | 1.74 | 0.072 | 1.272 | 0.271 | 2.397 | 3.565 | 94.682 |
| 352 | UT1434_OldCrow_std_29 | 73.562 | 0.256 | 13.249 | 1.694 | 0.074 | 1.454 | 0.239 | 2.699 | 3.692 | 96.919 |
| 353 | UT1434_OldCrow_std_30 | 71.621 | 0.283 | 12.872 | 1.703 | 0.038 | 1.37 | 0.22 | 3.151 | 3.519 | 94.777 |
| 414 | UT1434_OldCrow_std_31 | 71.867 | 0.25 | 12.553 | 1.687 | 0.004 | 1.38 | 0.231 | 2.378 | 3.267 | 93.617 |
| 415 | UT1434_OldCrow_std_32 | 70.018 | 0.273 | 12.287 | 1.679 | 0.039 | 1.351 | 0.259 | 1.597 | 3.482 | 90.985 |
| 416 | UT1434_OldCrow_std_33 | 72.198 | 0.264 | 12.371 | 1.871 | 0.008 | 1.324 | 0.275 | 2.24 | 3.46 | 94.011 |
| 417 | UT1434_OldCrow_std_34 | 72.48 | 0.272 | 12.668 | 1.732 | 0.087 | 1.323 | 0.245 | 2.338 | 3.529 | 94.674 |
| 418 | UT1434_OldCrow_std_35 | 71.668 | 0.293 | 12.433 | 1.724 | 0.046 | 1.301 | 0.229 | 1.916 | 3.569 | 93.179 |
| 419 | UT1434_OldCrow_std_36 | 74.272 | 0.296 | 12.982 | 1.702 | 0.037 | 1.347 | 0.249 | 2.812 | 3.702 | 97.399 |